A Millimeter Wave Electro-Optical Transmitter for Radio over Fiber Systems

Yejun Fu

A thesis

In the Department

Of

Electrical and Computer Engineering

Presented in Partial Fulfillment of the Requirements

For the Degree of Master of Applied Science at

Concordia University

Montréal, Québec, Canada

November 16, 2012

CONCORDIA UNIVERSITY

School of Graduate Studies

This is to certify that the thesis prepared

By: Yejun Fu I.D. 9560335

Entitled: A Millimeter Wave Electro-Optical Modulator for Radio over Fiber System

and submitted in partial fulfillment of the requirements for the degree of

Master of Applied Science

Complies with the regulations of the University and meets the accepted standards with respect to originality and quality.

Signed by the final examining committee:

_____ Raut, Rabin _____ Chair

_____ Sivakumar Narayanswamy ___ Examiner

___ Yousef R. Shaya_____Examiner

_____Xiupu zhang_____Supervisor

Approved by _____

Chair of Department or Graduate Program Director

_____

Dean of Faculty

Date_____

ABSTRACT

Millimeter wave radio over fiber (RoF) system has emerged with competitive advantages of high bandwidth and low distribution cost to meet the increasing demanding for high data rate wireless access. In RoF system, optical transmitter is a key device that is utilized to transmit radio frequency (RF) signal over optical fiber.

An optical transmitter design involves two important components: Mach Zehnder Modulators (MZM) and Disturbed Feedback (DFB) Lasers. Unfortunately, the DFB laser faces aging problem that its slope efficiency and threshold currents change over time and temperature; the MZMs suffer from bias voltage drift effect, which leads to an unsteady output power. Power fluctuation reduces gain stability, which is indeed a problem of RoF system.

The objective of this thesis is to develop an optical transmitter with low cost circuit design to overcome the above-mentioned issues, by utilizing print circuit board (PCB) integrated design. The proposed transmitter consists of an MZM, a DFB laser, a current control circuit, a Thermo Electric Cooler (TEC) control circuit, and a bias controller, with which the DFB laser produces constant optical power and the MZM bias controller provides an automatic bias control to obtain a

steady system gain. The designed optical transmitter consists of a stable optical source and electro-optical modulator (MZM).

Experiments are conducted to assess the performance of the designed optical transmitter:

(1) The DFB laser with control circuit produces a stable optical output power (10mW) at wavelength 1550nm. Temperature of the DFB laser has been investigated which fluctuates no more than 0.2°C.

(2) Flexible bias controller reduces the power penalty for the MZM. It is found that the MZM's output power (proportional to system's gain) biased at quadrature drifts more than 0.89dB in 30 minutes. On contrary, the output power, with bias controller, reduces its fluctuation less than 0.03dB. Experiments prove that the microcontroller is a more advanced technique for MZM's bias control design.

(3) The RoF system, consisting of designed optical transmitter and a commercial optical receiver, has been investigated, which provides a 30GHz bandwidth for a millimeter wave application. Moreover, by maintaining the bias voltage, the bias controller improves the RoF system's spurious free dynamic range (SFDR) by 5.35 dB.

(4) It is found that the RoF system provides a linear range about 10 dB for orthogonal frequency division multiplexing (OFDM) ultra-wide band (UWB) application, regarding the reference standard as -25dB. In addition, transmission distance impairment for OFDM UWB system is also carried out. We observe that optimum EVM of this link increases with the extended transmission distance.

ACKNOWLEDGEMENTS

I am sincerely grateful to my advisor, Dr. Xiupu Zhang, for the support and guidance he showed me throughout my research. I am sure it would have not been possible without his help.

A special thank goes to Dr. Bouchaib Hraimel for his assistance in project management and many valuable discussions and worthy suggestions that facilitated my research. It is a great honor to work with him in the past two years.

I would also like to acknowledge and extend my heartfelt gratitude the faculty, staff and colleague who shared their personal experience with me. It was a pleasure to meet and work with these people.

Besides, I would like to thank to my parents and Carol who boosted me morally. Without your support, encouragement and patient love, I could not have finished this work.

CONTENT

LIST OF FIGURES

LIST OF ACRONYMS

Acronyms	Definition
ADC	Analog to digital conversion
BS	Base station
CAGR	Compound aggregate growth rate
CS	Central station
CW	Continue-wave
CPBC	Constant average power bias controller
DFB	Distribute feedback
DWDM	Dense wavelength division multiplexing
DAC	Digital to analog conversion
EAM	Electrical absorb modulator
EMI	Electrical magnetic interference
ESD	Electrical statistic discharge
FTTA	Fiber to the antenna
FP	Fabry-Perot
FBG	Fiber Bragg grating
GUI	Graphic User Interface
GSM	Global system for mobile communication
IM DD	Intensive modulation with direct detection
LNA	Low noise amplifier

LED	Light emitting diode
$LiNbO_3$	Lithium Niobate
MZM	Mach zehnder modulator
NF	Noise figure
O/E	Optical/electrical
OPAM	Operational amplifier
PCB	Print circuit board
PIN	p-i-n structure
PD	Photodiode
PC	Polarizer controller
PA	Power Amplifier
RF	Radio frequency
RoF	Radio over fiber
SFDR	Spurious free dynamic range
SNR	Signal noise ratio
SIP	Single in-line package
SA	Signal analyzer
SMF	Signal mode fiber
TIA	Transimpedance amplifier
UMTS	Universal mobile telecommunication system

VSA	Vector signal analyzer
VNA	Vector network analyzer

Chapter 1 Introduction

1.1 Background

- Increasing demanding

The data traffic of mobile and portable devices, including text messaging, multimedia messaging, video call services, and high-speed internet accesses, are increasing day by day. According to Cisco's research (see in Figure 1.1), worldwide demand for mobile and internet traffic has continuously grown from 2009.

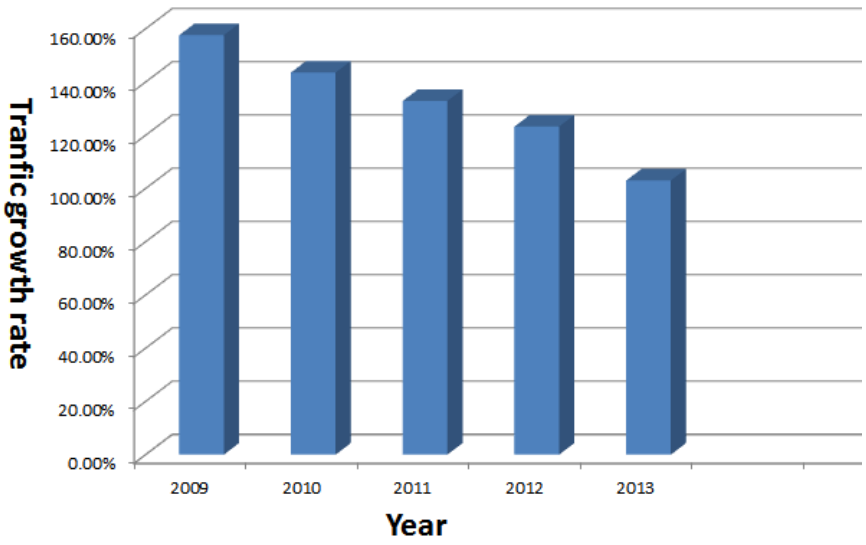

Figure 1.1 Mobile data and internet traffic growth rate [1]

The world's mobile data traffic expands at a compound aggregate growth rate (CAGR) of 150% between 2008 and 2013 [1]. Thence, the future wireless

access network will have to support gigabit data rates. However, current deployed mobile access network does not offer such high capability.

- Problem of conventional wireless access network

The spectrum of wireless access network is shown in Figure 1.2. Multiplicities of wireless access networks are located from 900 MHz to 5.2 GHz.

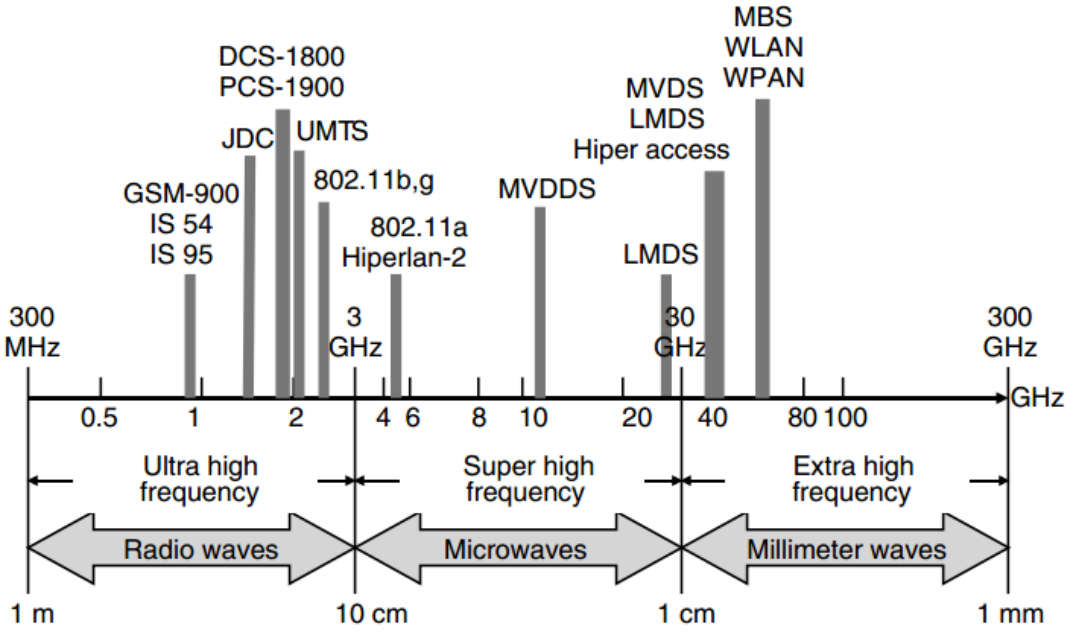

Figure 1.2 Radio spectrum utilized by a variety of current and next generation wireless access networks [2]

The problem of above available wireless access network is that these various systems are rapidly running out of frequency spectrum. Moreover, sharing at the same frequency will cause server congestion. Migrating to higher carrier frequencies (brings more bandwidth) is the only approach to future gigabit data rate wireless communication [3].

1.2 Millimeter-Wave RoF system

- Solution :millimeter wave band

Offering broad bandwidth, the millimeter wave is the most promising solution to achieve high capacity wireless access network. When it comes to the transmission media for millimeter wave signals, there are three possible options: air, coaxial cable, and optical fiber. The first option is limited by the high attenuation (about 15 dB/ km at 60 GHz) [4]; the second one is constrained by the coaxial cable bandwidth, high cost, and high transmission loss. Avoiding above problems, the millimeter wave over fiber transmission provides broader bandwidth, low loss (< 0.5 dB/km), and low cost. Furthermore, millimeter wave over fiber technique enables to deliver RF signals without interferences [5]. In a word, millimeter wave RoF technique has been considered as a cost-effective and reliable solution for the distribution of future wireless access networks.

- What is RoF Technology?

RoF is a technology that uses optical fiber to distribute RF signals from a central site (CS) to groups of separated base stations (BS), which consists of two different technologies: the radio frequency for wireless communications

and optical fiber for wired transmission. One of simple RoF link configurations called intensity modulation with direct detection (IM-DD) is shown in Figure 1.3 [6].

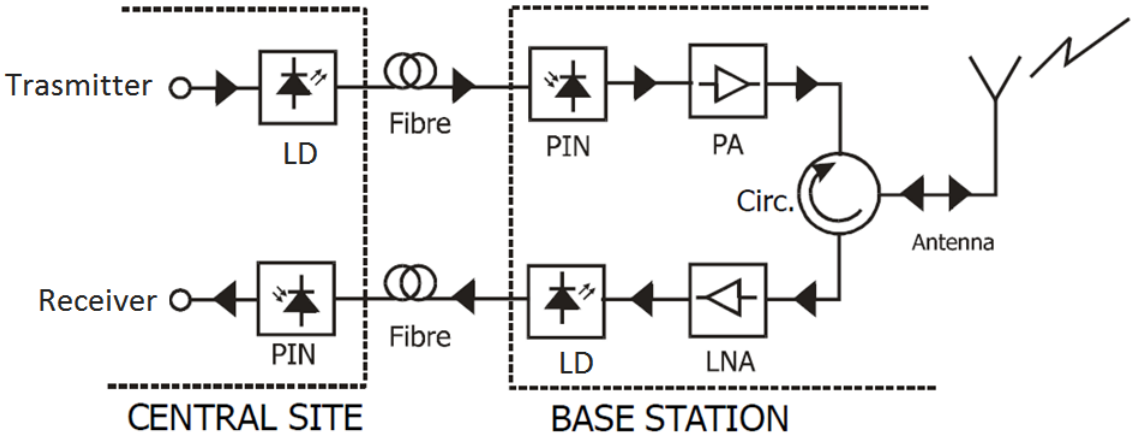

Figure 1.3 A basic RoF system

RF signals directly modulate the laser diodes in the CS, then the modulated optical signal is transported over fiber links to a BS, where the RF signal is recovered by direct detection in the P type-intrinsic-N type (PIN) photodetector. At last, the amplified signal is radiated by an antenna. Signals can be transmitted from a BS to the CS, in a similar way [7] [8].

- Benefits

RoF systems possess many advantages:

(1) Low attenuation- The attenuation loss of 0.5-inch coaxial cable (RG-214) is about 500 dB/Km, when it is operated at 5 GHz [9]. However, commercial

available Single Mode Fibers (SMFs) made from glass have attenuation loss below 0.25 dB/km and 0.5 dB/km at 1550 nm and 1300nm wavelength, respectively [10]. Signals can be transmitted over long distance optical fiber without much attenuation.

(2)Broad bandwidth- For single mode fiber, the overall available bandwidth is more than 50THz, except for several high attenuation windows [11]. This broadband property can be availed by Dense Wavelength Division Multiplexing (DWDM), which encompasses large number of closely spaced optical signals over a single fiber. In a 45-channel system spaced at 100GHz, the covered bandwidth could be 4.5THz [12]. The low-loss window around 1.55um wavelength is divided into conventional band and long-wavelength band(C band and L band), which provides a bandwidth of 95nm, corresponding to 11THz.

(3)Immune to Electro Magnetic Interference (EMI) - Fiber optical transmission is immune to EMI. It is a very attractive property, especially for privacy protection or secured communication. For instance, the aircraft carrier-USS Ronald Reagan has built 200 miles optical fiber through a ship-wide maze of plastic tubes for secured communications [13].

- Applications

Several applications of optical communication systems are discussed below:

(1)Fiber to the antenna (FTTA) - Connecting optical fiber to the antenna, we can obtain many advantages like low line loss, immunity to lightning or electric discharge, and reducing complexity of systems. [8].

(2)CATV- RoF systems can be used to distribute telephone services and broadcast of multiple video channels over television cables. Such system is also able to provide a wide range of services, such as telephone, internet and video broadcasts.

(3)Cellular networks- RoF technology is popular in the mobile communication networks, especially in a high densely populated area. The RoF system can provide flexible and effective installation of large numbers of BS in Global System (GSM) and Universal Mobile Telecommunication system (UMTS) for mobile communications, for instance during 2000 Sydney Olympics, Allen Telecom announced a fiber optic-based system. In first day, over 500,000 wireless calls were made from Olympic Park Venues, which indicates RoF systems are a successful solution for handling massive wireless accesses [14].

- Why 40GHz?

Today, due to the advances in electrical and optical components development, RoF systems can be designed with high frequency and sufficient signal to noise ratio (SNR) to transport RF signals for a considerable long distance. However,

many limitations will restrict the bandwidth and gain of the RoF system, such as modulators and power amplifiers. The recent RoF system focuses on 40GHz transmission, because the available electro optical modulator module only supports up to 40GHz bandwidth. Furthermore, only few venders can provide RF broadband amplifiers (40GHz) for millimeter wave applications. In this work, we adopt a 40GHz MZM and a 40GHz bandwidth power amplifier for the optical transmitter.

1.3 Review of schemes for optical transmitter

In millimeter wave RoF system, the optical transmitter plays an important role. The schemes of optical transmitter design can be sorted into two types: direct modulation and external modulation. Bandwidth and chirp limitation affect the system performance for the direct modulation. For a high bit rate application, an external modulation transmitter is often employed, the details of the above two techniques will be elaborated in Chapter 4.

Two types of external modulator are commonly used: Mach-zehnder Modulator (MZM) and Electrical Absorb Modulator (EAM). MZMs can provide wide bandwidth for long distance high-speed communication; EAMs are suitable for

medium distance and medium speed application. The details of above three modulation schemes for an optical transmitter are shown in Table 1.1

Configurations	Advantages	Disadvantages
Direct modulation	▪ The simplest scheme ▪ Low cost	▪ Limited modulation bandwidth of laser (not suitable for mm-wave band) ▪ produces chirp ▪ Temperature dependence
External modulation(MZM)	▪ Long distance application ▪ High bandwidth	▪ Expensive ▪ Bias drift effect ▪ Bulky size
External modulation(EAM)	▪ Highly integrated with a compacted size ▪ bias voltage drift free	▪ produces less chirp ▪ lower extinction ratio

Table 1.1Comparison of optical transmitter schemes

1.4 Review of key components in optical transmitter

- Optical sources

A laser source is an essential component in an optical transmitter. The word LASER stands for Light Amplification by Stimulated Emission of Radiation. Lasers can be clearly understood by regarding how it amplifies or generates certain wavelength of light by the stimulated emission of radiation.

Many kinds of optical sources are developed in these years, for example Light Emitting Diodes (LED), gas lasers, fiber lasers, and semiconductor lasers. One type of semiconductor lasers named as DFB laser is commonly used as a source in optical transmitter design. Because the DFB laser possesses compact size, narrow spectral width and low threshold current.

Drawback of this type of laser is that the wavelength emitted by a DFB laser is temperature dependent. The laser's wavelength changes with the increasing of temperature. For some applications, like dense wavelength division multiplexing (DWDM) systems with 0.8 wavelength spacing, the laser temperature must be controlled.

Figure 1.4 illustrates a laser diode with a 3mw output needs drive current about 85mA when it is operated at 10°C. However, if the temperature increases up to

90°C, the same output power will need a current of 125mA.The output power of lasers strongly depends on the temperature.

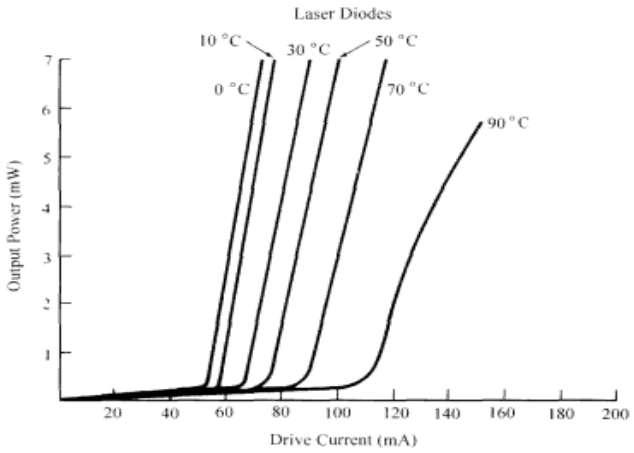

Figure 1.4 Dependence of I-L on temperature [15]

In a word, the drive current density and output power of lasers will change when it is subject to an environment with perturbations.

- Electro-optical modulators

In 1875, John Kerr discovered certain materials that would change their optical properties (refractive index) in response to an applied electrical field. The phenomenon that index changes proportionally to the squared electrical field is known as the Kerr effect [16]. Although the index changes are tiny, a light wave propagating through this medium could have a considerable phase change. The material- Lithium Niobate ($LiNbO_3$) is widely used as a substrate for MZMs. Distinguishing features of broadband characteristic, low chirp and low driving voltage (5V) make the MZMs become the dominate modulator in millimeter wave

RoF applications. We will elaborate the MZM concerning the structure, transfer function, and bias drift effect, in Chapter 3.

Main drawbacks of MZMs are high optical insertion loss (4~7dB), large size (~11cm), sensitivity to the polarization of optical input power and the transfer function shifting due to the temperature disturbing.

1.5 Objective

Many research works related to RoF systems have been intensively investigated. The primary objective of this thesis is to build a low cost optical transmitter, relying on available components, PCB board design, and microcontroller technique.

Constant optical sources and stable MZM output power play important role in this transmitter system: a current and temperate control circuit is designed to overcome the DFB laser's temperature dependence and aging problem; an arbitrary bias controller is implemented to compensate the MZM's bias drift effect.

Based on PCB design and experimental verification, the RoF system parameters are carried out, which involves the S-parameters, eye diagram, P_{1dB} compression

point, SFDR measurement. The results will be compared with different optical transmitters, and bias controllers.

A practical application of OFDM UWB signal transmitter for the RoF system is demonstrated, which aims to compare different modulation schemes. Moreover, the impairment of fiber length to the system performance is investigated. Most importantly, the optical transmitter is to be built for millimeter wave applications at an affordable cost.

1.6 General design specification

This optical transmitter design can be used for CATV, antenna remoting, microwave delay lines and other applications where it is need to transport RF over long distances without signal degradation. There are two PCB board designs: The first board carries DFB laser, current control, and temperature control units, which can generate a tunable optical power range from 9 to 15 dBm. The temperature control units can maintain the DFB laser from 26°C to 32°C; the other board contains logarithmic amplifiers, connectors and voltage regulators, and a 16F877A micro-controller located on a DIP40 socket. A six pins RJ-11 port is installed at the back of the board, which connect the 16F877a to a programmer ICD2. By using software MPLAB, the 16F877A can be reprogramed and developed for other applications. A LCD 16x2 char LCD are used to interface

with microcontroller and show the bias voltage and ADC sample value. This board is used to compensate the bias drift effect and maintain MZM's bias voltage. The bias controller can generate a bias voltage from 1.1 to 8.0V with an increment of 0.01V.

The external modulated transmitter operates at 1550 nm wavelengths are available for applications over the 40GHz frequency band and it is a fully integrated unit that contains both the optics and the control electronics. Only DC Power supply and the RF input signal are required for operation. A more detailed table for transmitter's specification can be found in Appendix E.

1.7 PCB and microcontroller design tools

In this work, the schematic design and PCB layout tools are the OrCAD and PCB Editor, respectively. The microcontroller-16F877A are developed and programed by microchip's MPLAB IDE software.

OrCAD 16.5 is demo version software, which limits the total components placed in the schematic. The OrCAD Capture can be used for not only schematic design but also simulation, which can export schematic results (net lists) to the circuit board layout utility (PCB Editor). The procedures of PCB design, including schematic design and PCB layout, are introduced in Appendix A.

MPLAB is an integrated development environment, which includes several functions for application development, hardware simulation, and debugging. It uses both assembly and C programming languages. In Appendix B, the software MPLAB, the microcontroller 16F877A and programmer ICD2 are introduced.

1.8 Thesis outline

This thesis is composed of five chapters and the rest part of the thesis is organized as follows:

Chapter 2 introduces a control circuit design for DFB lasers, containing automatic power control and temperature control. An experiment is set to verify the performance of this design.

Chapter 3 explicates the working principle of a bias controller for MZMs. The bias control algorithm is explicated and experiments are conducted to compare it with another bias control technique.

Chapter 4 states the structure of designed optical transmitter, and then we carry out several experiments to measure the RoF system's performance. Direct modulation and external modulation techniques are also compared.

Chapter 5 concludes the thesis and highlights recommendation for future works; the possible application after this work is addressed as well.

Chapter 2 Design of DFB Laser Controller

2.1 Introduction

As previously stated in Chapter 1, the DFB laser is strongly aging and temperature dependent. Its threshold current increases with the temperature. Optical sources in the market featuring with power and temperature controller are quite expensive, and average prices could reach 1500$ or more. Furthermore, some optical sources may have a quite large size and long warm-up time. For example, Anritsu MG9541A optical laser source needs one hour to warm up.

The purpose of the control circuit design is to achieve a low cost, small size and highly stable optical source by using low-cost electronic components. The current control circuit is used to maintain constant average optical power and the TEC control circuit is used to regulate the temperature of the laser diode. The DFB laser with these control circuits can be maintained to generate a constant optical power to overcome the problem of temperature and aging dependence.

This chapter is organized as follows: Section 2.2 introduces the basic structure of a DFB laser, the butterfly package and the working principle of TEC. Section 2.3 provides the circuit design of current controller. Section 2.4 shows the detailed design of TEC control circuit. In section 2.5, an experiment is carried out to evaluate the performance of the DFB laser using our designed current controller. In section 2.6, a summary is given.

2.2 Basics of DFB laser and TEC

The structure of a DFB laser, which consists of a Bragg grating, P type and N type semiconductor, is shown in Figure 2.1. The Bragg grating is built on the top of PN junction. The Bragg grating with a periodic variation index has a similar function of filter, which allows one longitudinal mode to exist.

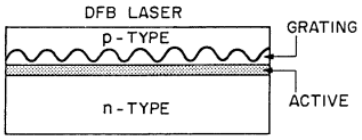

Figure 2.1 Structure of a DFB laser [18]

A more intuitive way to understand the function of Bragg grating is shown in Figure 2.2, which compares two typical output spectra between DFB lasers and (Fabry-Perot) FP lasers. Unlike the FP laser, the DFB laser has one longitudinal mode.

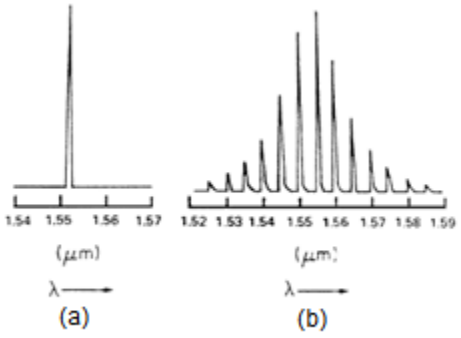

Figure 2.2 Output spectra of (a) a single longitudinal mode DFB laser and (b) a multi-longitudinal mode FP laser [15]

The DFB laser diode is usually integrated with PD and TEC, which has a butterfly package. As we can see in Figure 2.3, the fiber and PD are set at two sides of the laser diode. The photodiode measures the output power of the laser. The thermal resistor monitors the temperature of the DFB laser. The above components are mounted on a metal base. The TEC is stuck at the back of metal base, which stabilizes the temperature of laser.

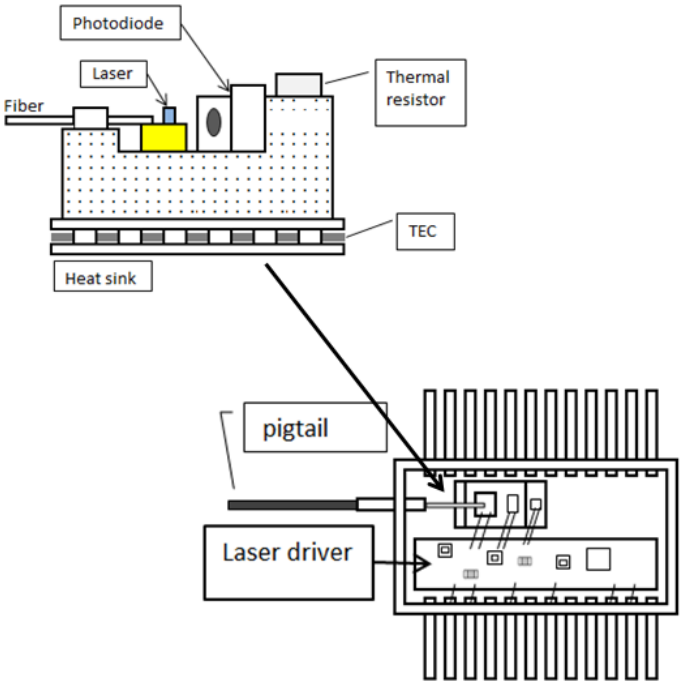

Figure 2.3 General structure of a packaged butterfly DFB laser

The TEC is an active cooling system, which is different from a heat sink- a passive device only used for dissipating heat. The TEC not only lowers the object temperature but also stabilizes it. TEC is highly reliable and has a compact size, and it is often used for the temperature controlling in laser systems.

Figure 2.4 presents one TEC unit, which consists of two arrays of P type and N type semiconductors. Electrical current (see in Figure2.4) circulates through an N-type semiconductor array, a P-type semiconductor array and inner copper connectors; meanwhile, heat can be absorbed and transferred from the top side to the bottom side. Changing the direction of the current, the direction of heat transfer can be reversed.

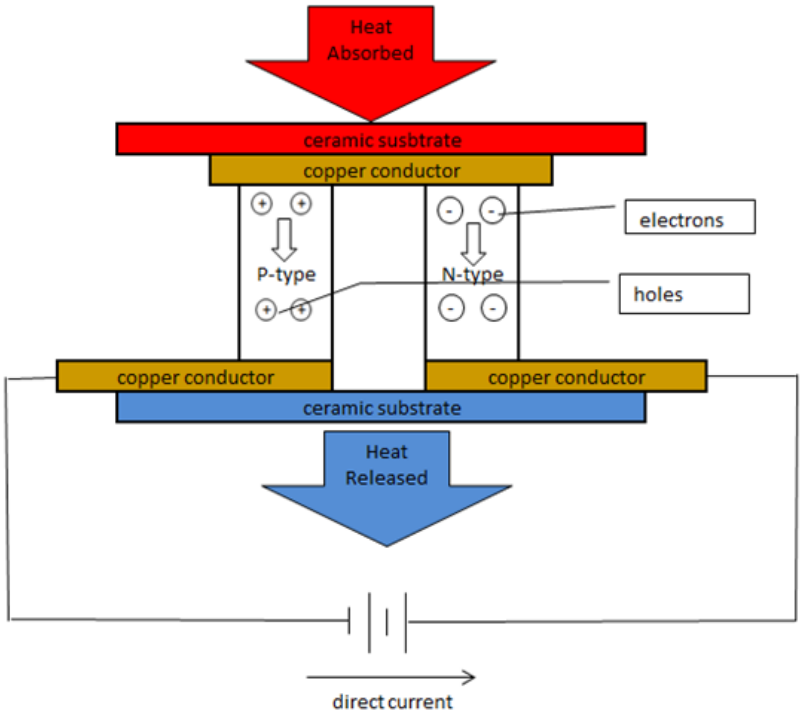

Figure 2.4 The schematic of a TEC unit

In order to provide a high efficiency of heat dissipation, many of above units are built and connected together. Figure 2.5 shows a three dimensional structure of TEC array.

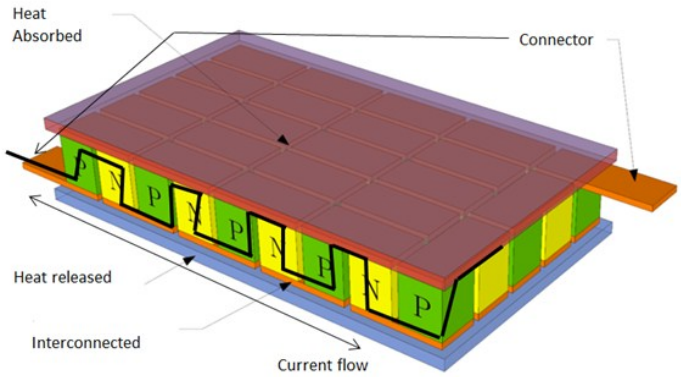

Figure 2.5 The structure of TEC array

2.3 DFB laser current control circuit

The purpose of current control circuit is to provide feedback control to the optical source and enable the laser to produce a continuous constant power. We use Alcatel 1905 DFB laser which is integrated with a TEC, PD and thermistor.

As known, a PD is located at the backside of the laser diode to monitor the optical power. By adding an inverse voltage, the PD produces a current, which is proportional to the driver current on the laser diode. We measure the P-I curve

and PD current of Alcatel 1905 DFB laser. Figure 2.6 presents that the laser drive current is proportional to the PD current.

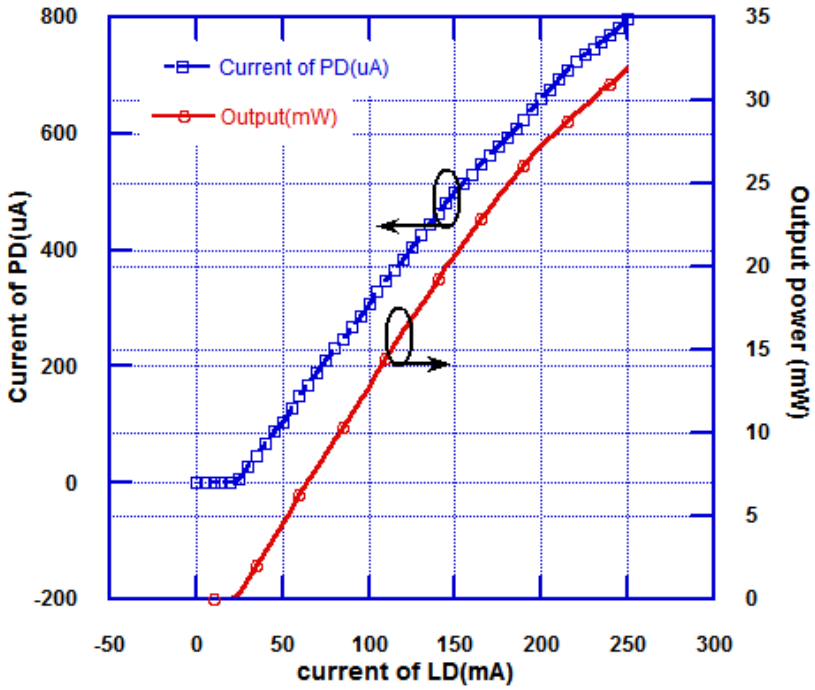

Figure 2.6 The P-I curve of Alcatel 1905

From the above figure, it is not difficult to predict that the output power will fluctuate in a large range, if the drive current is unstable. The current control circuit must be utilized to ensure the laser to produce a constant power.

We implemented the current driver by iC-WKN, which is an IC that can drive laser diodes in continue-wave (CW) mode with a maximum 300 mA current. The

IC includes integrated circuit protecting against electronic static discharge (ESD) [19]. The function of iC-WKN is shown in Figure 2.7.

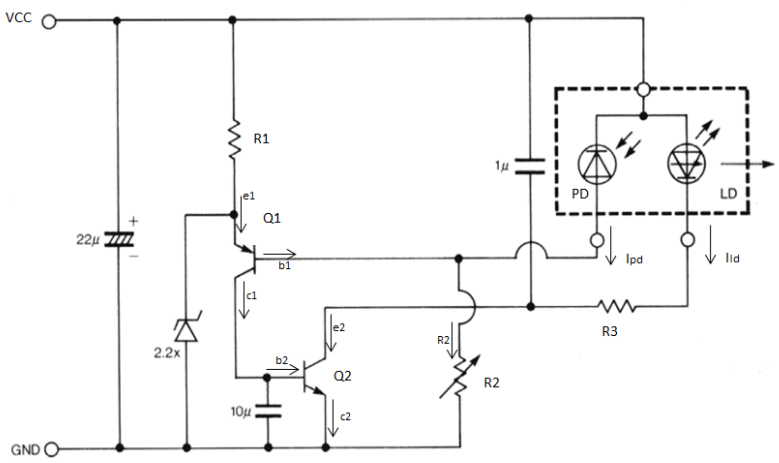

Figure 2.7 Schematic the current driver [19]

A PNP and a NPN transistor are used in the circuit to regulate the laser diode current in the feedback loop. The optical output power depends on gains of Q1, Q2 and values of R_2. We can derive the relation between I_{pd} and I_{ld}.

$$I_{pd} + I_b = I_{R2} \tag{2.1}$$

$$I_{c1} = \beta_1 I_{b1} = \beta_1 (I_{R2} - I_{pd}) \tag{2.2}$$

$$I_{ld} = \beta_2 I_{b2} = \beta_2 \beta_1 I_{R2} - I_{pd} \beta_2 \tag{2.3}$$

In equation (2.3), I_{pd} is proportional to the output power of the laser diode, if the laser diode power increases, I_{pd} will increases and I_{ld} will decrease accordingly.

By changing the value of the resistor R_2, the output power of laser diodes can be adjusted.

From equation (2.3), if R_2 value is small, the laser diode will require a high drive current, which may damage the laser diode. By setting the value of R_2, the output power can be limited. Here we set R_2 equal to the sum of two resistors (names as Rm_fix and Rm_tuning) [19],

$$Rm\_fix + Rm\_tuning = V(MDA)/I(MD) \tag{2.4}$$

where V(MDA) equals 0.5V, and the absolute maximum PD current I(MD) is around 1 mA. Therefore, the minimum value of R_2 should be $500\,\Omega$ which corresponds to a maximum laser diode driver current, about 350mA. To avoid the laser diode overload, we add a fixed value resistor about $634\,\Omega$ that can limit the maximum laser diode current of 0.79mA. A trim resistor is added to adjust the output power.

2.4 TEC control circuit

The purpose of TEC controller is to compensate for the thermal effect of laser diodes. Figure 2.8 represents a typical structure of TEC control circuit which contains four transistors. As discussed before, the function of TEC is determined by the direction of current. By letting Q1 and Q4 or Q2 and Q3 open, the bi-directional current can operate TEC for heating or cooling.

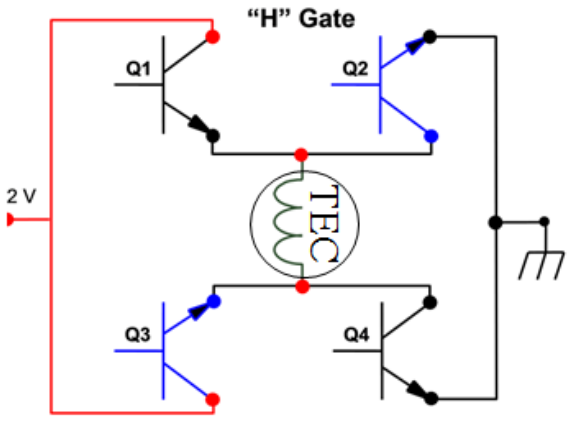

Figure 2.8 A H gate TEC control configuration

A TEC module HY5620 has been implemented which is a subminiature proportional temperature controller. This device can be used to heat or cool a DFB laser and maintain the temperature. A thermistor bridge can precisely measure and regulate the temperature of the TEC. It can deliver up to +/- 2 Amperes of current to a TEC [20].

To make TEC control circuit work properly, additional required components are needed. Figure 2.9 shows the schematic design which contains HY5620, r_{set}, R_{loop}, C_{loop}, $R_{\_Crnt\_Cool}$ and $R_{\_curnt\_heat}$.

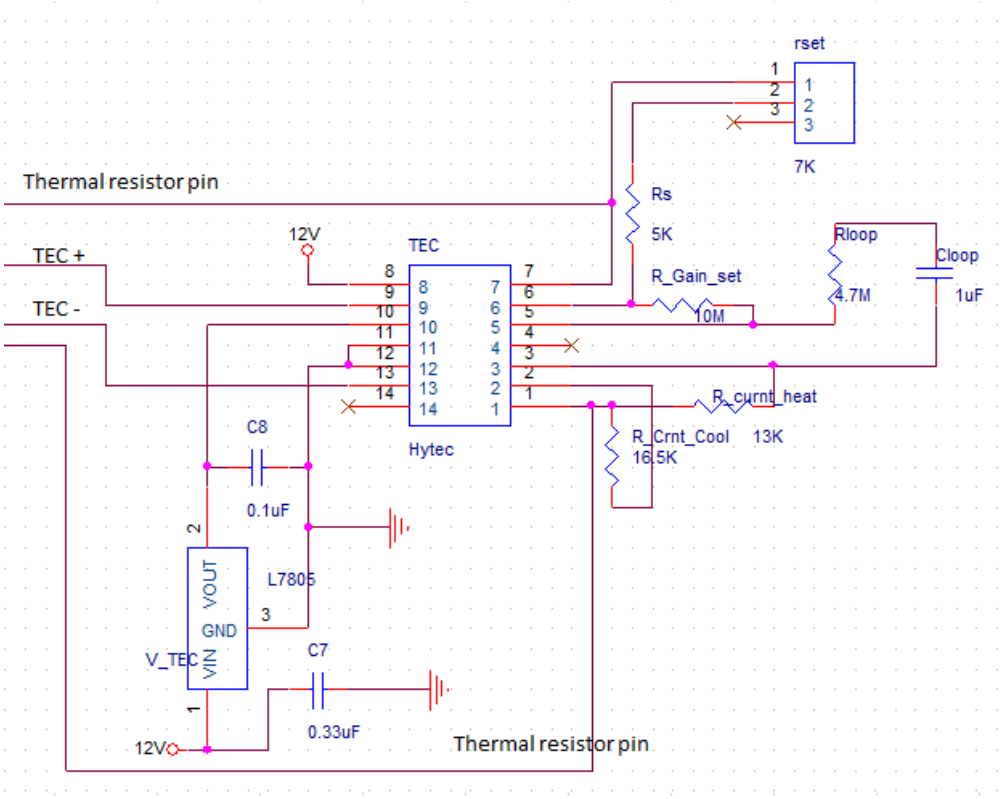

Figure 2.9 Schematic of temperature controller

To operate the TEC control circuit, components of capacitor and resistor are interpreted as follows: Temperature set resistor (r_{set}): r_{set} indicates the temperature of laser diode when it is stabilized. If resistance of the thermistor in Alcatel 1905 is equal to r_{set} that indicates the circuit is stabilized.

The relation between resistance and temperature is shown in Figure 2.10. For example, when we set a given temperature to 25°C, the resistance of r_{set} is 10kΩ.

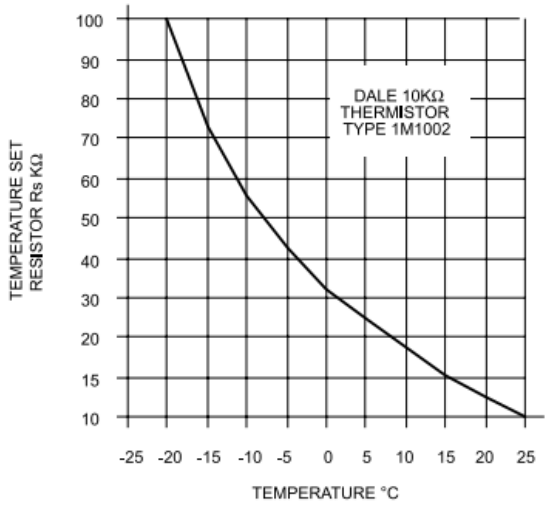

Figure 2.10 Temperature configuration [20]

Loop stability (R_{loop} and C_{loop}): R_{loop} and C_{loop} will determine the time that the current goes through TEC when it reaches 66% of its final temperature [20]. In this project, R_{loop} is set 4.7 MΩ, and C_{loop} is set 1 μF, which indicates the loop time is around 5 seconds.

Current limit resistors ($R_{\_Crnt\_Cool}$ and $R_{\_curnt\_heat}$): These resistors are used to protect the TEC and limit the maximum current, when the TEC works in the cooling or heating cycle. Since the maximum current, used for TEC in Alcatel DFB laser, is around 1.3 A, $R_{\_Crnt\_Cool}$ is set to 16.5 KΩ.

The working principle of TEC control circuit is: when the temperature of the Alcatel 1905 laser is higher or lower than the given temperature, the temperature control will turn on. A maximum cooling current flows into the TEC, or maximum heating current flows out of the TEC. Once the TEC cools or heats the Alcatel 1905 laser to the given temperature, the current through the TEC will decrease to maintain the temperature.

2.5 Evaluation of DFB laser controller circuit

As previously stated in Chapter 1, we use OrCAD and PCB editor as the schematic and layout tools. The schematic drawing contains the control circuits and Alcatel 1905 laser is rendered in Figure 2.11.

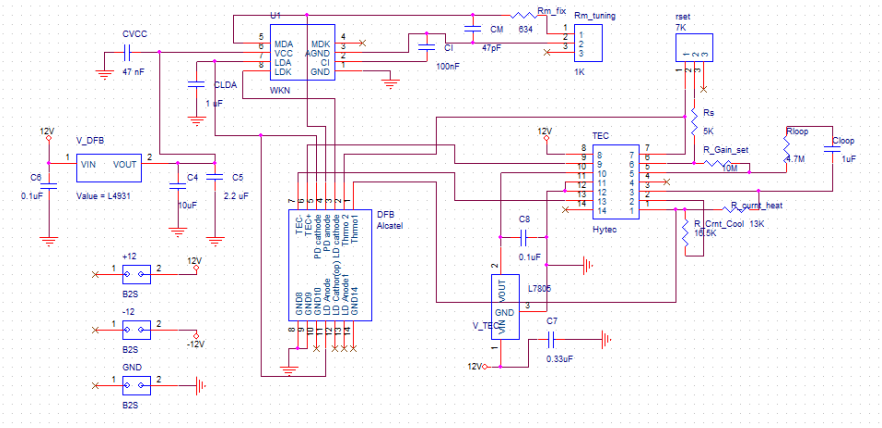

Figure 2.11 Schematic drawing of laser drive and TEC

The final layout is shown in Figure 2.12. The DFB laser is located in the middle, the current and TEC control circuits are placed at left and right side of the board, respectively.

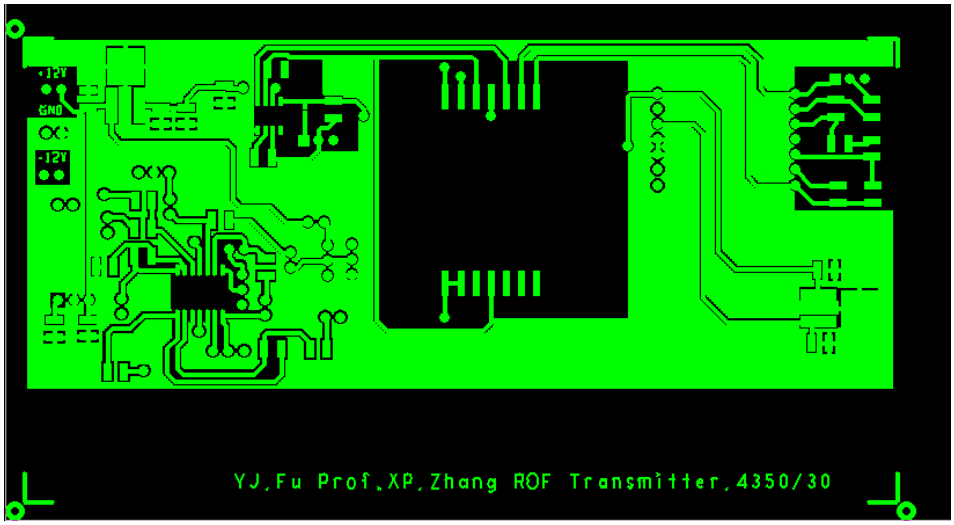

Figure 2.12 PCB layout of transmitter

To test the stability of the Alcatel 1905 DFB laser, a thermal meter is built with a microcontroller -PIC16F877A and a temperature sensor DS18B20. The code of this thermal meter can be found in Appendix C. The DS18B20 digital thermometer provides 12-bit Celsius temperature measurements. It has an operating temperature range from -55°C to +125°C. The resolution of the temperature sensor is 12 bits, corresponding to an increment of 0.0625°C [21].

We set up an experiment to evaluate the performance of the Alcatel 1905 DFB laser and Figure 2.13 is the experimental setup. The laser current is controlled by

a resistor (R_{m_tuning}). TEC can cool down or heat up the laser diode by the resistor "r_{set}" (see in Figure 2.11). A power source provides +12V, -12V, and +5V for the laser and thermal meter. A portable power meter (EXFO) measures the output power.

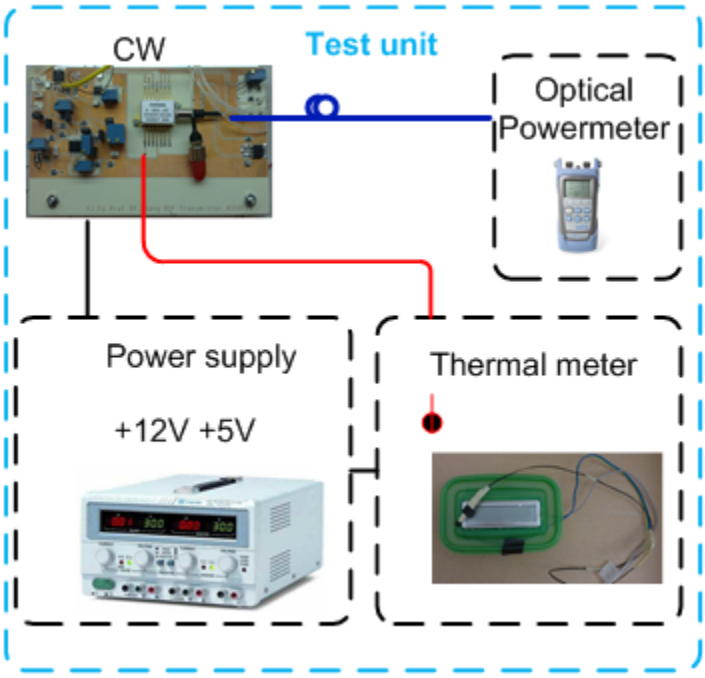

Figure 2.13 DFB laser experimental configuration

As mentioned before, the purpose temperature of laser diode is decide by the resitance of r_{set}. In Figure 2.14, changing r_{set} from 5 kΩ to 12 kΩ,the laser's

temperature increases at first then becomes stable. It illustrates the small value of r_{set} will produce a lower stabled temperature as well.

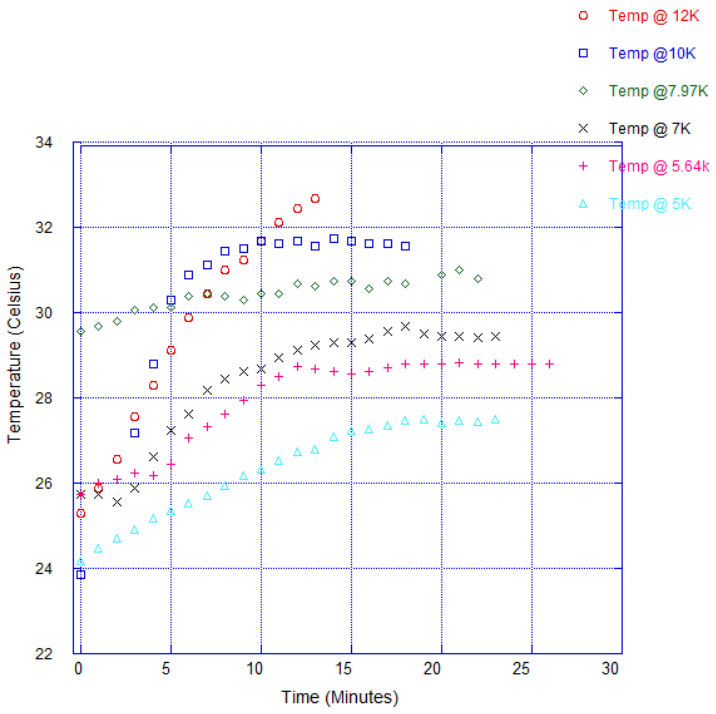

Figure 2.14 Temperature vs. rset resistor

The output power of the Alcatel 1905 laser is maintained at 20 mW. For the different values of r_{set}, it can be seen the temperature of Alcatel 1905 laser becomes steady with fluctuation less than 0.2°C, after 20 minutes.

2.6 Summary

In this chapter, firstly, we have introduced the basics of the DFB laser and TEC, which include the physical structure and working principle. Then, we have explained the detailed design of the current controller and TEC controller. In the end, we have investigated experimentally the performance of the Alcatel 1905 DFB laser in term of the temperature at a 20 mW optical output power.

Figure 2.14 shows that the temperate of the laser can be maintained. The circuit has set a current limitation, which can protect the laser diode from accidental current overload. The laser and control circuits cost less than 400$. The board only has a size of 3”×6”. Our results indicate that the current and TEC controller can successfully stabilize the Alcatel 1905 laser. The DFB laser with a steady optical power is a reliable and perfect light source for optical transmitters.

Chapter 3 Design of Mach Zehnder Modulator Controller

3.1 Introduction

- Problem: MZM bias drift

The MZM is a preferred modulator for millimeter wave communication, because it offers a broad bandwidth up to 40GHz. However, MZM has drawbacks of high optical insertion loss, large size and is polarization sensitive. Furthermore, the MZM is temperature sensitive. If the MZM is exposed in a fluctuating temperature environment, its transfer function will drift over time. For this reason, MZM requires a bias controller to compensate the bias drift.

- Solution: Bias controller

Many techniques have been developed to reduce bias drift. We provide an overview of the present state of MZM bias control technology [22] [23]:

(1) The pilot tone technique: It uses a low frequency signal in a feedback circuit to maintain the bias voltage. However, this technique has a problem that MZM with low tone signals may generate strong in-band intermodulation distortion, resulting in a smaller dynamic range.

(2) Microcontroller: This technique is relied on a microcontroller to monitor PD current that is proportional to MZM output power. Detecting PD current fluctuates; the microcontroller can correct the bias voltage. Beside the high price, most of these commercial bias controllers have a big size and only work at maximum, minimum or quadrature transmission bias points.

(3) Operational Amplifier: unlike a microcontroller, this technique mainly adopts operational amplifiers in feedback circuit to compensate the bias drift. Limitation of this technique is that the circuit only can work at one bias point.

- Purpose: Low cost, multifunction and arbitrary bias point control

The purpose of our circuit design is to develop an arbitrary bias controller based on microcontroller technique. We provide a low cost and compact bias control circuit for an MZM. It relies on an effective method that can operate the MZM at any bias points by automatically finding the maximum and minimum transmission bias points. The bias controller can also be easily programmed to provide more flexible MZM driver for many other applications.

This chapter is organized into five sections. In Section 2, we will introduce the basics of MZM, such as structure, transfer function and nonlinearity. Section 3 is devoted to describe the principle of our proposed bias control circuit. In Section 4,

experiments are carried out to verify the performance of our bias controller. The summary is drawn in Section 5.

3.2 Basics of MZM

- Structure and transfer function

Lithium Niobate ($LiNbO_3$) is a widely used electro-optical material to modulate the light in an MZM. Figure 3.1shows a simplified structure of MZM consisting of two waveguides, two Y junctions and RF/DC electrodes. Assuming that the modulator is an ideal device with no dispersion, no nonlinearity and no coupling loss at point A and B; the phase shift at the lower branch is $\Phi(t)$.

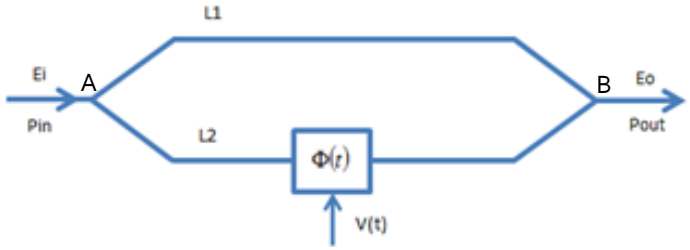

Figure 3.1 Simplified structure of the MZM

Optical signal is launched into MZM, then it is split into two waveguides at point A. A voltage V(t) applied at low branch introduces phase change. The two signals are combined at point B and the output optical field is [22]

$$E_{out} = \frac{1}{\sqrt{2}}\left[\frac{E_{in}}{\sqrt{2}} e^{-i(knL_1)} + \frac{E_{in}}{\sqrt{2}} e^{-i(knL_2+\Phi(V))}\right] \tag{3.1}$$

where n is the refractive index of $LiNbO_3$. L_1 and L_2 are the length of two waveguides. Equation (3.1) can also be rewritten as

$$P_{out} = P_{in} \cdot \frac{1}{2}\left\{1+\cos\left[\frac{\Delta\Phi(V)}{2}\right]\right\} = P_{in}\cos^2\left(\frac{\Delta\Phi(V)}{2}\right) \tag{3.2}$$

Obviously, the different phase of two branches plays an important part in equation (3.2). In practice, two branches often introduce a phase difference. Equation (3.3) used to describe the relation between the phase shift and the applied voltage is shown as follows [23]

$$\Delta\Phi(V) = \phi_o + \left(\frac{2\pi}{\lambda}\right)\frac{\alpha V}{d} L \tag{3.3}$$

where ϕ_0 is the original phase difference. This quantity may change due to fabrication tolerance. α is linear electro-optical coefficiency; L and d are the length and width of the $LiNbO_3$ crystal, respectively; λ is the wavelength of light and V is the applied voltage.

When the phase shift equals to 90°, a special parameter V_π is used to specify the efficiency of electro-optic modulator, which indicates that the bias voltage can change the MZM transfer function from the maximum to minimum point [23].

$$V_\pi = \frac{\lambda d}{2\alpha L} \tag{3.4}$$

Substituting equation (3.4) into (3.2), the ratio of input and output power can be simplified as [23]

$$\frac{P_{out}}{P_{in}} = \cos^2\left[\phi_o + \frac{\pi V}{2V_\pi}\right] \tag{3.5}$$

The equation (3.5) is also known as the MZM power transfer function. Figure 3.2 presents a typical transfer function of an MZM, which shows the relationship between the input electrical signals and the corresponding output optical signals.

V_{b0} is the important bias voltage that will determine the E/O conversion efficiency. For example, if the input signal is bipolar, the MZM is often biased at quadrature

points (V_{b0} works at quadrature points), which let the MZM have the best linearity and the largest swing of the signal voltage.

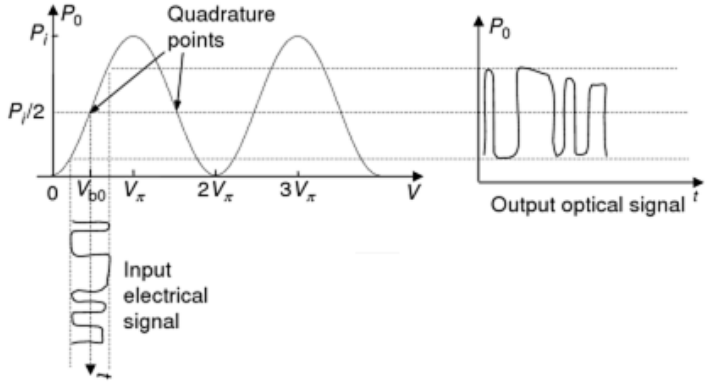

Figure 3.2 Electro-optic modulator transfer function and input/output (electrical/optical) waveform [23]

- Nonlinearity

However, the transfer function of the MZM is not exactly linear; it is a sine wave, so the nonlinear part of the MZM transfer function introduces a distortion for RoF systems. If the applied electrical signal is $V(t) = V_m \cos(\omega t)$, the MZM works at quadrature point, the original phase difference is 90°, the output power can be expanded as a Bessel series [23]:

$$P_{out} = \frac{P_{in}}{2} + P_{in} J_1(x)\cos(\omega t) - P_{in} J_3(x)\cos(3\omega t) + P_{in} J_5(x)\cos(5\omega t) + \ldots \quad (3.5)$$

In equation (3.5), the first term is the average power, the second term is the linear output, the third and fourth terms are higher order nonlinear harmonics. In order to avoid higher order distortions, the input signal should be applied with a lower magnitude voltage. In that case, the high order terms in equation (3.5) can be neglected. In many applications, quadrature bias point controlling is used to suppress the nonlinear distortion.

- Relation between PD current and transfer function

The MZM transfer function is proportional to its output power which can be detected by a PD. In this project, we adopt an AVANEX X-cut AM-40 MZM as a modulator which combines high linearity with low driving voltage and covering the frequency up to 40 GHz. It also has an Integrated PD with a responsivity of 10^{-3} [24]. The PD monitors the optical output power of MZM, which is adopted as a feedback source to control the bias point of the MZM. A simple relation between the input optical field and the output current can be written as

$$I \approx R_0\left(e(t)e^*(t)\right) \tag{3.6}$$

where R_0 is the responsivity of the PD. If a RF signal is fed to the MZM, an electrical signal will modulate an optical signal and the optical field at the PD can be expressed as:

$$e(t) = \sqrt{P_0}\left(1 + mv(t)\cos\omega_{RF}t\right)e^{j\omega_c t} \tag{3.7}$$

where ω_{RF} is the RF frequency, ω_c is the optical carrier frequency, P_0 is the optical power, m is the modulation index, $v(t)$ is the baseband envelop of the modulated electrical signal. Therefore, the approximate current at PD is

$$I \approx R_0\left[e(t)e^*(t)\right] = R_0 P_0\left(1+mv(t)\cos\omega_{RF}t\right)^2 \tag{3.8}$$

Measured transfer function of the AM-40 MZM modulator and the PD current is shown in Figure 3.3.

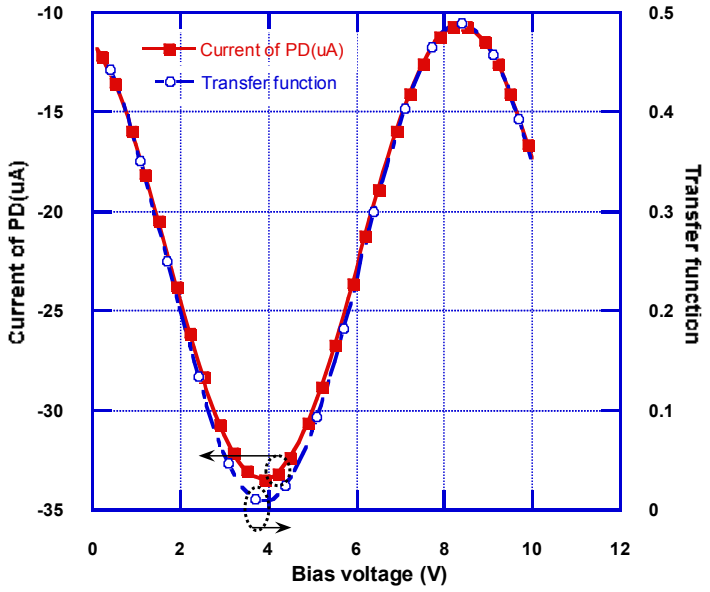

Figure 3.3 Transfer function and PD current of AM-40 MZM

Obviously, the transfer function is proportional to the PD current (see in Figure 3.3). By using a microcontroller to monitor the PD current, we can adjust the bias voltage to overcome the MZM's bias shift effect.

3.3 Bias controller based on Microchip 16F877A

The block diagram of bias control circuit is shown in Figure 3.4. The MZM (AM-40) has an integrated PD to monitor its own output power. The OPAM is used as a transimpedance amplifier (TIA) to convert PD current into voltage. The microcontroller (16F877A) has three functions: analog to digital conversion (ADC), Error correction and digital to analog conversion (DAC). DAC0832 module can provide a DC bias voltage to the MZM. The LCD is implemented to display the bias voltage.

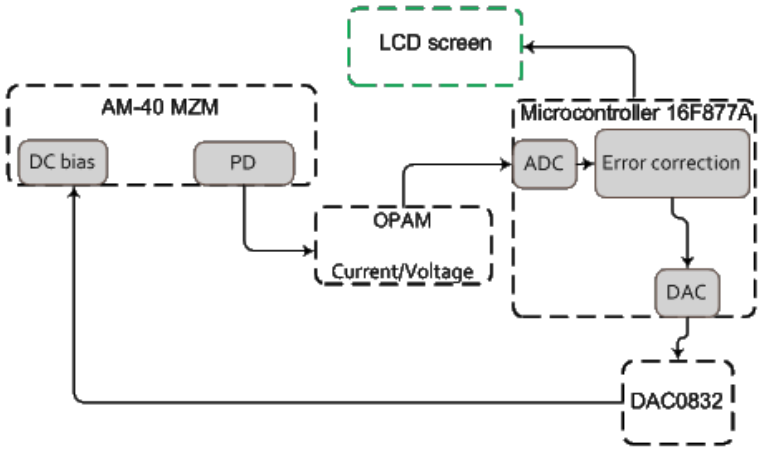

Figure 3.4 Diagram of bias controller

If there are any changes in MZM's transfer function, it will be reflected on PD output current and eventually detected by the microcontroller. The error correction function will decide the value of correction voltage to be applied on the MZM. However, details of this function will be elaborated later. Once the

correction voltage is ready, DAC will send a command to DAC0832 for adjusting the bias voltage to compensate the bias shift. In Figure 3.5, we show the detailed working flow of bias controller which can be identified into three phases: (a) initiation, (b) transfer function sweeping and (c) error checking.

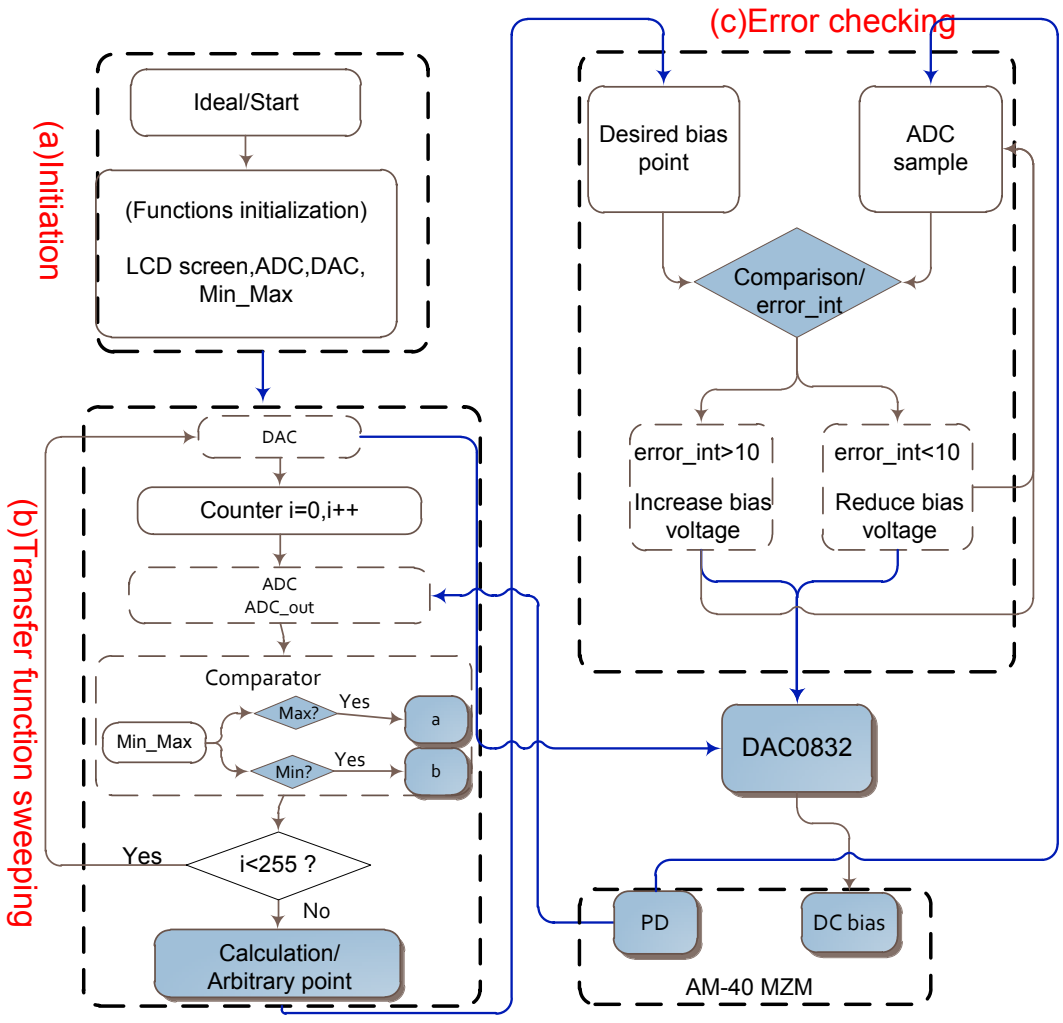

Figure 3.5 An algorithmic state chart of the bias controller

- (a) Initialization

The process begins with initial functions. The circuit contains eight ADC channels, one DAC convertor and one LCD screen. We have to define the ADC convertor channel, LCD display pattern, ADC input analog ports, DAC digital output ports and type of registers.

- (b) Transfer function sweeping

Before using the MZM, we have to measure the characteristic transmission function. The purpose of transfer function sweeping is to utilize microcontroller for recording the MZM's transfer function then provide a desired bias voltage to the MZM.

As shown in Figure 3.5(b), we start with DAC which provides a DC bias voltage of 1.0V to the MZM. Then the ADC fetches 500 samples of PD voltage and calculates the average value (see in Figure 3.5). This average sample result marked as ADC_out is passed to the following function block-comparator (see in Figure 3.5) to find t he maximum and minimum value. The results are stored in variable "a" for maximum value, and variable "b" for minimum value (see in Figure 3.5). The DAC, ADC and Comparator processes will be repeated for 255 times. Because DAC provides an increment of 30mV for each time, the transfer function sweeping would be able to cover from 1.0V to 8.68V. By this way, the microcontroller could record the MZM's transfer function and bias it at arbitrary bias points.

- (c) Error checking

After above processes, the MZM should be biased at a desired bias point (see in Figure 3.5(c)) and the microcontroller will keep running an error checking function which compares the ADC sample result from PD with desired bias point. The comparison result is stored in a variable “error_int” which is used to indicate whether the bias has drifted. For example, in Figure 3.6, the MZM is bias at 5.0V and the desired bias point is B corresponding to an ADC sample value of 800. If the transfer function shifts to the right side (red dash line), the error checking function will sample the PD and the corresponding sample value is 850. After comparison, the “error_int” equals to -50. By judging this value, DAC can send a command to DAC0832 and correct the original bias voltage from 5.0V to 5.1V. Then the microcontroller will run error checking again to ensure the compensation process is entirely completed.

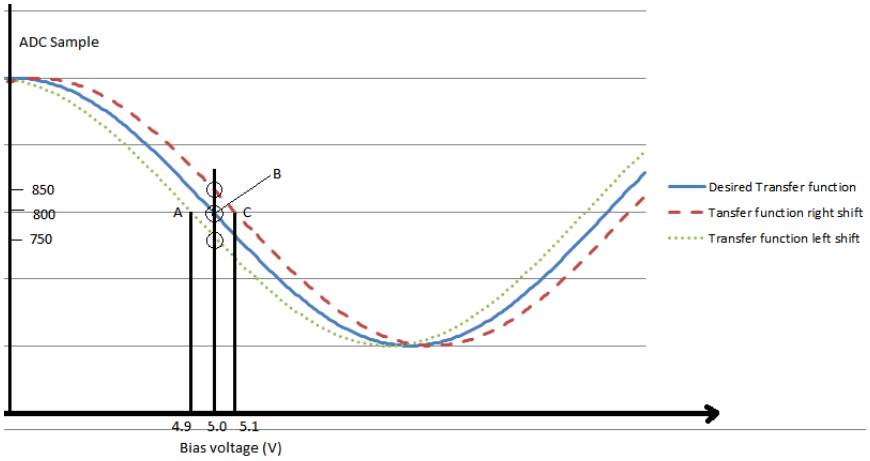

Figure 3.6 Bias shifts Vs. ADC sampling

The purpose of error checking function is keeping the MZM works at it qurdrature point(point B in Figure 3.6). No matter which side the tranfer function has drifted, the error check function can adjust the bias voltage to ensure the MZM works at correct qurdrature points (A or C in Figure 3.6).

The above three steps provide a general understanding for the function of the bias controller. The complete code can be found in Appendix D.

3.4 MZM bias control circuit evaluation

The circuit is designed in OrCAD with the same procedures mentioned in Appendix A. Figure 3.7 shows the schematic drawing of the bias controller. The designed circuit contains 16F877A, DAC, LCD, bandpass filter and logarithmic amplifier (see in Figure 3.7) which can be used for other applications.

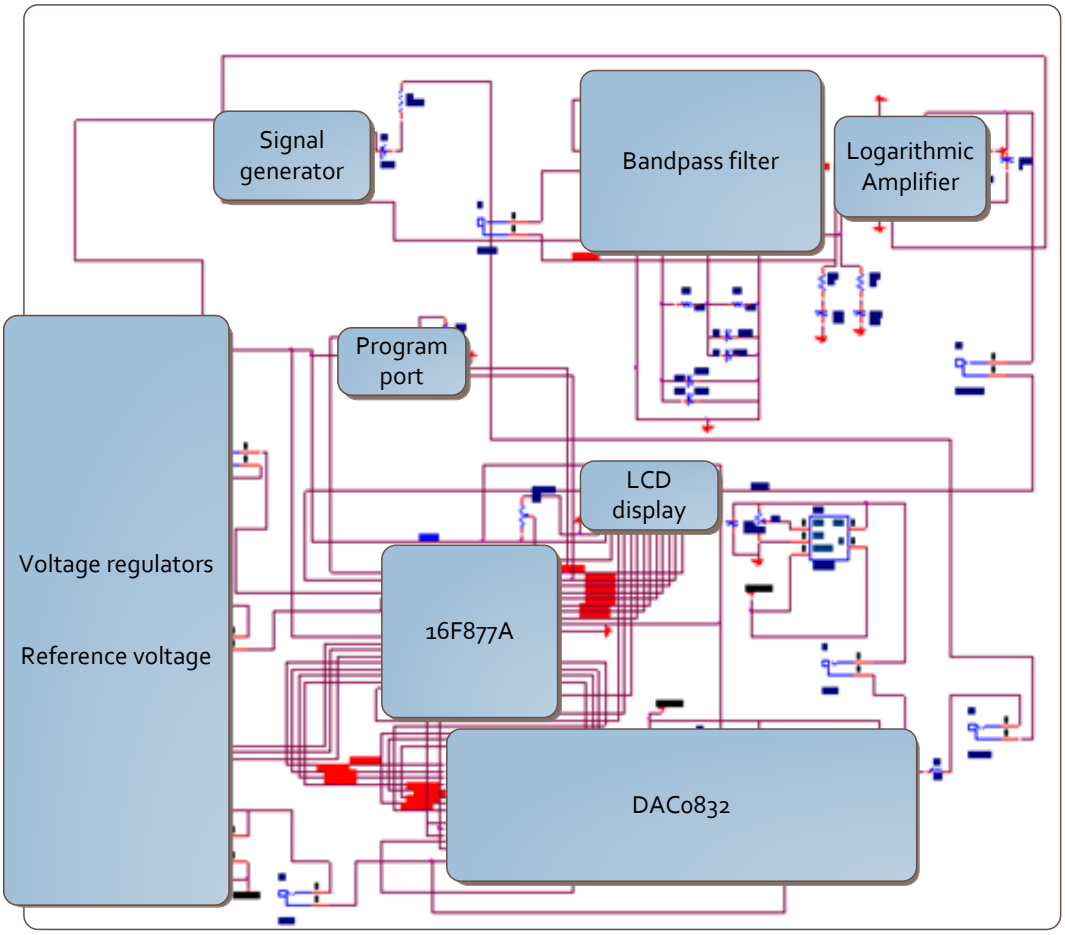

Figure 3.7 Schematic design of bias controller

The PCB board is fabricated by *Centre de Recherche en Electronique Radiofréquence* (CREER). The PCB layout of the bias controller is shown in Figure 3.8, which has a size of 3.4’’× 3.4’’.

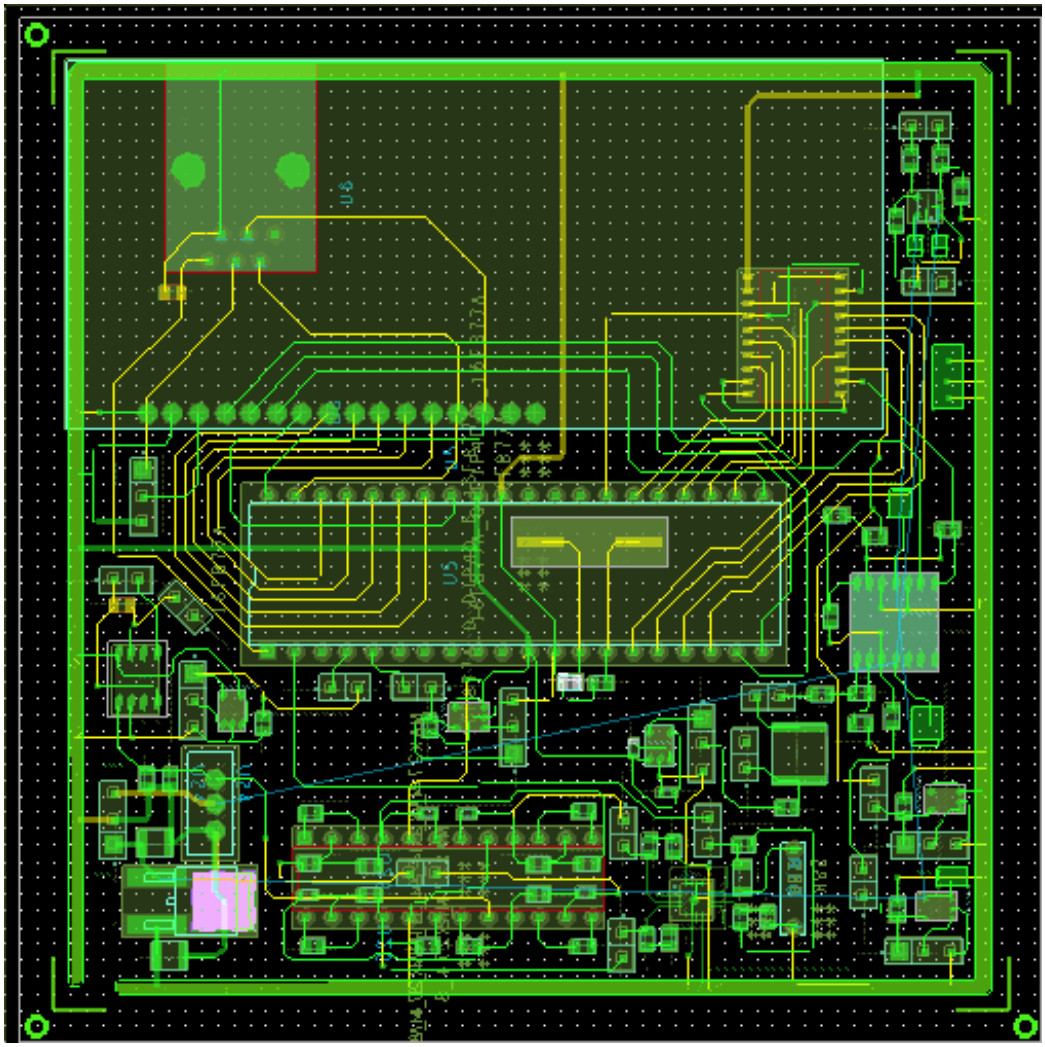

Figure 3.8 PCB layout of bias controller

In Figure 3.9, an experimental configuration is conducted to verify the bias controller. Anritsu MG9541A serves as a light source providing CW laser to the AM-40 MZM at 1550nm. Since the MZM is polarization sensitive, a polarization controller (PC) is installed between MG9541A and MZM. An EXFO power meter measures the output power of MZM.

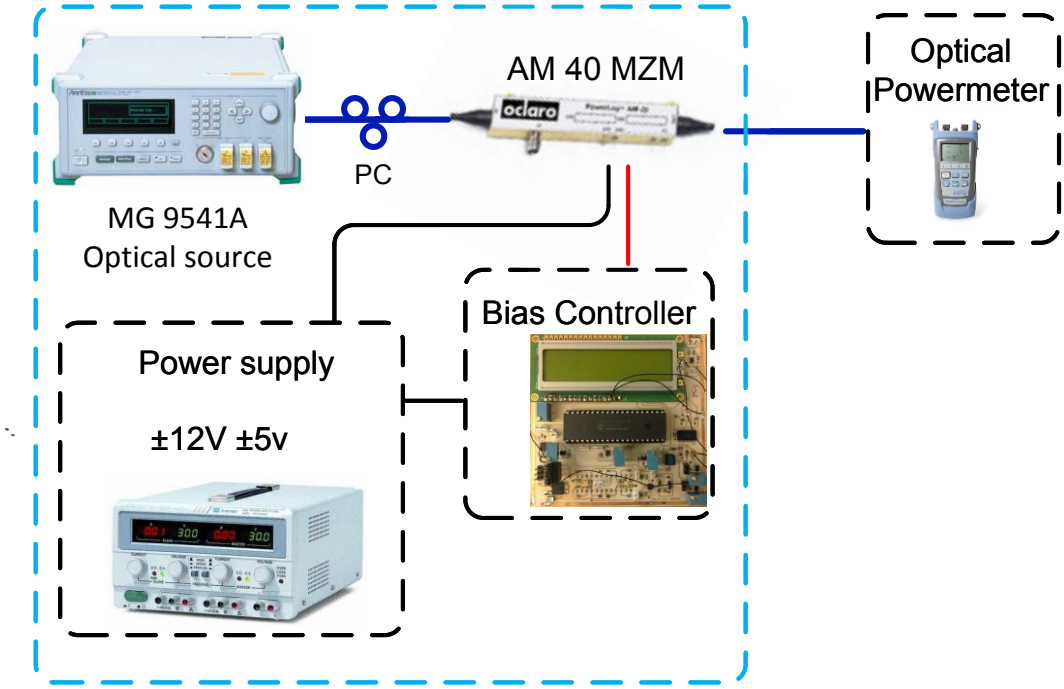

Figure 3.9 Experimental configuration of bias controller

The transfer function of MZM is P_{out}/P_{in}. The input power P_{in} is a constant power. The MZM output power (P_{out}) is proportional to the transfer function. Usually, we

measure the optical output power to evaluate the performance of bias controller. Figure 3.10 shows that our bias controller maintains the MZM output power at 1.05mW for 120 minutes.

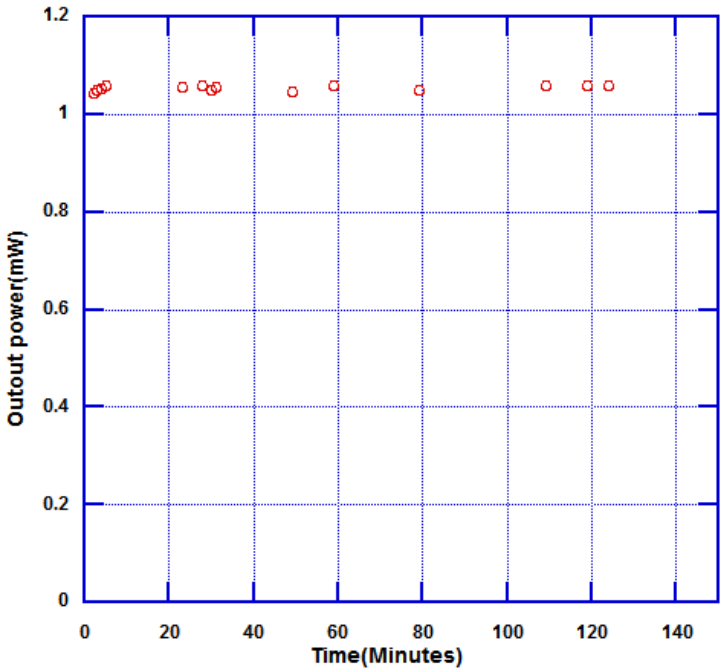

Figure 3.10 A stable MZM output power driven by bias controller

We also find that a more steady output power can be achieved by changing the value of the variable “error_ int” (see in Figure 3.5). The experimental results in Figure 3.11 show the modified error_int (error_7 in Figure 3.11) can make the

power fluctuate less than 0.03dB. On the contrary, the previous code, with the error_10, has an error shifting around 0.06dB.

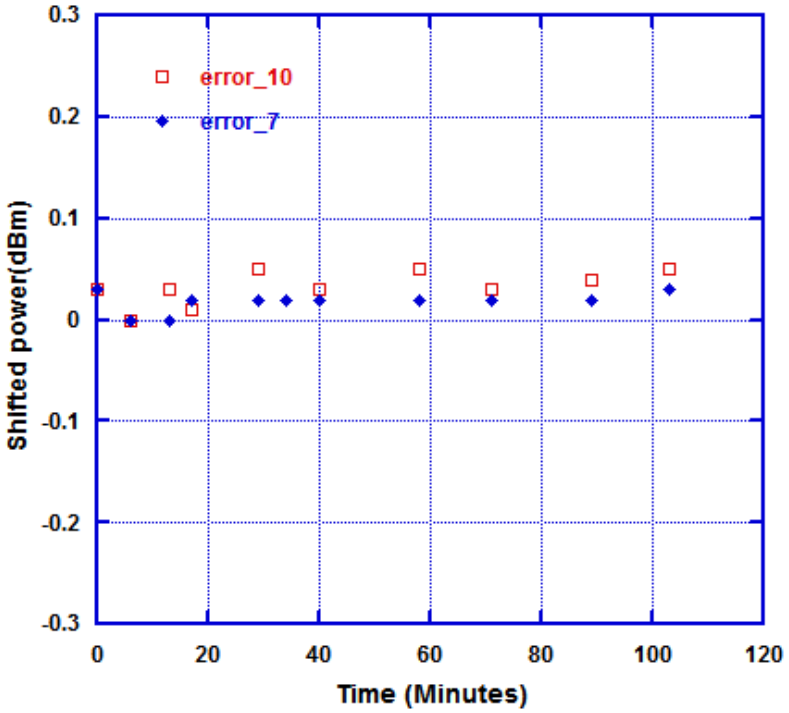

Figure 3.11 Variable error_10 vs. error_7

A bias controller design published at World Scientific and Engineering Academy and Society (WSEAS) is shown in Figure 3.12. Optical power generated by DFB laser goes into MZM unit and the output power is measured by a power meter OMM6810-B.

A constant average power bias controller (CPBC) circuit monitors the TIA (represent the PD power) and generates the desired bias voltage to the MZM. A

data collection unit (DAQ) is used to gather information regarding the optical output power, PD current and Bias voltage.

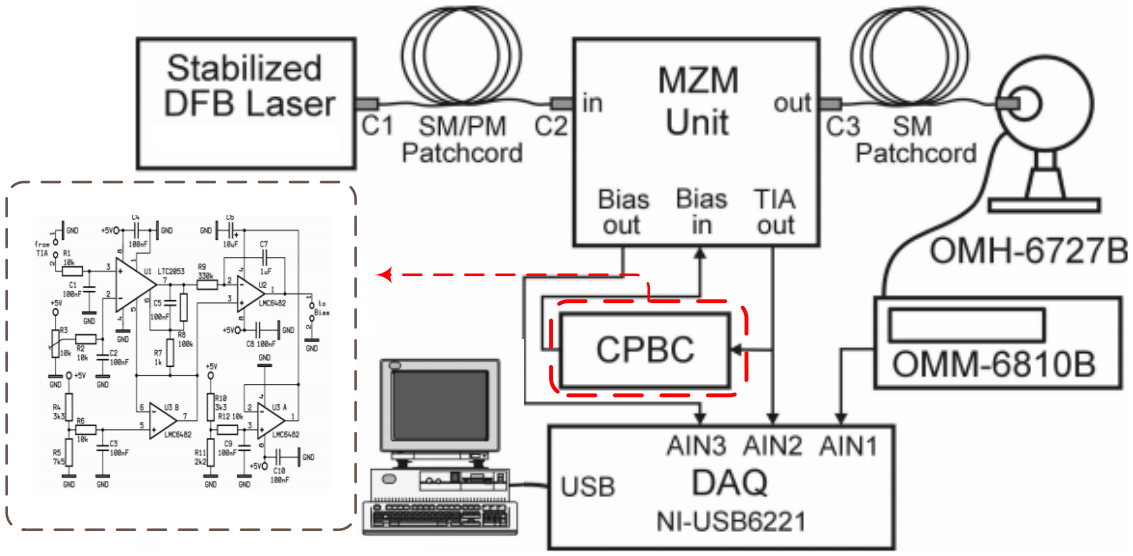

Figure 3.12 The arrangement of the measuring system [25]

The CPBC circuit is mainly built with operational amplifiers, a technique we mentioned previously. The TIA output voltage is fed into CPBC that will compare this voltage with a reference voltage and generate a differential voltage to compensate the bias drift.

Performance of CPBC is compared with our bias controller and the result is presented in Figure 3.13. The experiment result of CPBC is marked as OPAM (red circle); our bias controller is marked as microcontroller (blue diamond). The CPBC can sustain the output power with fluctuation less than 0.35dB. Our bias controller can maintain the optical power steadily around -0.5dBm with a

fluctuation no more than 0.1dB. Figure 3.13 indicates the microcontroller technique can provide a more accurate bias control method.

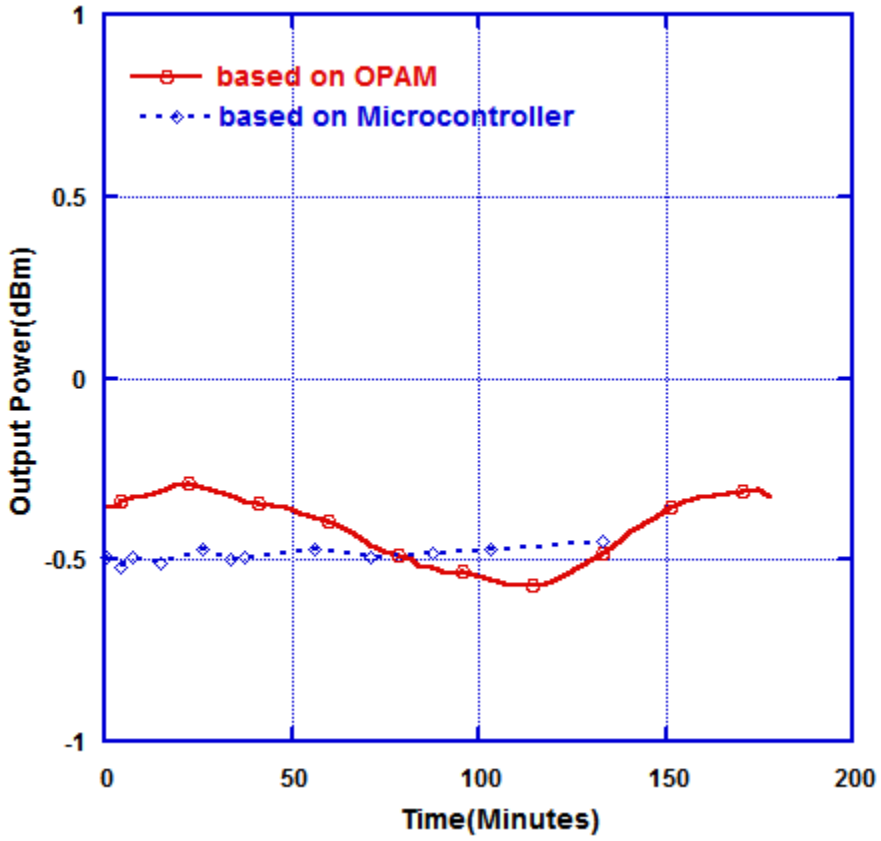

Figure 3.13 The MZM output power control by two bias controllers: CPBC Vs. Microcontroller

3.5 Summary

This chapter has presented a comprehensive overview concept of bias control circuit. Firstly, we introduced and compared different techniques used for bias controller. Then, we described the basics of MZM including its structure, transfer function and nonlinearity. We explained the main function of bias controller. At

the end, an experiment was set up to evaluate the control circuit. The result obtained from experiment shows that the bias controller is feasible to maintain the output power of MZM. We found the microcontroller is a more advanced technique for bias controlling. We provide a low cost and compact bias control circuit for MZM. The whole board costs less than 100$ with a compact size of 3.4''×3.4''. Furthermore, the bias controller can be programmed for other applications.

Chapter 4 Design of Optical Transmitter

4.1 Introduction

An optical transmitter is highly demanded for RF over fiber, antenna remoting and CATV transmission applications. Many modulation schemes have been developed for optical transmitter design and we provide an overview of two most popular methods. In Figure 4.1(a), the RF signal directly modulates a laser's current, which is known as direct modulation. Instead of directly modulating the laser, in Figure 4.1(b), a laser diode serves as continuous wave and RF signals modulate intensity of light by an optical modulator, which is known as an external modulation.

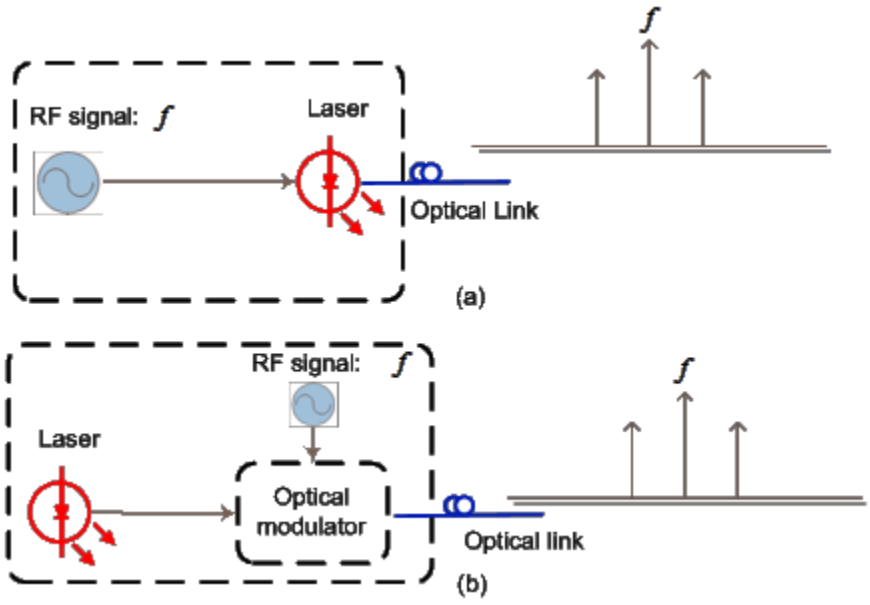

Figure 4.1 Optical transmitter (a) direct modulation (b) external modulation

The laser diode in direct modulation technique has two functions: a laser source and a modulator. Although the direction modulation is the simplest scheme, it is hard to be applied for high frequency, like millimeter wave systems. Limitations of bandwidth and laser nonlinearity make it impossible to modulate millimeter wave signals directly on a laser. Thus, at high frequencies, such as above 10GHz, external modulation is a preferable solution.

In this chapter, we utilize an external modulation scheme for our optical transmitter. The low noise, narrow line width Alcatel DFB laser is adopted as a CW light source. The broadband optical modulator AM-40 MZM is employed to provide the modulation bandwidth up to 40 GHz. Combing with the previously stated MZM bias controller and DFB laser control circuit, the designed optical transmitter can be utilized for millimeter wave band applications.

This chapter is organized as follows: Section 2 introduces the structure of designed optical transmitter. From Section 3 to Section 7, we conduct experiments to evaluate the transmitter's performance including S-parameter, 1dB compression point, noise figure, SFDR and eye diagram. Section 8 and 9 present UWB OFDM signal transmission over a RoF system. At the end, we draw out the summary, including a table of the system's parameter.

4.2 Structure of optical transmitter

Figure 4.2 shows the structure of our optical transmitter. The Alcatel 1905 DFB laser is served as 10mW CW laser at 1550nm. Meanwhile, the current and temperature driver maintain the optical output power. The AM-40 MZM modulates RF signals into optical form that is transmitted over optical fiber. As mentioned before, the bias drift of MZM limits the system performance. A precise bias controller is used to compensate bias drift, which enables the transmitter has good output power stability. Since the AM-40 MZM has a high insertion loss of 6 dB, a commercial power amplifier (ZVA +213) is used to increase the system gain.

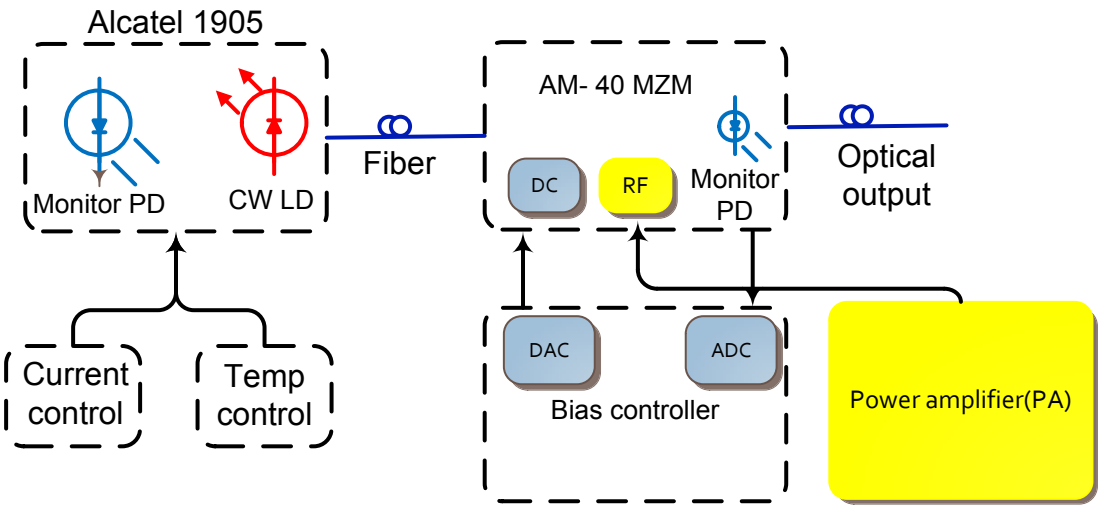

Figure 4.2 Diagram of optical transmitter

Figure 4.3 shows the final PCB board after soldering. The MZM is not mounded on the PCB board, because we have to share this MZM for other experiments. The most common operating bias points of MZMs are negative slope quadrature, positive slope quadrature, minimum transmission (also called null) and maximum transmission point [26]. In this work, experiments are conducted with the MZM operated at positive slope quadrature point corresponding to a bias voltage around 1.8V.

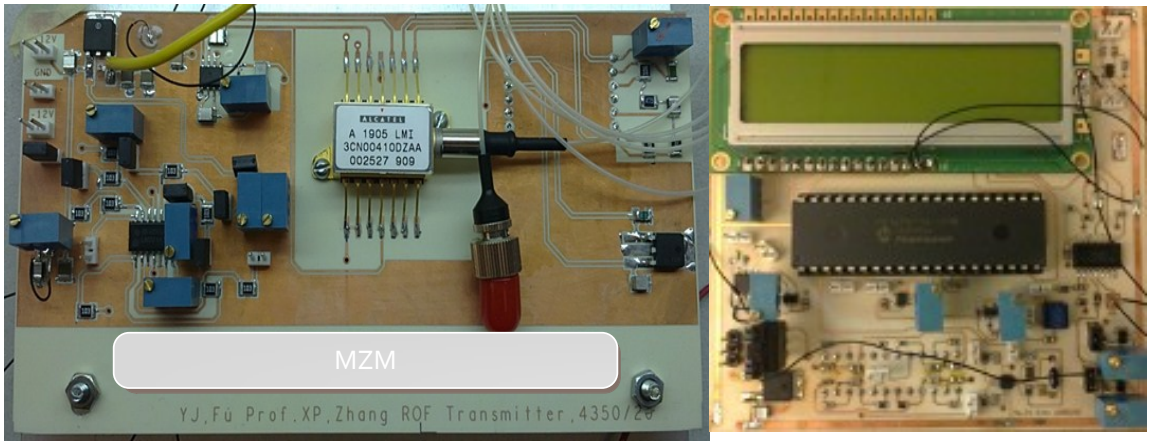

Figure 4.3 The fabricated optical transmitter

The optical transmitter is well fabricated. Several experiments will be carried out to demonstrate that this product can work as we expected. The following section will show the experiment details and results.

4.3 Link S-parameters

- **Setup**

Figure 4.4 describes the experimental configuration to measure the S-parameters. The RoF system consists of the designed optical transmitter, a commercial optical receiver-DSC 720 and a PA. The Agilent E5071B vector network Analyzer (VNA) is used to measure S-parameters. Before jumping into measurements, a short load, an open load and a 50 ohms load are required to calibrate the VNA.

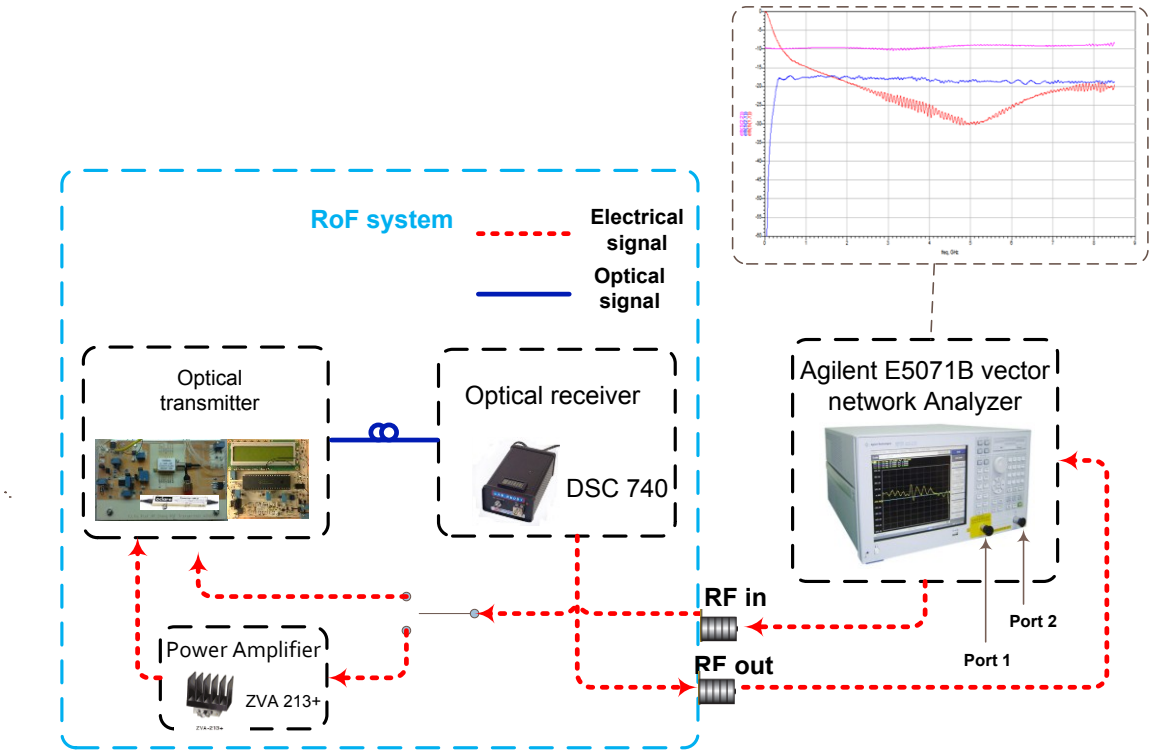

Figure 4.4 S parameters testing

From VNA's port 1, RF signals from 300 KHz to 8.5GHz are sent into incident port of DUT (the RoF system). The transmitted signals are fed back to VNA's port 2. Thus, the VNA can analyze the system's return loss and transmission coefficient.

- Result(without PA)

We record S-parameters at two bias voltages in Figure 4.5. Experiment result indicates that two bias points of 8.01V (maximum transmission point) and 5.0V (minimum transmission point) can largely change the system's gain.

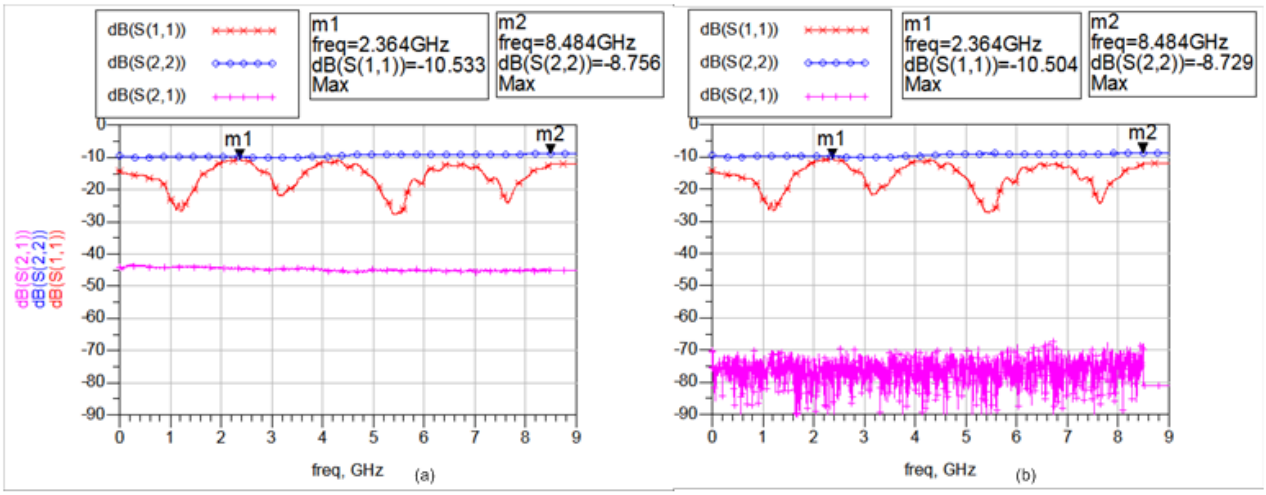

Figure 4.5 S-parameters at bias voltage of (a) 8.01V and (b) 5.0V

In Figure 4.5 (a), the S11 is below -10.533dB (see maker m1) and the S22 is less than -8.756dB (see marker m2). The S11 and S22 have few changes when the MZM is biased at 5.0V, in Figure 4.5 (b). However, the systems gain (S21)

decreases dramatically, from -45 dB at maximum transmission point (bias voltage of 8.01V) to -75 dB at minimum transmission point (bias voltage of 5.0V).

- Result (with PA)

The system gain (S21) is low (-45 dB) even MZM is biased at the maximum transmission point, so a PA (ZVA +213) is added into RoF system to provide a gain of 27dB. The measured s-parameters are shown as follows:

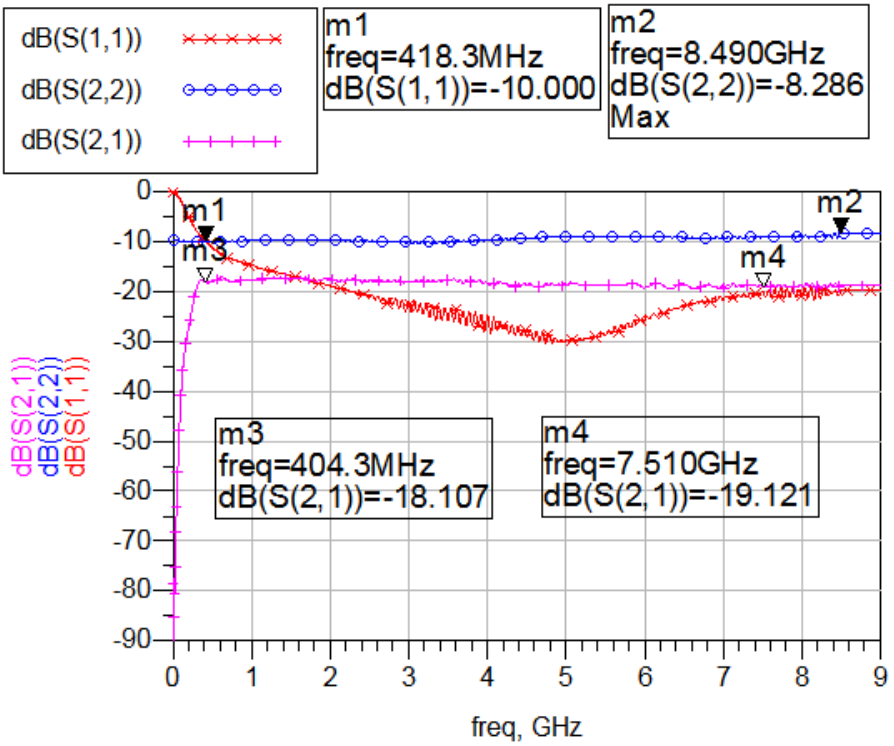

Figure 4.6 RoF system S-Parameter with PA

In Figure 4.6, the S11 parameter is below -10dB after 418MHz (see m1) and S22 is no more than -8.286dB (see m2). From 404MHz to 8.5GHz, the system produce a stable gain curve around is -18 dB (see m3 and m4).

- Result of 40GHz measurement

The Agilent E5071B (VNA) only covers a maximum bandwidth up to 8.5 GHz. To evaluate the system performance at millimeter-wave frequencies, we measure the S-parameter at CREER by using VNA Anritsu 37269B which can test S-parameters up to 40GHz. A 100GHz U^2t photodetector is adopted to replace the DSC740 (optical receiver), since the DSC740 only has a 3-dB detection bandwidth of 26GHz. Figure 4.7 shows the S-parameters of the RoF system.

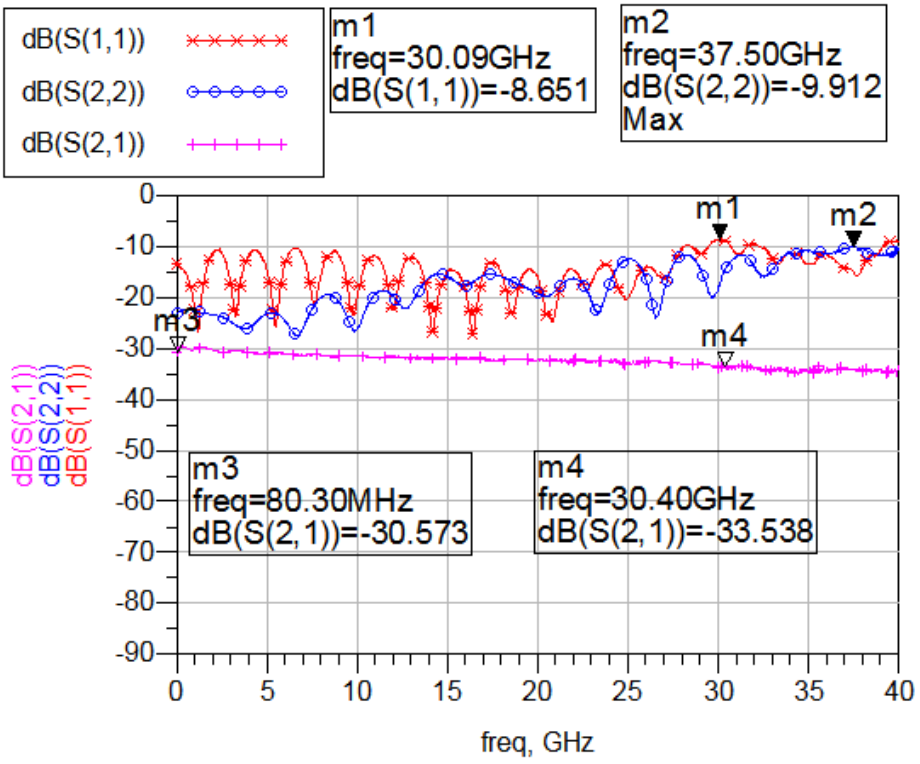

Figure 4.7 RoF system S-parameters for 40GHz

The return loss S11 is below -10dB, except for frequencies around 30GHz, which

corresponds to a worse performance of -8.65 dB. The S22 is less than -9.9 dB, which indicates the output port of U^2t photodetector is well matched. The 3dB cut off frequency of our RoF system is around 30.40GHz.

4.4 Eye diagram

- Setup

In this experiment, we evaluate RoF system by analyzing the “eye diagram” which is often used to assess the performance of communication systems. Figure 4.8 shows the experiment setup.

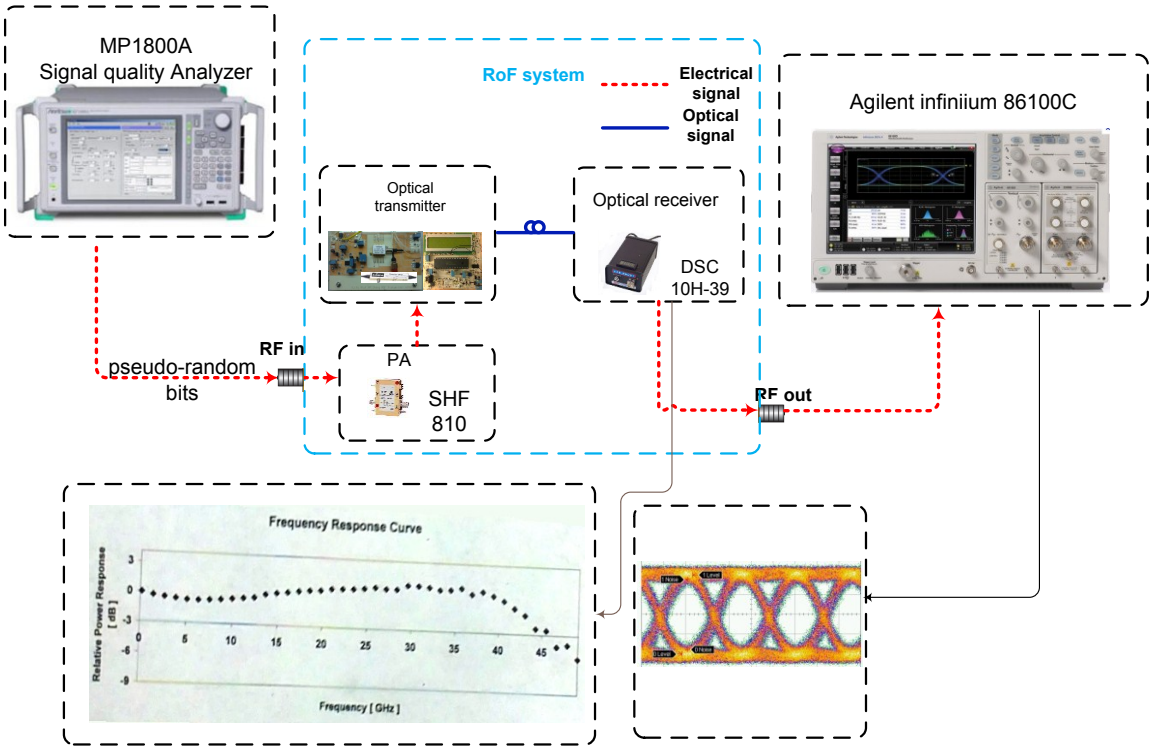

Figure 4.8 The experimental setup for eye diagram

MP1800A is a pulse pattern generator with four channels of parallel data output lines. It can produce PRBS pattern up to 2^{31}-1 bits. A 40GHz wideband PA-SHF810 is implemented to deliver a sufficient gain for RF signals. The PA cascaded with an attenuate mainly provides a gain of 10 dB. Optical receiver-DSC10H-39 offers a detection bandwidth of 45GHz. Agilent infiniium 86100C Oscilloscope is used to analyze the eye diagram.

- Result

The pulse generator provides pseudo-random bits for the RoF system, with a 1 V_{p-p} input signal at a bit rate of 40Gbps. For each displayed bit period, there will be Highs, Lows, and Up and Down transitions (see in Figure 4.9). With a properly trigger, the measured results are repeatedly displayed which looks like an eye (see in Figure 4.9).

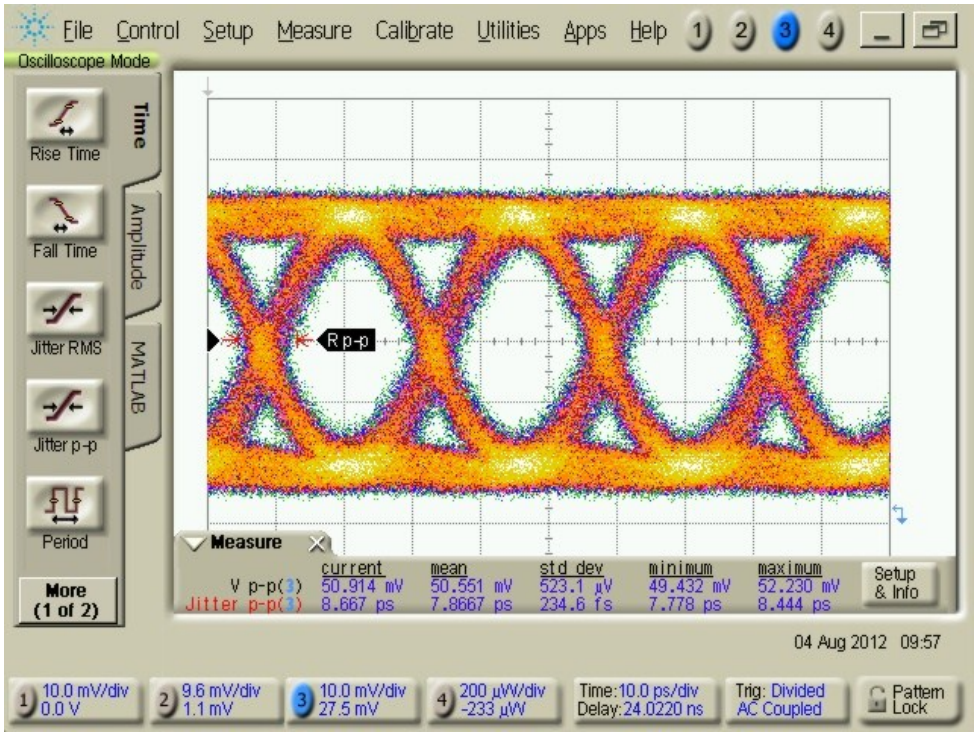

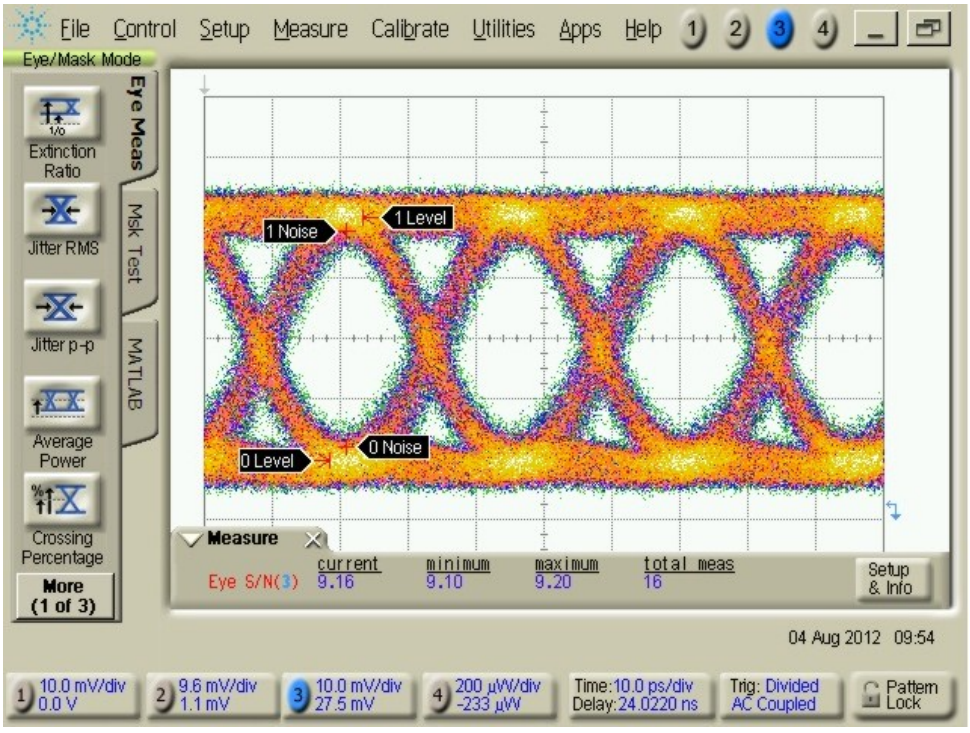

Figure 4.9 Measured eye diagram of RoF system at 40Gbps

Figure 4.9 shows the output voltage swing (V_{p-p}) has reached 50.914 mV and the Q factor (S/N) is 9.16.

4.5 1dB compression point (P_{1dB})

The P_{1dB} is a commonly used figure of merit to shows the gain relationship between output power and input power for RF amplifiers. A typical RF amplifier (nonlinear device) response is shown in Figure 4.10.

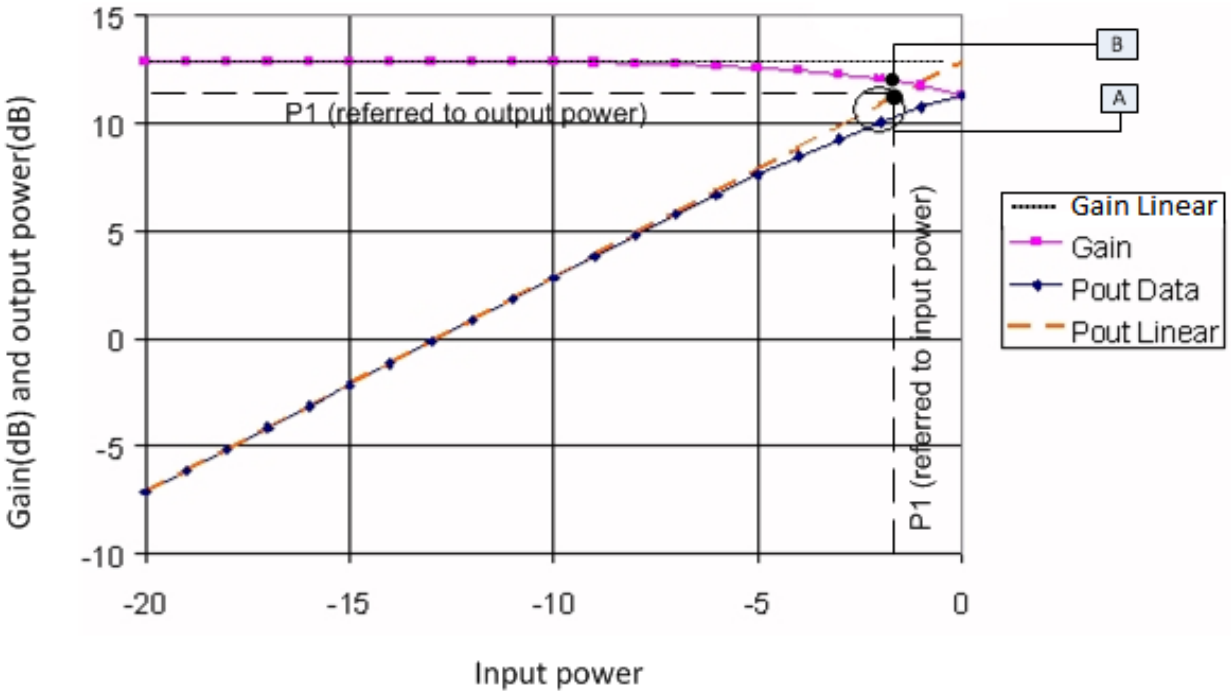

Figure 4.10 input and output characteristics of an amplifier

Figure 4.10 plots the input, output power data, and gain of an amplifier, with linear and nonlinear curves. The measured output power (P_{out} data) is plotted

against the ideal linear response (P_{out} linear), where these two lines diverged by 1 dB is noted as the P_{1dB} point (see point “A” in Figure 4.10). However, by comparing measured gain curve with the ideal linear gain response, we also can obtain P_{1dB} point (see point “B” in Figure 4.10). It is also known as a swept-power gain compression method, which not only can be used for amplifier but also our RoF system.

We use the same experimental setup, which is shown in Figure 4.4. Sweeping the RF input power from -30dBm to -5dBm, the VNA measures the system’s gain to obtain the P_{1dB} point.

- Result

To evaluate system's gain at different transmission points, we measure the RoF system's gain with fourteen different MZM bias voltages, from 1.1V to 8.1V. A table containing six $P_{1\ dB}$ points and corresponded bias voltages is shown in Figure 4.11.

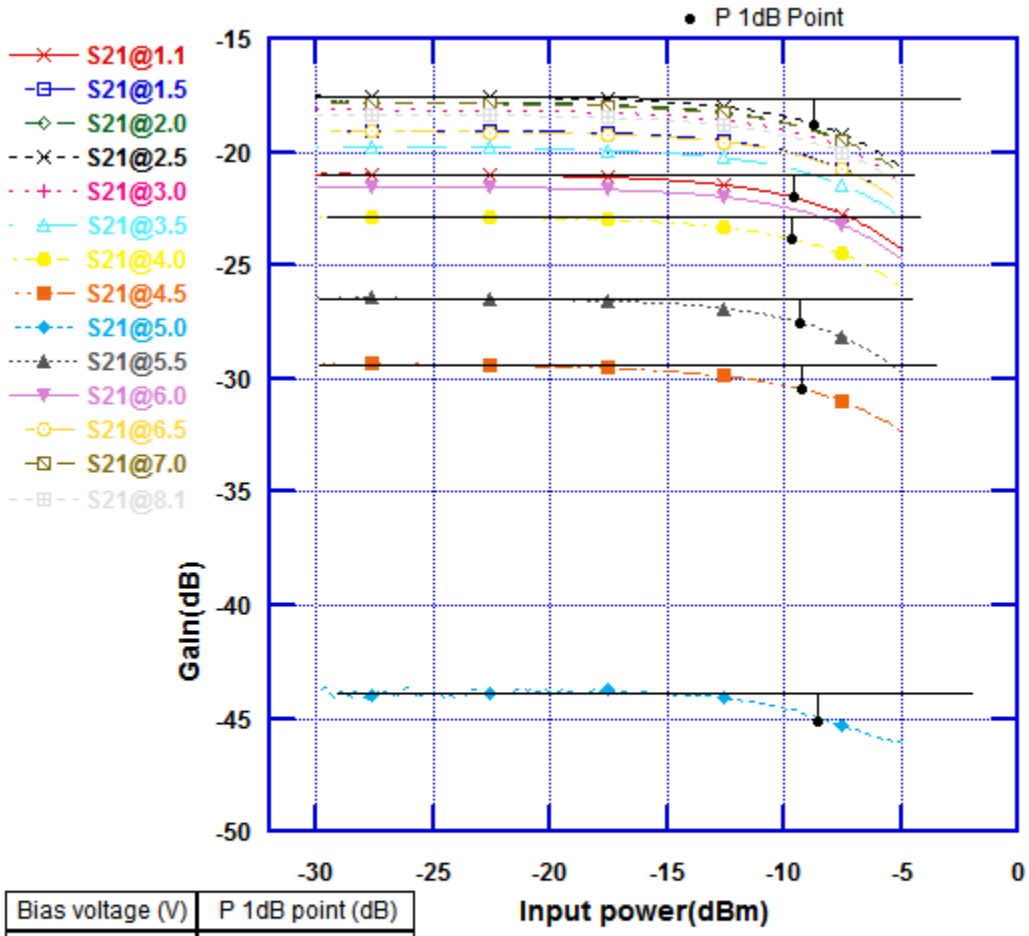

Bias voltage (V)	P 1dB point (dB)
1.1	-9.58
2.5	-8.73
4.0	-9.67
4.5	-9.24
5.0	-8.56
5.5	-9.32

Figure 4.11 P_{1dB} point at different bias points

For a transmitter, usually P_{1dB} is referred to output power. In our circumstance, the system gain changes with different bias voltages, therefore, the P_{1dB} is defined as input power. In Figure 4.11, we measured several P_{1dB} values, and the average value of RoF system's P_{1dB} is -9.18 dB, approximately.

- Stability of system's gain

As mentioned before, the system's gain is affected by the bias voltage. The bias drifting leads to an unstable gain curve. In Chapter 3, we only evaluate the bias controller by measuring the output power of the MZM; however, we can also investigate the bias controller by testing the system's gain as a function of time. We set the RoF system at fixed bias voltage and measure the system's gain several times, in Figure 4.12.

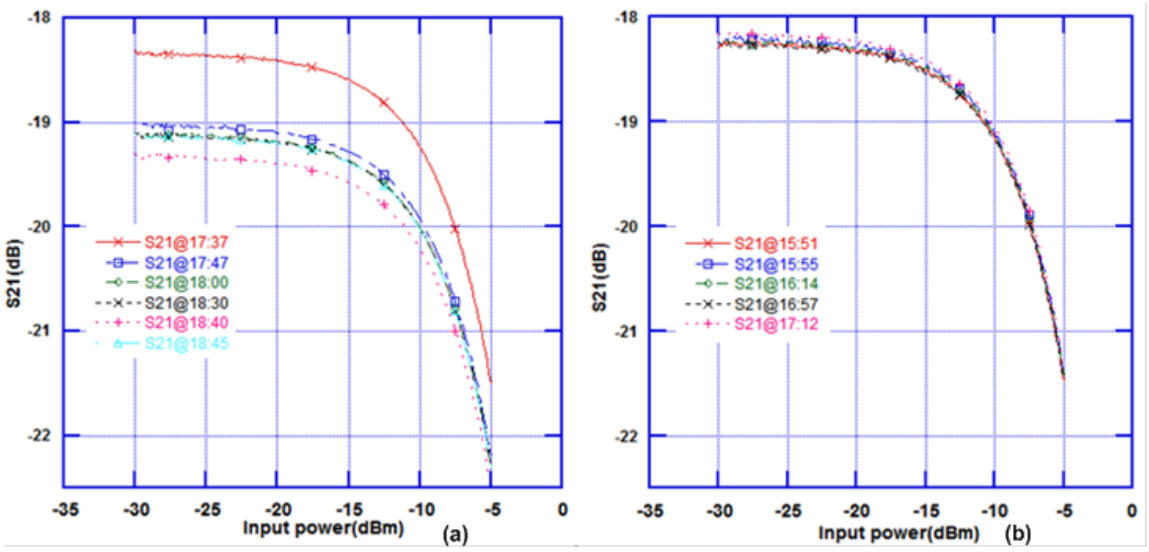

Figure 4.12 System gain (a) without bias controller and (b) with bias controller

Figure 4.13 compares the system gain with and without bias controller. In Figure 4.13(a), we start to measure the S21 at 17:37(time), after 10 minutes the S21 curve drops down about 0.7dB. At 18:40, it almost decline around 1dB. However, in Figure 4.13(b), the gain curve is stable with a shifting no more than 0.2 dB, in one hour. The bias controller has a good ability to maintain a steady system gain curve.

4.6 Noise figure

We measure the RoF system's noise figure (NF) which is a parameter of the degradation in signal to noise ratio between input and output. A low NF means a little noise is added by the system. Figure 4.13 shows the experimental setup.

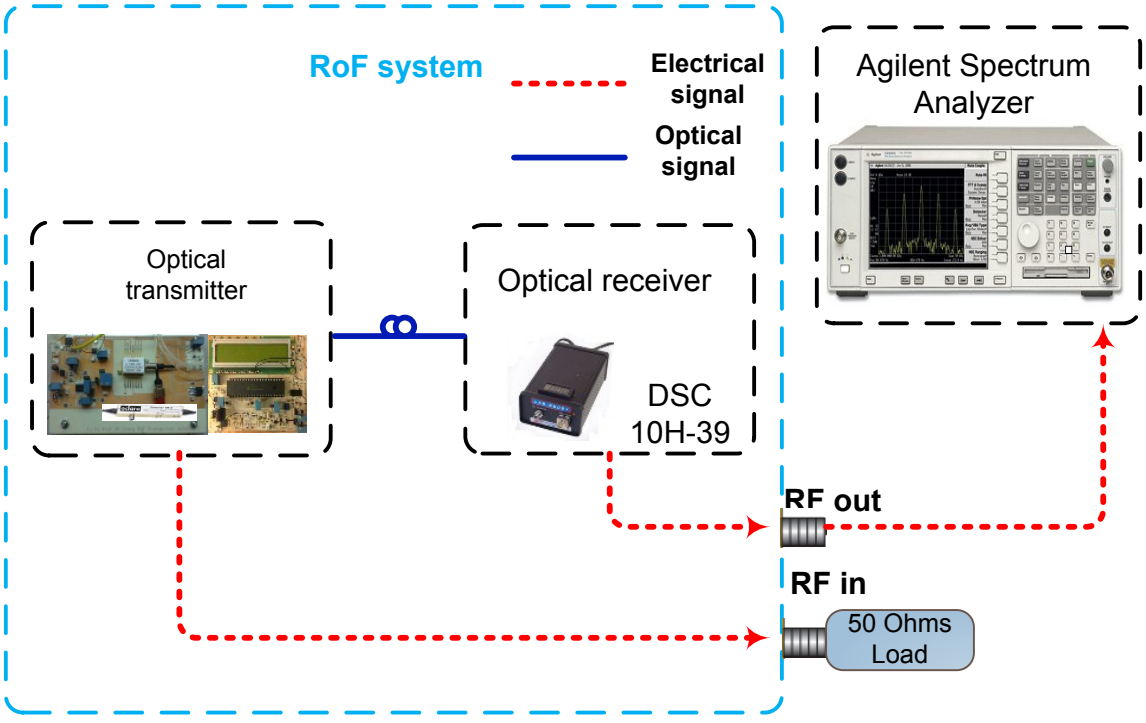

Figure 4.13 Noise figure experimental configuration

A 50 Ohms load is mounted on the RF input port, the spectrum analyzer (SA) measures the power spectral density of the thermal noise. The measured noise floor is around -141.54dBm/Hz.

The input noise power can be calculated by $P = K_b T \Delta f$ =- 174.288dBm where, where Δf is the resolution bandwidth, *T* is room temperature, and K_b is Boltzmann's constant. The RoF system gain is -18 dB. The Noise figure can be calculated by

$$NF = \frac{S_i}{S_o}\frac{N_o}{N_i} = G\frac{N_o}{N_i} = -18 + (-141.54 + 174.288) = 14.748dB \tag{4.2}$$

where S_i and N_i represent the signal and noise levels available at the input to the RoF system, S_o and N_o represent the signal and noise levels available at the output.

4.7 Spurious free dynamic range (SFDR)

SFDR can be understood as a range from the smallest signal power level that can be detected in a system (a signal just above the noise level), to the largest signal power level that can be introduced into a system without creating detectable distortions. In Figure 4.15, when the power of the third-order intermodulation single is equal to the noise floor (see point “a”), the corresponding fundamental output signal power (see point “b”) divided by the noise level is the value of SFDR.

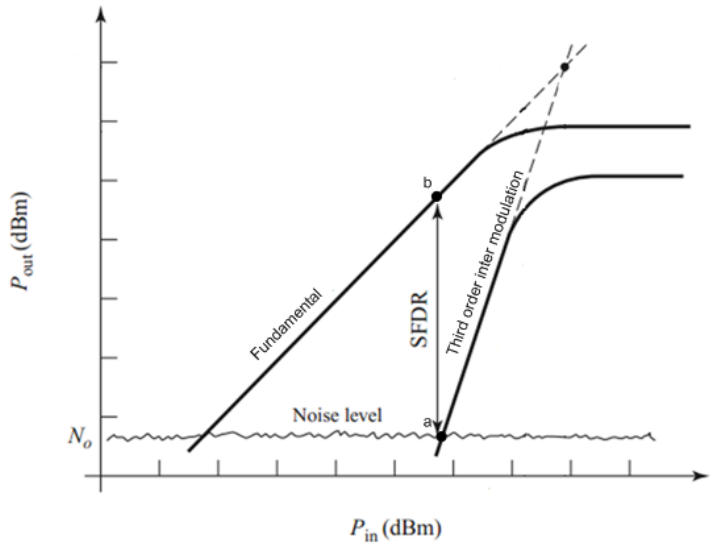

Figure 4.14 Illustration of SFDR range

- Setup

Figure 4.15 presents an experimental setup to analyze the SFDR. Two signal generators produce two equal amplitude signals but differ in frequency by 4.0 MHz from each other (f_1:4.960GHz and f_2:4.964GHz). A microwave hybrid combines two tones and feeds them to the RoF system. Two tones and intermodulation signals are sent into the SA where power level of two tones and intermodulation signals can be observed.

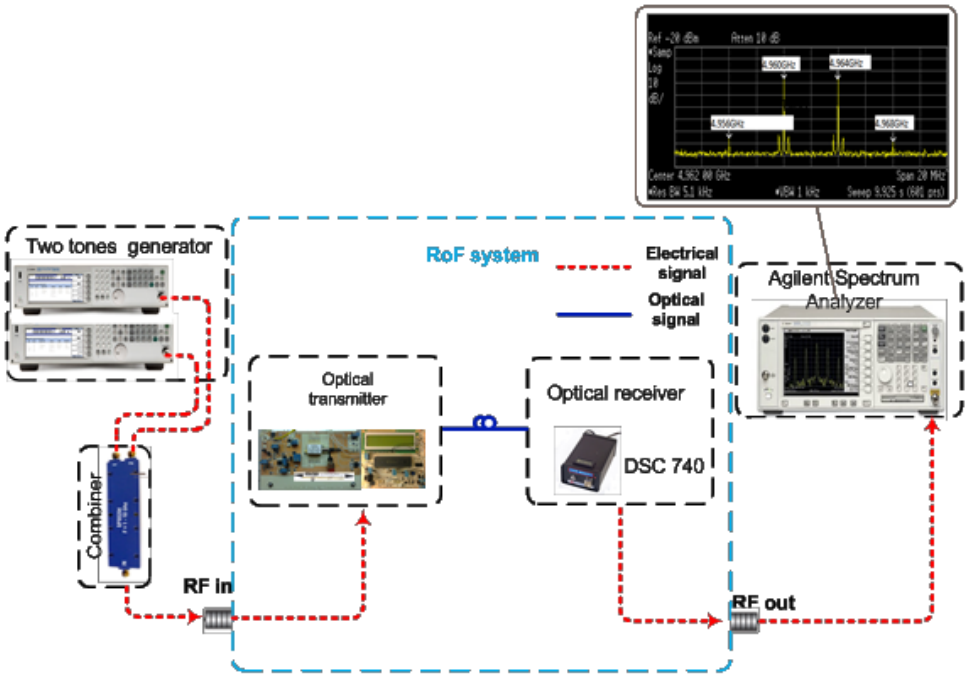

Figure 4.15 SFDR measurement configuration

Since the RoF system is not linear, the intermodulation distortion occurs when two tones (f_1:4.960GHz and f_2:4.964GHz) are injected into the system. The intermodulation output signals occur at ($2f_1$-f_2: 4.956GHz), and at ($2f_2$-f_1: 4.968GHz), which is close to f_1 and f_2 (see in Figure 4.16). Third order intermodulation signals will increase 3 dB for every increased 1 dB the input signals.

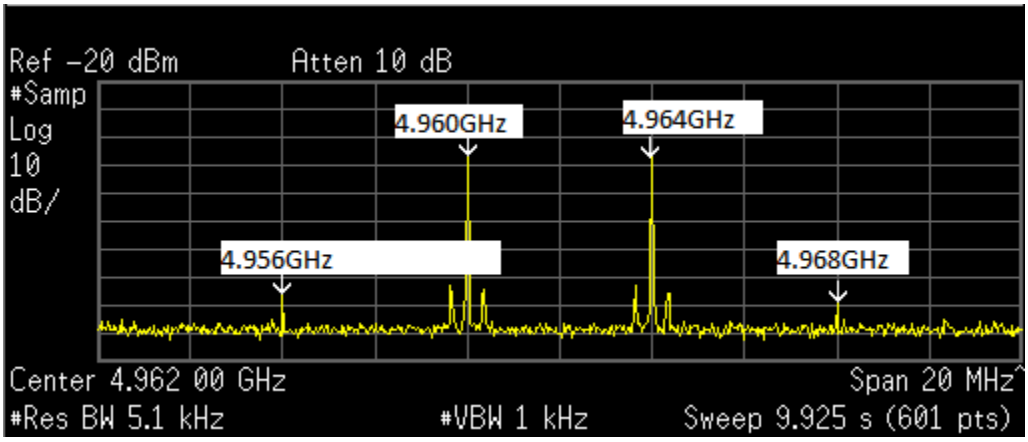

Figure 4.16 Output frequency spectrum for two tones and 3rd intermediations

- Result

We measure two input signals power level (f_1 and f_2) and four output signals power level (f_1, f_2, $2f_1$-f_2, and $2f_2$-f_1) then plot them in Figure 4.17. The above

signals are recorded for two times: with bias controller (Marked as “with_B_”) and without bias controller (marked as “without_B_”).

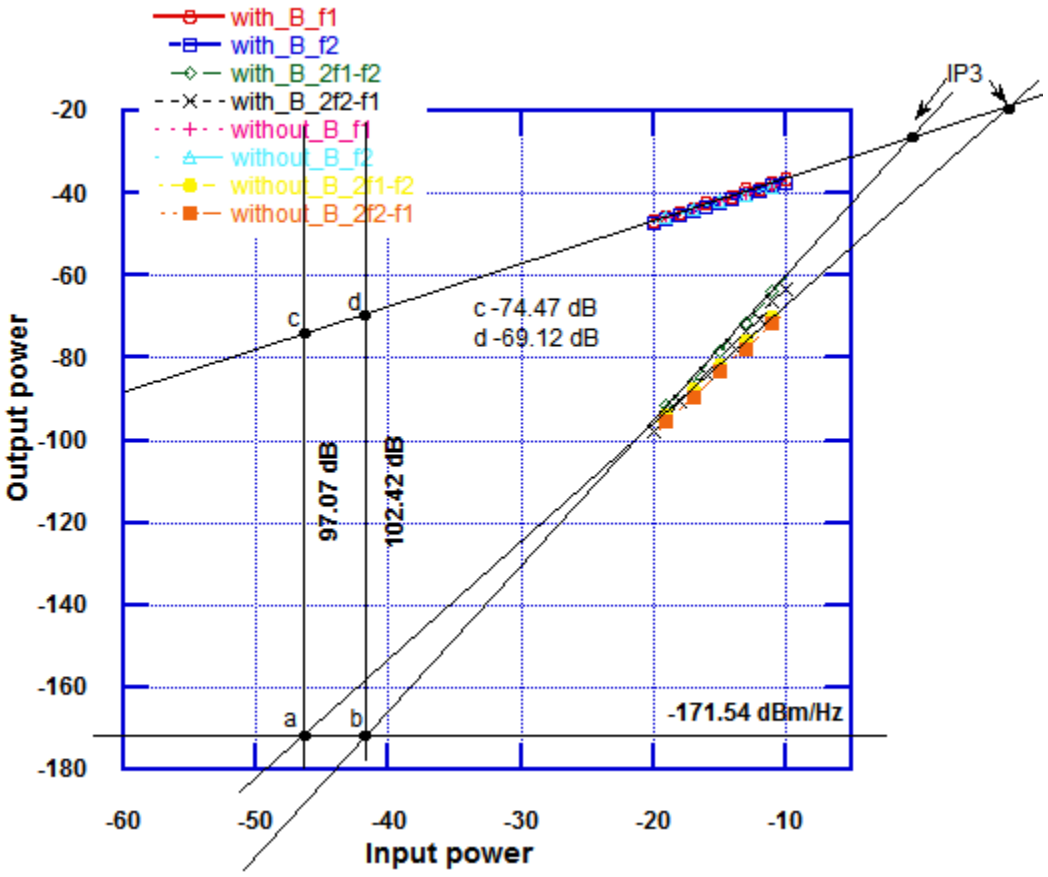

Figure 4.17 SDFR of optical link with and without bias controller

Figure 4.17 illustrates two tones and the third order intermodulation signals’ output power vs. input power. If we linearly extend portions of these plots (see in Figure 4.17), they would eventually intersect at the Third Order Intercept point (IP3). If we draw a noise floor of the system (-171.54dBm/Hz in this system), and linearly extend above plots, which will give us two intersect points (“a” and “b”, see in Figure 4.17). According to the definition, the SFDR is the power of point “c” or “d” divided by noise floor. Since the power is measured in dB, we can subtract

noise floor from output power “c” or “d” to calculate SFDR value. Learning from Figure 4.17, the RoF system has a SFDR of 104.2 dB with a bias controller, and a SFDR of 97.07 dB without bias controller. The bias controller can suppress the nonlinearity and provide a larger SFDR by maintaining the MZM at the quadrature bias point.

4.8 UWB OFDM transmission in RoF link

An application of transmitting UWB OFDM signal over RoF system is carried out. The EVM measurements are used to evaluate the system's performance, which can identify sources of signal degradation, such as carrier leakage, phase noise , I-Q imbalance and non-linearity. The OFDM is a popular modulation solution for short distances and high data rate applications. The UWB OFDM signal consists of 128 subcarriers which can be data carriers, pilot carriers, guard carriers, or null carriers. Each carrier has a 4.125 MHz bandwidth, and the total six groups occupy 528 MHz bandwidth. Figure 4.18 and Figure 4.19 illustrate UWB band groups and band #1 structure, respectively.

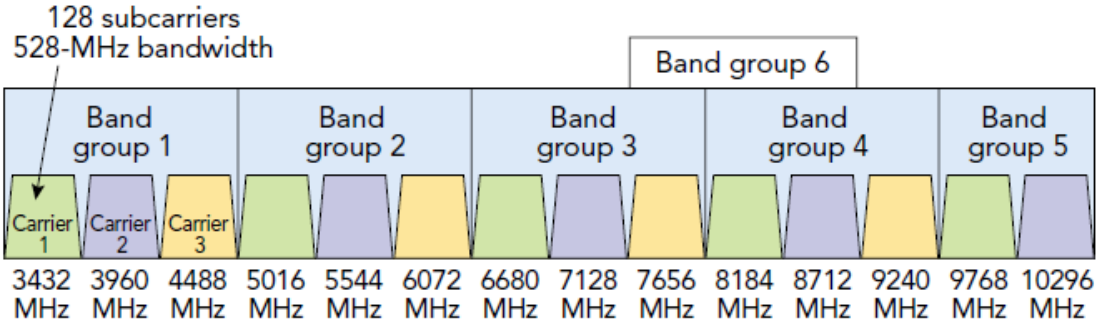

Figure 4.18 The spectrum allocation for UWB six band groups and extends from 3.1 to 10.6 GHz [27]

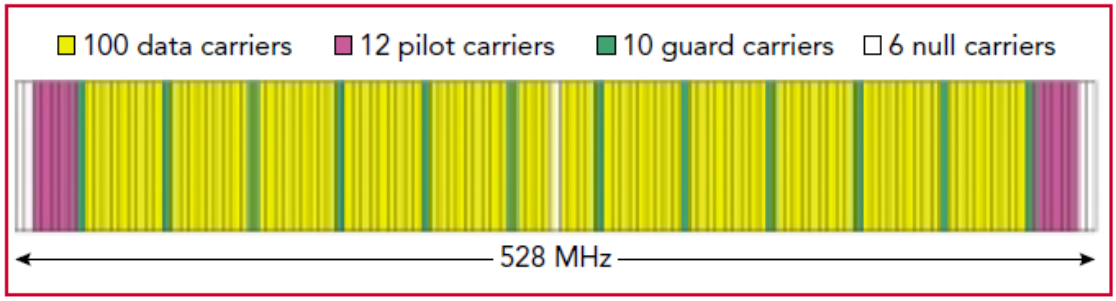

Figure 4.19 The 128 subcarriers of a UWB OFDM signal [27]

- Setup

The experimental configuration is shown in Figure 4.20. The AWG 7122B with RFXpress generates group 1 carrier 2 UWB OFDM signal which has a center frequency of 3.96GHz and bandwidth of 528MHz. The spectrum analyzer (Advantest u3772) measures the channel power of UWB signals. The input channel power is -13dBm with a data rate of 480Mbps and a package size of 1024. Combining a low noise power amplifier (LNA) with an attenuator, we can tune the input power from -13dBm to 8dBm. At the receiver, a LNA is also implemented to improve the system's gain. The Agilent Infiniium DSO81204B oscilloscope tests the EVM performance of received OFDM UWB signals.

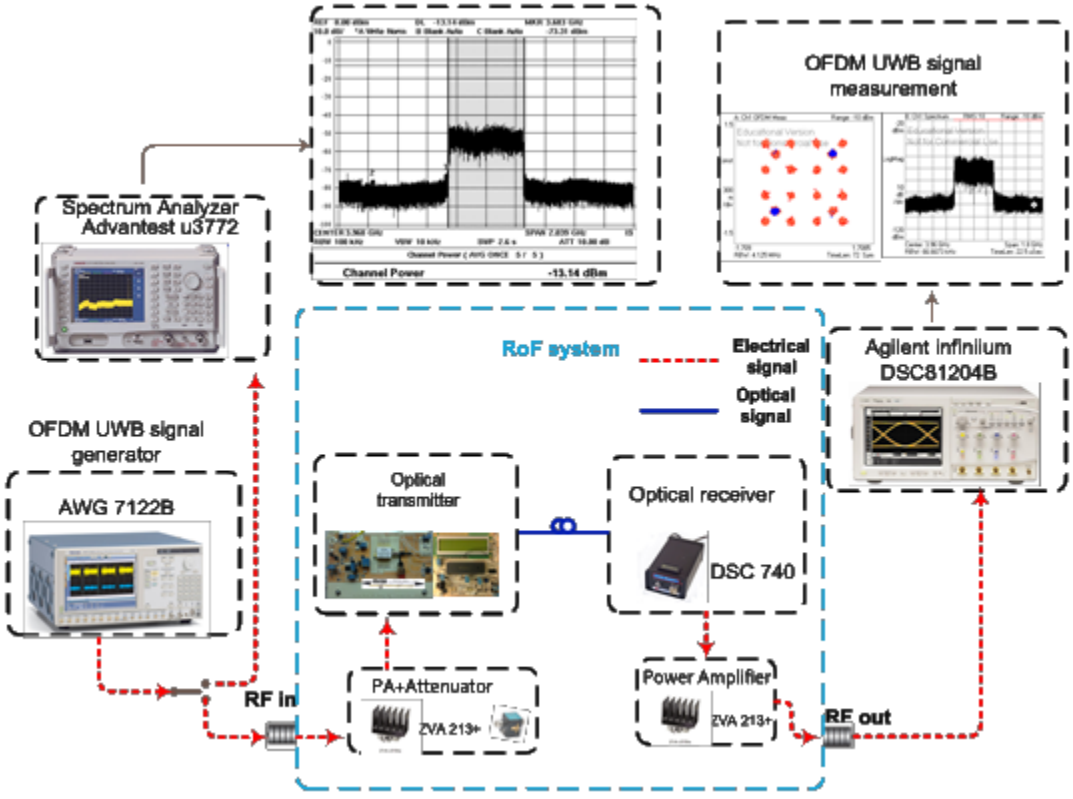

Figure 4.20 OFDM UWB experimental configuration

- Result

The oscilloscope contains vector signal analyzer software (VSA)-89600 which provides flexible tools for demodulating and analyzing UWB OFDM signals. Figure 4.21 shows a screen shot of measured result, including constellate diagram, spectrum of channel signals, and channel's composite error summary.

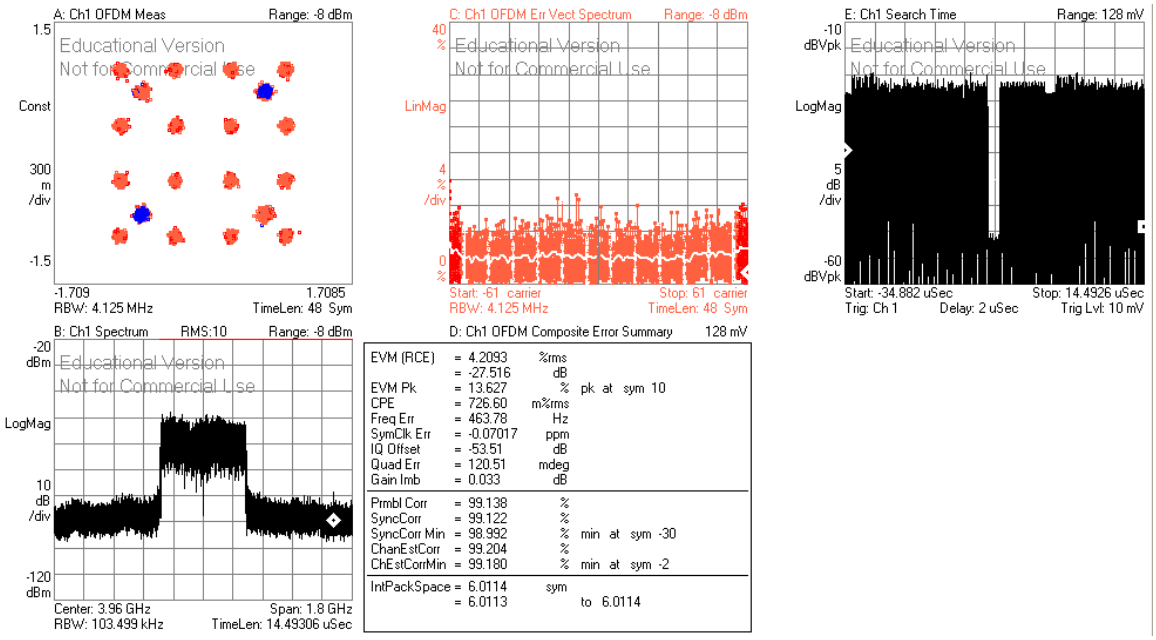

Figure 4.21 Measurement result by VSA

Figure 4.21provides lot of system information. In this experiment, we mainly use EVM value to investigate system's performance. Figure 4.22 is the measurement result. Tuning the input channel power from -13dB to 8dB, we measure the EVM as a function of input power.

In Figure 4.22, when input power is low, the EVM reduces with an increasing

input power until it reaches to the optimum point “a” (see in Figure 4.22) that corresponds to the lowest EVM of -27dB. If we continue to increase the input power, the EVM will start to increase, because the OFDM signal starts being affected by the system’s nonlinearity.

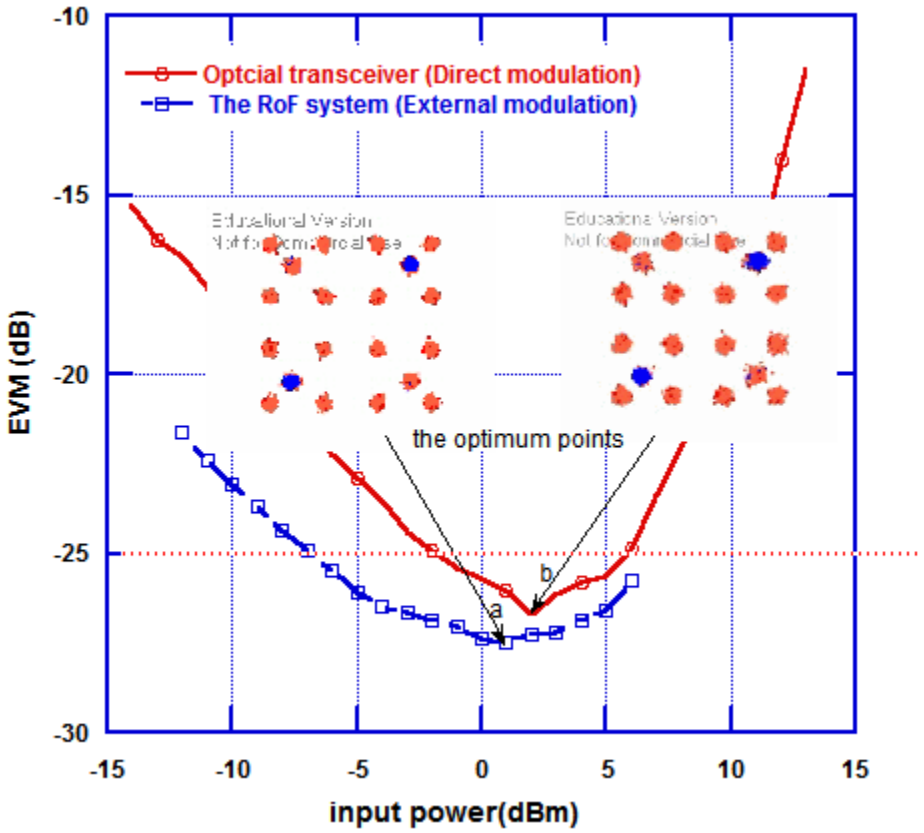

Figure 4.22 EVM performances between direct and external modulations

We also compare EVM of our RoF system with an optical transceiver that mainly uses direct modulation technology. In Figure 4.22, the RoF system has a good linearity of the input power from -7 dBm to 7 dBm (referred to EVM of -25 dB). Our RoF system (blue diamond line) has a larger linear range and lower optimum

point than the optical transceiver (red circle line). The external modulation is a more advanced technique than direct modulation.

- Stability of EVM

Similar to Section 5, we also investigate the performance of bias controller by observing the EVM with or without the bias controller, respectively. Figure 4.23 shows the measured EVM in 200 minutes.

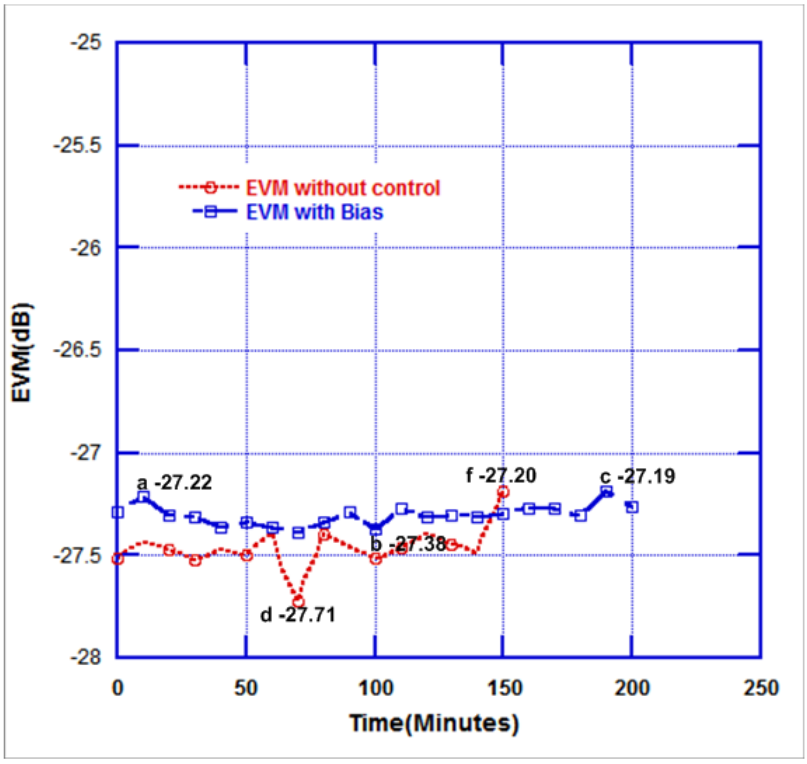

Figure 4.23 EVM with and without bias control

In Figure 4.23, the system with bias controller (blue square line) has a smoother EVM curve, except the point a, b, and c which has a fluctuation of 0.2 dB. However, the system EVM performance without bias controller is out of our

expectation, which has a fluctuation no more than 0.5dB. Here, we may be able to conclude that the EVM performance is not sensitive to the bias voltage drift.

4.9 Impairment of transmission distance for OFDM UWB RoF System

- Setup

Based on the experiment in Section 4.8, we attempt to increase the transmission distance to investigate the impairment of transmission distance for an OFDM UWB RoF system, regarding the EVM performance. Figure 4.24 illustrates the experimental configuration which uses almost the same setup in Section 4.8, but only changes the transmission distances.

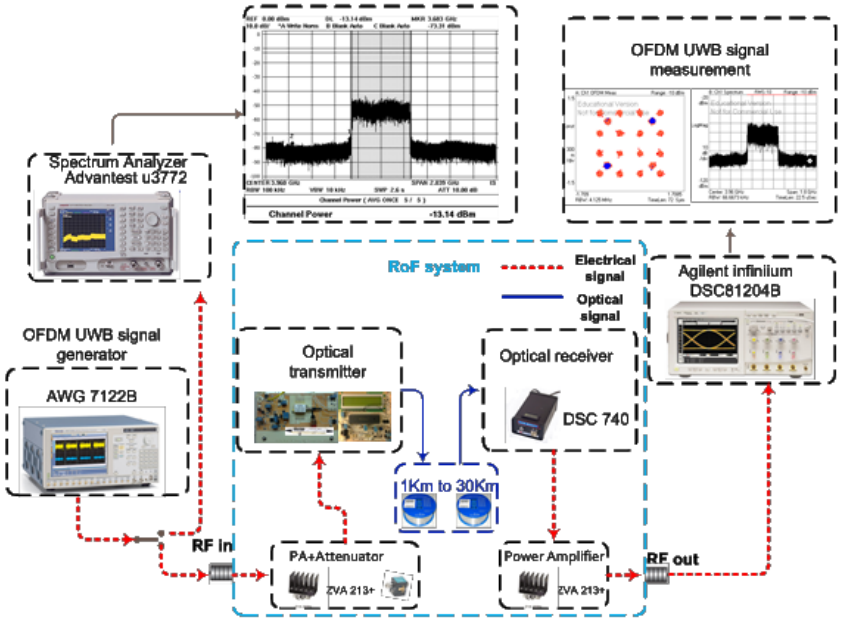

Figure 4.24 Experimental setup of OFDM RoF system with different spools of fiber

- Result

Figure 4.25 shows the measured EVM at different transmission distances from 1km to 30km, and the optimum EVM points are marked with a black dot.

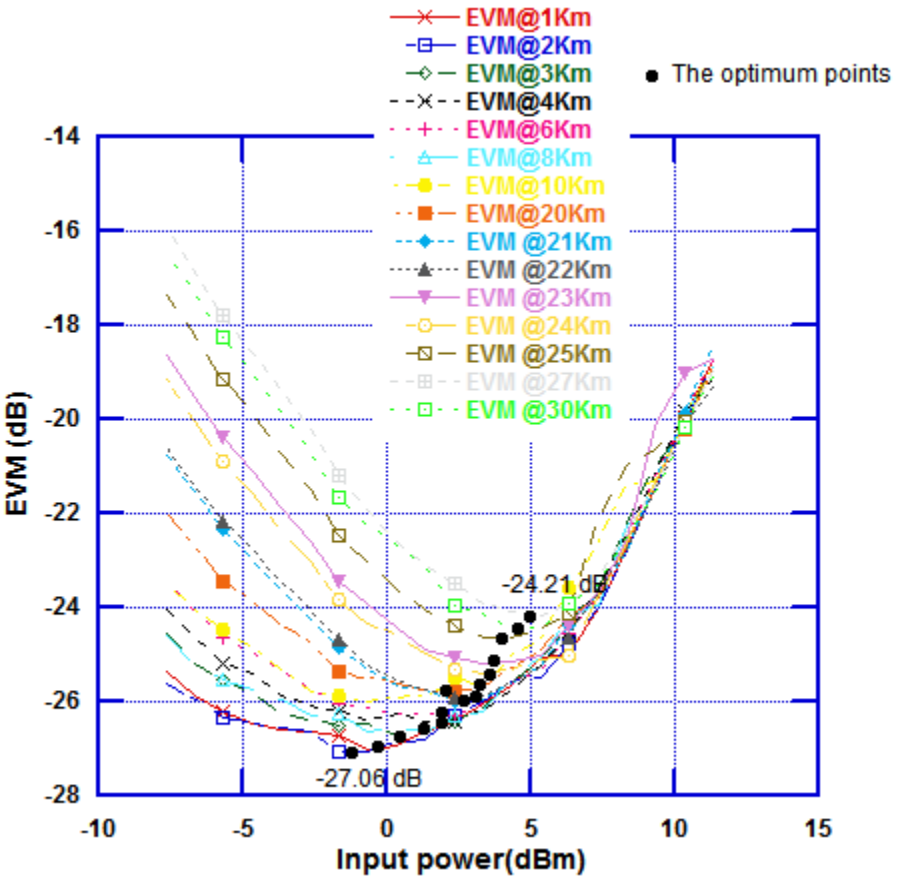

Figure 4.25 EVM measured at difference distances

In this experiment, we combine one 1, 2, 4, 8, and 20Km fiber spool to make a transmission distance that ranges from 1Km to 30Km. Adding extra adaptors and patch cables will introduce loss, for example a 3Km fiber may has a higher

loss than 4 Km fiber, and that is the reason why the transmission distance of 27Km brings a lower optimum point than a 30Km transmission distance(see in Figure 4.24).

The EVM optimum point increases from -27.06 dB to –24.21 dB, when we extend the transmission distances. From Figure 4.25, we also find that when the input RF power is low, the loss introduced by different distance limits the EVM performance. However, for a high input power, the intermodulation effect dominates the system, and signal to noise ratio (SNR) remains the same value, which lead to the same EVM.

4.10 Summary

In this chapter, we compared two different modulation techniques for optical transmitter and introduced the structure of our optical transmitter. Then, several experiments were carried out to evaluate the RoF system's performance. In Section 8, we compared EVM performance of two different modulation systems. In Section 9, we investigated the impairment of transmission distance for OFDM UWB RoF system.

Chapter 5 Conclusion

5.1 Summary

This Master thesis has provided a study of electro-optical modulator integrated optical transmitter design for RoF millimeter wave system, by using PCB circuit design and microcontroller technique. In this work, functions of fabricated board have been explicated and verified. Many issues about the optical transmitter are presented.

Firstly, the thermal effect and power control have been shown as the main problem for the DFB laser. It is pivotal for a DFB to produce a steady output power in optical transmitter design. Experiments show that our laser control circuit can maintain the DFB laser output power at 20mW with a temperature fluctuation less than 0.2°C. The designed laser source features as low cost, stable, and short warm up time (less than 20 minutes).

Secondly, bias drift effects on the MZM has been reduced by using the demonstrated algorithm. By revising the code, the bias controller can operate the bias voltage more precisely. It has been proved that the microcontroller is a more advanced technique for bias controlling which processes low cost, flexible, and

multifunction. We have demonstrated that the bias controller steadily maintains the MZM's output power with a fluctuation no more than 0.1dB.

Thirdly, employing the designed optical transmitter and a commercial optical receiver, we have carried out several experiments to evaluate the RoF system that can provide a 3dB bandwidth of 30.4GHz. We have shown the feasibility of a 40Gbps data link over the RoF system, which has a good Q factor of 9.16. From the experimental results, the bias controller has a good performance to maintain system's gain and improve the SFDR around 5.35 dB. In a nutshell, the designed optical transmitter is viable for millimeter wave band applications with a low cost no more than 500$ (cost of the MZM are not included).

Furthermore, we have compared two modulation schemes for the OFDM UWB signal transmitted over the RoF system. From the results, we conclude that the external modulation system has a larger linear range and better EVM performance than direct modulation system. It is also found that EVM performance is not sensitive to the bias voltage drift.

At the end, we have investigated impact of fiber length on the EVM performance for OFDM UWB RoF system. Expanding the optical length from 1 to 30 km, the optimum EVM point grows exponentially 2.5dB (referred to input power). We conclude that the main reason of signal degradation in this system is MZM's nonlinearities and chromatic delay introduced by optical fiber.

5.2 Future lines

We recommend that further research be undertaken in the following areas:

- smaller size, component relocation

Firstly, the microchip 16F877A and display module take up lots of space on the PCB board. To reduce the board size, future design could choose these components with a compacted package, such as surface mount chips. Moreover, the board is designed with two layers and plenty of components can be placed at the backside. Secondly, the power dissipation was not concerned when the parts were placed. During the measurement, the temperature of the PCB board, close to voltage regulators, is considerably high. Therefore, the location of some components, such as the power regulators may not appropriate. We suggest to replace voltage regulators with single in-line packages (SIP).

- More functions for lasers and more accurate bias voltage for MZMs

Press keys, a screen, and a temperature sensor can be added to set and display the DFB laser's parameters (drive current, optical output power, and laser's temperature). Moreover, this board can offer sophisticated functions, for instance laser diode overload protection, high temperature warning, and shutdown precaution process. In addition, changing components, such as a more advanced

microcontroller, 12 bit ADC/DAC and more accurate reference voltage regulators, the bias controller can provide a more precise operation with an accuracy of 1mV.

- Application: low noise tunable optical source

Adding an ultra-narrow Fiber Bragg Grating (FBG) and a circulator to the DFB laser, a noise suppression laser source can be achieved. A low pilot tone is being sent to the laser, then goes into circulator and FBG that will reflects this signal back to the microcontroller. Comparing the reflected signal with the original pilot tone, the microcontroller uses PMW function (integrated in microcontroller) to control a TEC plate (attached under the FBG), which can shift the FBG's transmission peak, thermally. The above processes can be understood as a wavelength locker. If the DFB laser's carrier frequency shifts, the microcontroller and the TEC will act as a tunable filter to correspondingly alternate FBG's center wavelength. Therefore, the fluctuations that fall out of the peak frequency are rejected [28].

BIBLIOGRAPHY

[1] Cisco, "Cisco Visual Networking Index: Forecast and Methodology, 2008–2013," Cisco, 2009.

[2] C. H.Lee, "Microwave Photonics", CRC Press, 2007.

[3] B.Razavi, "Gadgets gab at 60GHz," *Spectrum, IEEE,* vol. 45, no. 2, pp. 46-58, 2008.

[4] Smulders, "Characterisation of propagation in 60 GHz radio channels," *Electronics & Communication Engineering Journal,* vol. 9, no. 2, pp. 73-80, 1997.

[5] X. Z. a. J. Y. Zhenbo Xu, "Frequency upconversion of multiple RF signals using optical carrier suppression for radio over fiber downlinks," *Optics Express,* vol. 15, no. 10, pp. 16737-16747, 2007.

[6] K. K. Masataka Nakazawa, in *High Spectral Density Optical Communication Technologies*, Springer, 2010, p. 337.

[7] S. K. Hamed AI-Raweshidy, Radio over Fiber Technologies, Norwood: ARTECH HOUSE.INC, 2002.

[8] A. Ng'oma, "Radio-over-Fibre Technology for Boradband Wireless Communication Systems," 2005.

[9] K. D.Wake, "A Novel Swithched Fiber Distributeed Antenna System," in *European Confernce on Optical Communications*, 2004.

[10] C. DeCusatis, Handbook of Fiber Optic Data Communication, New York:

2007.

[11] L. D.K.Mynbaev, Fiber Optic Communications Technology, New Jersey: Prentice Hall, 2001.

[12] EMcore, "Dense Wavelength-division Multiplexing," EMcore, 20 11 2012. [Online]. Available: http://www.fiber-optics.info/fiber_optic_glossary/dense_wavelength-division_multiplexing_dwdm.

[13] D. McGray, "wired," wired.com, 2003. [Online]. Available: http://www.wired.com/wired/archive/11.09/navy.html.

[14] K. G. Stavros A.Kotsopoulos, "Handbook of Research on Heterogeneous Next Generation Networking," Idea Group Inc, 2008, p. 584.

[15] K. T. Ajoy Ghatak, "An Introduction to fiber otpics," New York, Cambridge University Press, 1998, p. 233.

[16] P. Weinberger, "John Kerr and his Effects Found in 1877 and 1878," *Philosophical Magazine Letters ,* 2008.

[17] E. Säckinger, "Broadband Circuits For Optical Fiber Communication," in *Optical fiber*, JOHN WILEY & SONS INC, 2005, p. 11.

[18] G. Agrawal, in *Fiber-Optic Communication Systems*, NY, John Weily & Sons, Inc, 2002, p. 101.

[19] i. Haus, "15V CW LASER DIODE DRIVER iC WKN datasheet," [Online]. Available: http://www.ichaus.de/upload/pdf/Wkn_b1es.pdf.

[20] H. Microsystems, "HY5650 TEC Controller Operating Manual," hytek

microsystems, [Online]. Available: esl.eng.ohio-state.edu/~rstheory/iip/hy5650_manual.pdf.

[21] M. I. DELEVOR, "Programmable Resolution 1-Wire Digital Thermometer," maxim integrated, 2008. [Online]. Available: http://www.maximintegrated.com/datasheet/index.mvp/id/2812.

[22] H. Al-Rweshidy, Radio over Fiber Technologies for mobile Communications Networks, Artech House, 2002.

[23] R. Hui, Fiber optic measurement techniques, Academic Press, 2009.

[24] oclaro, "20/40G Intensity modulators for analog applications," Oclaro, Inc. , [Online]. Available: http://dev.oclaro.com/product_pages/Powerlog_AM-40.php.

[25] J. ŠVARNÝ, "Limited Applicability of the Constant Optical Power Controller to the Integrated Intensity Electro-Optic Modulator," in *10th WSEAS International Conference on ELECTRONICS, HARDWARE, WIRELESS and OPTICAL COMMUNICATIONS*, 2011.

[26] J. Yao, "A Tutorial on Microwave Photonics," *IEEE Photomics Society Newsletter,* 2012.

[27] Wikipedia, "UWB," [Online]. Available: http://en.wikipedia.org/wiki/Ultra-wideband.

[28] Y. P. C. L. M.-J. P. Jean-Francois Chiche, "Ultra-Narrow Bragg Grating for Active Semiconductor Laser Linewidth Reduction through Electrical Feedback," in *Fibre Grating Sensors*, Quebec City, 2007.

[29] K. Brunham, Writer, *Introduction to orcad.* [Performance]. Embedded soulutions, 2002.

[30] M. T. Inc., "Quick Guide to Microchip Development Tools,"2008.

[31] M. T. Inc, "28/40/44-Pin Enhanced Flash Microcontrollers," 2003.

APPENDIX

A: PCB design flow- OrCAD and PCB editor

- OrCAD

In this section, we briefly introduce the design flow of schematic design by using Or-CAD and Figure A.1 illustrates its graphic user interface (GUI) operation windows.

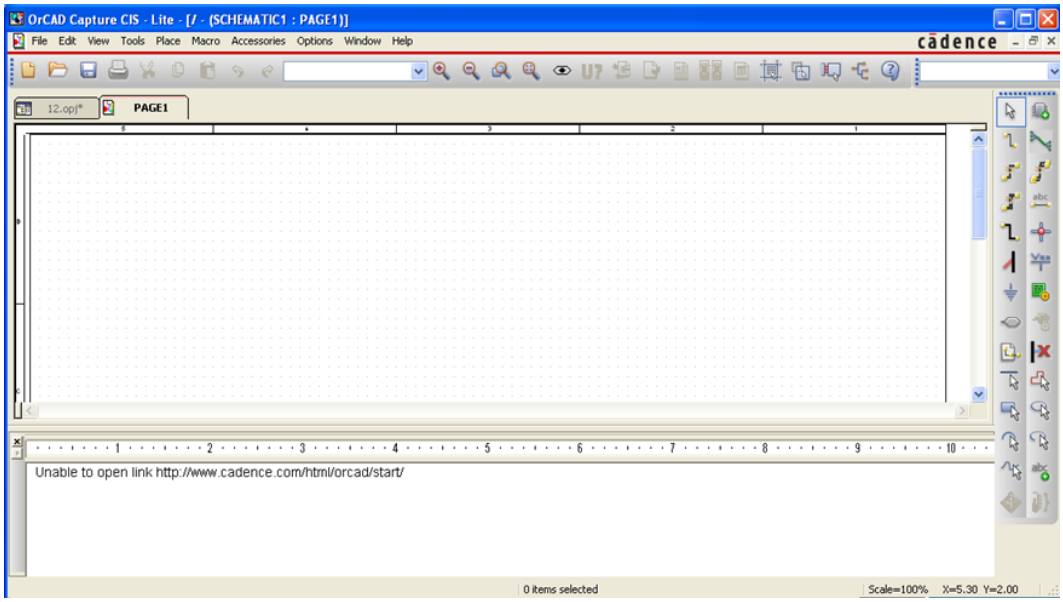

Figure A.1 Windows capture

For the schematic design, we can follow the flow in Figure A.2.

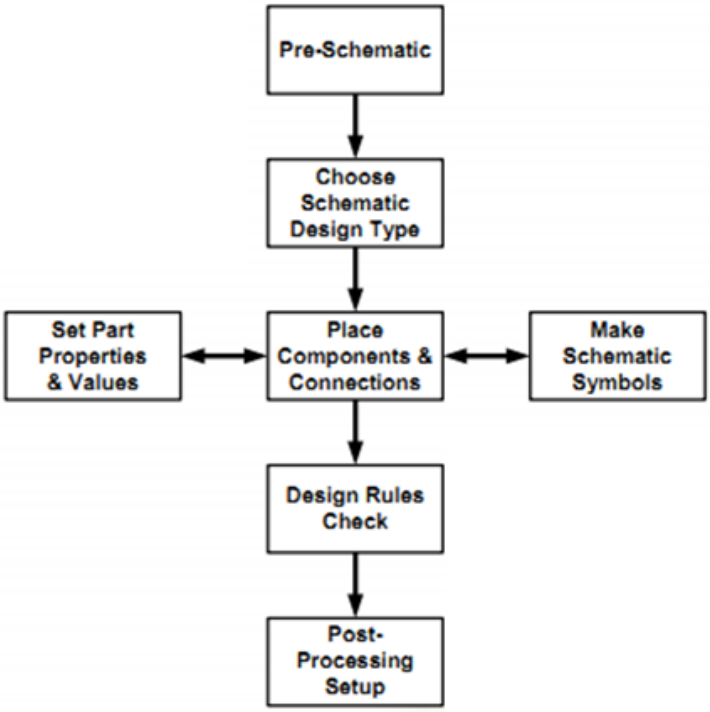

Figure A.2 Capture design flow [29]

At first, we need to select the components (ic, capacitors, resistors, etc.) from the library. For each component, a symbol must be created, which is a physical view of the component that contains all the pins of the component and properties. Each component used in schematic design must have an associated footprint used for PCB Layout. The capture provides most of the libraries. However, a few special symbols might need to be created, according to datasheet, as an additional symbol library for a new design. Cadence provides a software named PAD design that can let you draw special component footprint. Meanwhile, Footprint Maker could also yield the standard diameters of most common

components. For example, in this design, HY5620 TEC driver is a special model. We have to make a footprint according to its datasheet.

Second, procedure can be ended by placing to schematic board and then connecting all components by wires. All the properties of parts must be set, for example values, PCB part names, symbols etc. Components must be placed in the schematic and connected by wires. Beside, for some designs, extra symbols may also need to be placed, for instance texts, test points, power and ground symbols.

At the end, the design rules check (DRC) should be executed to ensure above processes that are meet all constraints which defined by users.
A DRC checking must be examined the schematic. If it is passed, a net list file will be generated, which can be used in the PCB editor layout.

- PCB editor

Figure A.3 displays a blank board file opened in the PCB Editor. There are six working areas in this design window. Various tools are placed in toolbars and many aspects of component characteristics can be controlled, like trace highlights, etching edits, DRC checks, etc. Any characteristics can be regulated

in these toolbars, including visible or hidden line and component locations. The command window presents information and allows users to type commands. The worldview window provides an overall view of the location and the size of the design windows corresponds to the actual PCB. The status bar shows the coordinates of the crosshairs. The P and A field indicate the coordinates. Here are several important procedures in PCB layout work.

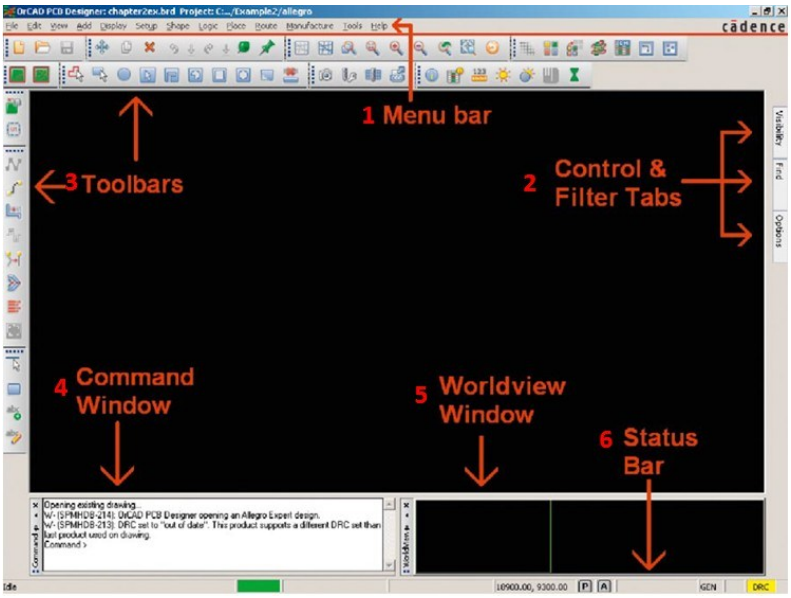

Figure A.3 PCB editor windows

Creating board: After importing the net list, a border outline needs to be created. It could be done by opening the PCB Editor then going to Setup and selecting Design Parameter in Figure Under the Display menu, the grids can be set up, which is an important parameter. At the Design tab, the size of the work place and the drawing extents can be set suitably. The whole units for this project are

mils and inches. Because, the PCB board is fabricated at the University of Montreal and it has to meet the specific requirements for the machine.

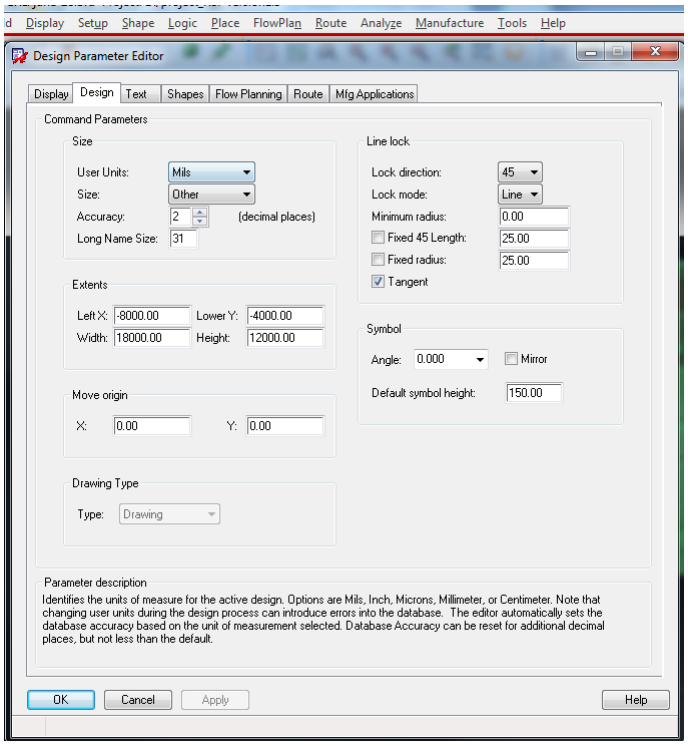

Figure A.4 PCB editor design parameter configuration

A board can be added by clicking the Add button then choosing Rectangle, in Figure A.4. In the Options, by selecting Board Geometry as the Class and Outline as the subclass, a board outline of dimensions 6000 Mils by 3400 Mils can be established. PCB Editor also provides a command window. Writing “x 0 0” means a point is set at location (0, 0); then writing again “x 34000 6000” sets the upper right coordinates of the rectangle. A Board outline can be created by these two commands.

For some applications, multilayer may be needed. Figure A.5 shows a window to set up multilayers. The window shows the default two layers PCB and inserted two more FR4 and two more copper layers(GND, VCC), which is a four layer PCB.

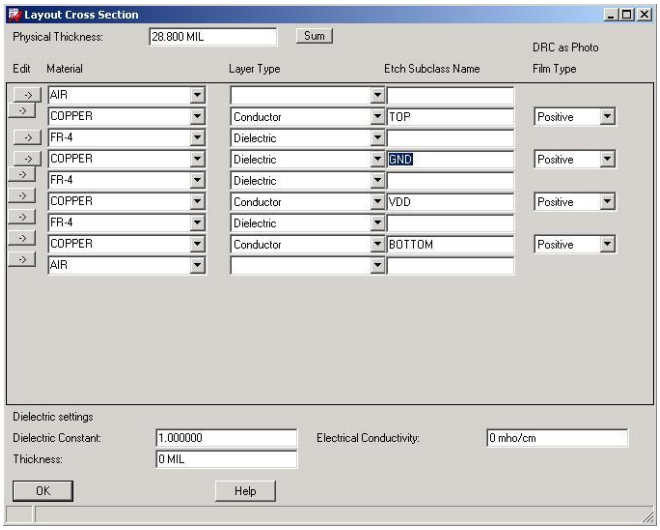

Figure A.5 Multilayer configuration

Setting up constraint conditions and VIAs: Before placing and routing circuit, a set of router specifications need be set down. Several important design rule constraints need be defined.

Defining Trace Width and Spacing Rules: Line width choice can be made based on several key factors. The first is the thickness of PCB board. Depending on the capability of PCB board parameters, a minimum line width is recommended on datasheet. The second factor is the current limitation. For a

certain value of current, a line width can be calculated out by equations [29]. The third factor is the frequency of signal, which decides the width of lines. In this project, all signals are low frequency, so the line impedance is not concerned. The line space is important when the signal is high voltage and big current. In this project, since a sufficient area can be used to route, it is not a key factor and it was set as 15mils. Rogers RO4000® high frequency circuit materials are selected as PCB board. The RO4350B has a dielectric constant of 3.48 and thickness of 30mils. In this design, the signal line width is 15mils. For high speed signals and highly integrated circuits, to limit the circuit size, the line width and space could be a crucial factor. What's more, these parameters also depend on the fabrication capability. All the PCB circuit is made by Polytechnique de Montreal, and the minimum line width is 6mils, the minimum line space is 10mils.

Assigning cutting marks, Alignment donut, and vias: Since Polytechnique de Montreal has its own requirements for all design. Four right angle etching line with a length of 200mils and width of 20mils are set at the corner of circuit. These four marks are cutting marks. In a word, the inside of four right angle area is the real size of circuit. During the manufacture, vias are also important. The holes, which connecting top layer and bottom layer have a relatively small size. In order to insure the accuracy, three alignment holes with a shape of donuts are mounted at the outside of layout. These donuts have a 66mils inner and 120mils outer diameter. The vias, in this design, are set as a 31mils hole with a 60 mils pad.

Placing components and routing: After finishing above procedures, parts can be placed. Choosing Place button at manual from the menu bar can place parts. The Placement dialog box is shown in Figure A. 6.

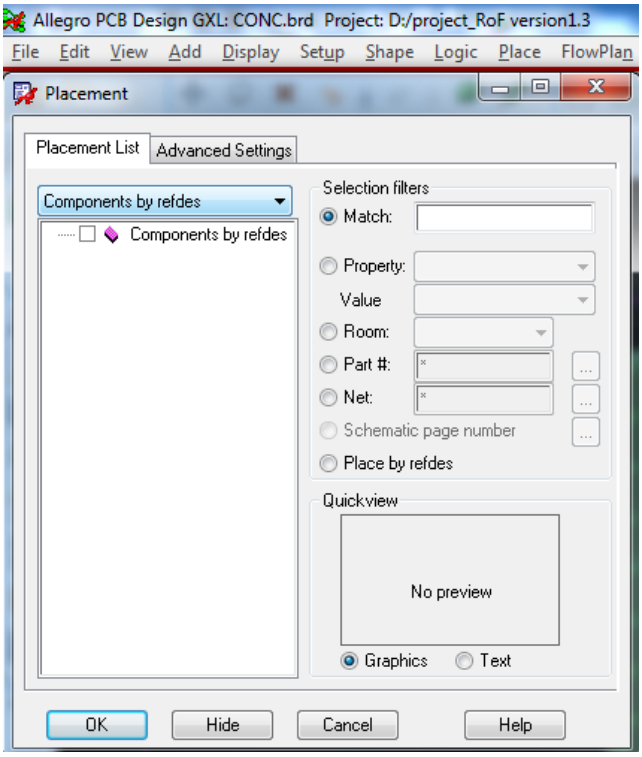

Figure A.6 Manually placing components

One of components can be selected in the sub tab-Component by refdes box. Once it was been selected, the part is automatically transferred to the design window. When the entire components are placed, the board is ready to route. Clicking one, trace will be highlighted. Selecting Add Connect button and clicking the trace will show as an etching line with real line width. In some conditions, a via is need to connect traces between two different lays.

DRC checking and generating gerber and drill files: At this stage, all the components, lines are placed and routed. A procedure named as design rule checker (DRC) should be executed. A message indicates whether there are errors. Then PCB Editor generates a design file used to fabricate the final board. The most common file applied in manufacturing system is Gerber file. The design file that is required by Polytechnique is Gerber RS-274X. Figure A.7 shows a dialog box which can configure the parameter of the gerber file. The Gerber file should have a precision of 2.4, which can be defined at Format option. The integer places are two and the decimal place is four.

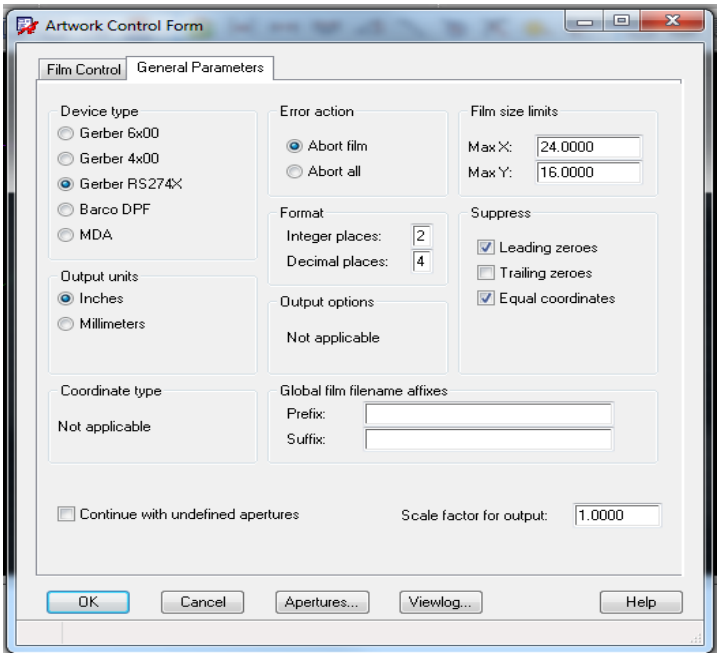

Figure A.7 Artwork control form1

Choose Yejunfu-S1B and Yejunfu-S1T layer, in Figure A.8. S1T indicates this is top layer, the other S1B is bottom layer. Undefined line with option is eight mils. This decides the size of extra texts. In Figure A.8, the bottom of the board has a line with the name of the circuits, the designer, the types and width of board. This line is made by etching line with a line width of eight mils.

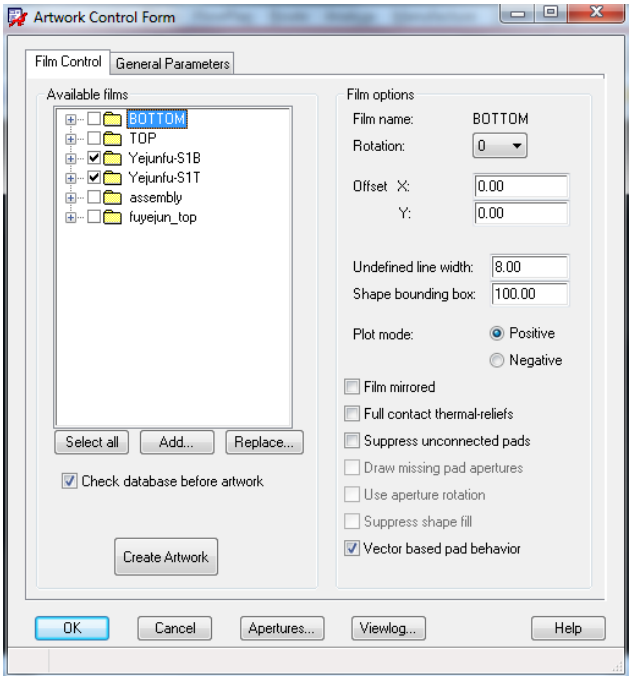

Figure A.8 Artwork control form2

By finishing above procedures, the final gerber file of top and bottom layout can be generated. A drill file in form of dxf contains all the via information, like alignment donuts, cutting marks and diameters of vias, is also need by Polytechnique de Montreal.

In brief, the PCB design follows five processes:

Start with schematic design with OrCAD

Generate netlists and transfer to PCB layout

Set up board size, constraint management, line and via size

Place components and route the board

Generate Gerber files and drill files

B: MPLAB Tool and PIC 16F877A

MPLAB is an integrated development software which can be used to program the microchip. Figure B.1 displays the working windows of MPLAB. It is a Microchips Integrated Development Environment and includes several components for application development, hardware simulation and debugging. It uses both Assembly and C programming languages with MPLAB.

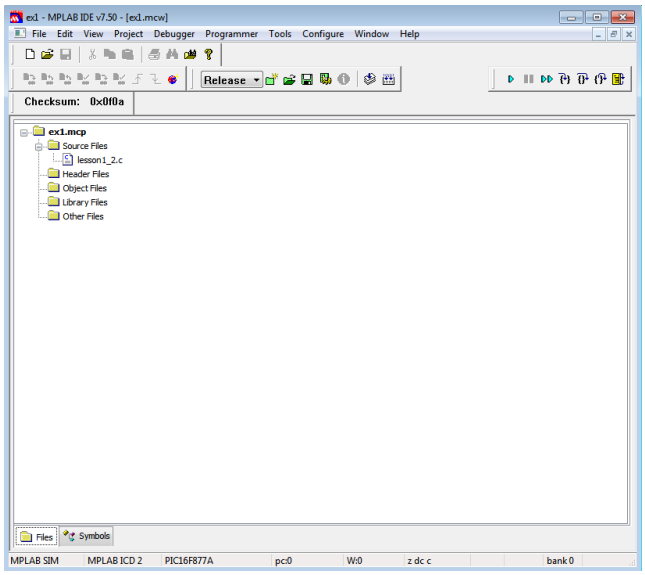

Figure B.1 Work windows of MPLAB

Figure B.2 shows the programmer MPLAB® ICD 2 used in this project. It is an all-in-one programmer, a low cost, real-time debugger and programmer for PIC® MCUs. “Using Microchip Technology's proprietary In-Circuit Debug functions, programs can be downloaded, executed in real time and examined in detail with the debugging functions of MPLAB. Setting watch variables and breakpoints from symbolic labels in C or assembly source code, the program can single steps through C source lines or into assembly code. MPLAB ICD 2 can also be used as a development programmer for supported MCUs [30].”

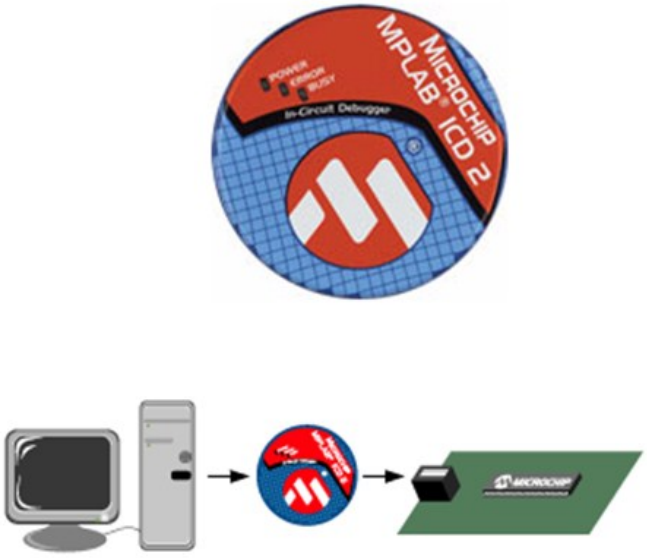

Figure B.2 Programmer ICD 2 [30]

By using a USB cable, the ICD 2 connects the design user's PC and the target board. It allows users to look into the target board's microcontroller, view variables and registers at breakpoints with MPLAB watch windows.

Microcontroller PIC 16F877A

A microcontroller (MCU) is a small scale computer on a single integrated circuit containing a processor core, memory and programmable input output peripherals, which can be used for embedded applications [42]. In this project, microchip PIC16F877A is adopted, which is CMOS FLASH-based 8-bit microcontroller pack with 40 pins. Figure G.3 shows the pin diagram of 16F877A. In order to test and debug the final board, a DDIP package is selected. PIC16F877A features 256 bytes of EEPROM data memory, self-programming, an ICD, 8 channels of 10-bit Analog-to-Digital (A/D) converter, 2 additional timers, 2 capture/compare/PWM functions, a synchronous serial port, which can be configured as either 3-wire Serial Peripheral Interface (SPI™) or the 2-wire Inter-Integrated Circuit (I²C™) bus, and a Universal Asynchronous Receiver Transmitter (USART) [31]. The PIC61F877A provides 8 channels (A/D) which makes it ideal for more advanced level A/D applications.

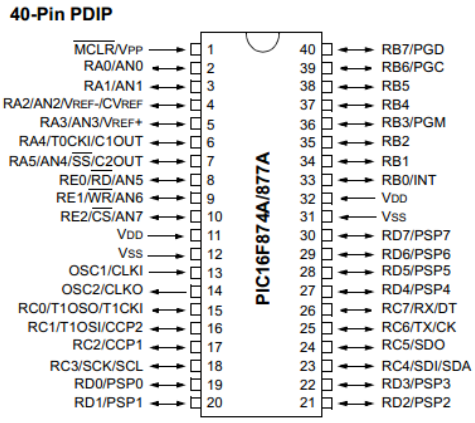

Figure B.3 Pin diagram of 16F877A

C: Code for thermal meter

```
#include "pic.h"

__CONFIG(0x2F0A);
#define uchar unsigned char
#define uint unsigned int
#define DQ RD5
#define DQ_HIGH() TRISD5=1
#define DQ_LOW() TRISD5=0;DQ=0
#define RS RD0
#define RW RD1
#define E RD2
#define CS RD3
#define WR RD4
//#define ILE RD5
//#define XFER RD6
uchar pacmanopen[] = {0x0E,0x07,0x03,0x01,0x03,0x07,0x0E,0x00,'\n'};
uchar pacmanshut[] = {0x00,0x0F,0x1F,0x01,0x1F,0x0F,0x00,0x00,'\n'};
//Display Config.
#define MAX_DISPLAY_CHAR 19
//LCD Registers addresses (PORT B)
#define LCD_CMD_WR       0x00
#define LCD_DATA_WR      0x01
#define LCD_BUSY_RD      0x02
#define LCD_DATA_RD      0x03
//LCD Commands
#define LCD_CLS              0x01  //clean the screen, cursor to 0 position,
#define LCD_HOME             0x02  //cusor to 0 position
#define LCD_SETMODE          0x04
#define LCD_SETVISIBLE   0x08
#define LCD_SHIFT            0x10
#define LCD_SETFUNCTION        0x38// 0x20 8 bit one line*******0x38 8 bit two
lines
#define LCD_SETCGADDR          0x40
#define LCD_SETDDADDR          0x80
#define E_PIN_MASK       0x04
#define Newline          0xC0
void disp(uchar num1,uchar num2,uchar num3,uchar num4);
void disp1(uchar num1,uchar num2,uchar num3,uchar num4);
void lcd_init();
void adc_init();
void lcd_wait();
void clearscreen();
void wrcmd(uchar cmdcode);
void wrdata(uchar data);
```

```
void pause(uint num);
void eat();
void Delay_mS(uint D);
void clearscreen ();
void adc_start() ;
void InitialiseADC (unsigned char ADC_Channel);
void adc_enable(unsigned char channel) ;
void adc_read();
void readout(uchar data);
uint temper;
uchar a1,a2,a3,a4;
void delayus(uint,uchar);
void delayus1(uchar);
void delay(uint);
void write_byte(uchar date);
uchar read_byte();
void get_tem();
////-------------------------------------------------//
uint i;
uint advalf0;
uint adval0;
uint adval1;
uchar text[] = {'0',',','0','0','0'};
uchar text1[] = {'T','e',' ','0','0','.','0','0',' ','C'};
void main()
 {
   uint i,lednum,lednum1;
   float dacout;
   uchar a0,a1,a2,a3,a4;
   lcd_init();
   adc_init();
   TRISC=0x00;
  // PORTC=0x00;
               while(1){
                        lcd_init();
                             wrcmd(Newline);
                            get_tem();
                       }
 }
/************** adc_enable ******************/
void adc_enable(unsigned char channel) {
  ADCON0 = (channel << 3) + 0x81;  // ADC on, Fosc/32
}
/************** adc_read ********************/
void adc_read() {
  ADGO = 1;                     // start A/D-conversion
```

```
  while(ADGO)                    // wait
    continue;
}
/************** adc_start ******************/
void adc_start() {
   uint adres0;
   uint adres1;
    float advalf1;
    float advalf2;
    adc_enable(0);               // chanel 0
    adc_read();                 // begin
    adres0 = ADRESH;              // AD-Wert save
    adres0 = adres0 << 8;
    adres0 = adres0 | ADRESL;
advalf1=(adres0/1023.0)*255.0;//==2.3843
   adval0=advalf1*1;
return;
}
/*********************************************************/
void adc_init()
{
        TRISA=0x07;//set the port 1 2 3 as input

        TRISB=0x00;
        PORTA=0;

        ADCON1=0x8e;   //set up the up and low value
        Delay_mS(10);
}
 void pause(uint num)
 // Utility routine to pause for
 // a period of time.
  { while(num--)
     {/*do nothing */
     }
  }
/**************DRIVER*************************************************************/
void lcd_init()
// Initialise the LCD Display.
 { TRISB = PORTB = 0x00;
   TRISD=0x00;
   wrcmd(LCD_SETFUNCTION);               // 8-bit mode - 2 line - 5x7 font.
   wrcmd(LCD_SETVISIBLE+0x04);            // Display no cursor - no blink.
   wrcmd(LCD_SETMODE+0x02);
   //wrcgchr(pacmanshut, 8);              // Automatic Increment - No Display shift.
   //wrcgchr(pacmanopen, 0);
```

```
  wrcmd(LCD_SETDDADDR);                    // Address DDRAM with 0 offset 80h.
 }
void clearscreen ()
 { wrcmd(LCD_CLS);
  wrcmd(LCD_SETDDADDR+0x00);
 }
void wrcmd(uchar cmdcode)
        {
        PORTB=cmdcode;
        RS=0;

        RW=0;

   Delay_mS(1);
        E=1;

        Delay_mS(1);
        E=0;

        return;
        }
void wrdata(uchar data)
        {
        PORTB=data;
        RS=1;

        RW=0;

        Delay_mS(1);
        E=1;

        Delay_mS(1);
        E=0;

        return;
        }
void Delay_mS(uint D)
        {
        unsigned int i,j;
        for(i=0;i<D;i++)
        for(j=0;j<1000;j++);
        }
void disp(uchar num1,uchar num2,uchar num3,uchar num4)
{
  uchar *textptr = text;
    uint i;
```

```
      text[0] = num1;
      text[2] = num2;
      text[3] = num3;
      text[4] = num4;
    for(i=0;i<5;i++)    // Write the String.
      {
        wrdata(*textptr++);
        pause(10);
      }
}
void disp1(uchar num1,uchar num2,uchar num3,uchar num4)
{uchar *textptr1 = text1;
      uint i;
      text1[3] = num1;
      text1[4] = num2;
      text1[6] = num3;
      text1[7] = num4;
    for(i=0;i<10;i++)    // Write the String.
      {  wrdata(*textptr1++);
        pause(10);  }
}
//************DAC FUNCTION*************************************//
void readout(uchar data){
PORTC=data;
          CS=1;CS=0;

    WR=1;WR=0;

Delay_mS(1);
          WR=1;CS=1;

          return;}
void reset()
{         uchar st=1;
          DQ_HIGH();

    delayus1(0);   //2uS
          while(st)
          {  DQ_LOW();
             delayus1(250); //500uS
                  DQ_HIGH();

        delayus1(19);//40uS
        if(DQ==1)
                          st=1;
                  else
```

```
                        st=0;
        delayus1(250);  //500uS   }
}
void write_byte(uchar date)
{       uchar i,temp;
        DQ_HIGH();

 delayus1(0);
        for(i=8;i>0;i--)
        {       temp=date&0x01;   //01010101
                DQ_LOW();
       delayus1(2);               //7~15.8uS
                if(temp==1)
                        DQ_HIGH();
                else

                        DQ_LOW() ;

       delayus1(25); //25~51.8us

                DQ_HIGH();

                date=date>>1;    //00101010

        }

NOP();NOP();NOP();

NOP();NOP();}

uchar read_byte()

{       uchar i,date;

        static bit j;

        for(i=8;i>0;i--)

        {       date=date>>1;

                DQ_HIGH();

     delayus1(0);    //2.2us

                DQ_LOW();
```

```
        delayus1(1);  //3.8uS

                DQ_HIGH();

              delayus1(0); //5.8uS

                j=DQ;

                if(j==1)

                        date=date|0x80;//1000 0000

        else
          date=date|0x00;
              delayus1(22);   //17~ 37uS    //18~56 19~ 60uS        //45US (22/20)}
          return (date);}
void get_tem()
{         uchar tem1,tem2,num;
          float aaa;
          reset();
          write_byte(0xCC);//
          write_byte(0x44);//
    //write_byte(0x4E);/
          delay(2000);
disp1(a1,a2,a3,a4);
          reset();
          write_byte(0xCC);
          write_byte(0xBE);
          tem1=read_byte();
          tem2=read_byte();
          aaa=(tem2*256+tem1)*6.25;
    temper=(int)aaa;
          a1=temper/1000+48;
          a2=temper%1000/100+48;
          a3=temper%100/10+48;
          a4=temper%10+48;
          delay(2000);
    delay(2000);
    delay(2000);}
void delayus(uint x, uchar y)
{uint i;
uchar j;
          for(i=x;i>0;i--);
    for(j=y;j>0;j--);}
void delayus1(uchar x)
{ uint i;
```

```
  for(i=x;i>0;i--);   }
void delay(uint x)
{         uint a,b;
          for(a=x;a>0;a--)
                    for(b=110;b>0;b--);}
```

D: Code for bias control

```
#include "pic.h"
#include "stdlib.h"
__CONFIG(0x2F0A);
const float bb[]={3.72,3.73,3.74    ,3.75   ,3.76   ,3.77   ,3.78   ,3.79   ,3.8    ,3.81
        ,3.82   ,3.83   ,3.84   ,3.85   ,3.86   ,3.87   ,3.88,3.89,3.9,
3.91    ,3.92   ,3.93   ,3.94   ,3.95   ,3.96   ,3.97   ,3.98   ,3.99   ,4.00   ,4.01   ,4.02
        ,4.03   ,4.04   ,4.05   ,4.06   ,4.07   ,4.08   ,4.09   ,4.1,
4.11    ,4.12   ,4.13   ,4.14   ,4.15   ,4.16   ,4.17};
const float cc[]={3.72,3.73,3.74    ,3.75   ,3.76   ,3.77   ,3.78   ,3.79   ,3.8    ,3.81
        ,3.82   ,3.83   ,3.84   ,3.85   ,3.86   ,3.87   ,3.88,3.89,3.9,
3.91    ,3.92   ,3.93   ,3.94   ,3.95   ,3.96   ,3.97   ,3.98   ,3.99   ,4.00   ,4.01   ,4.02
        ,4.03   ,4.04   ,4.05   ,4.06   ,4.07   ,4.08   ,4.09   ,4.1,
4.11    ,4.12   ,4.13   ,4.14   ,4.15   ,4.16   ,4.17};
unsigned char texta[] = {'D',' ','0','0','0','0'};
#define uchar unsigned char
#define uint unsigned int
#define RS RD0
#define RW RD1
#define E RD2
#define CS RD3
#define WR RD4
#define ILE RD5
#define XFER RD6
uchar pacmanopen[] = {0x0E,0x07,0x03,0x01,0x03,0x07,0x0E,0x00,'\n'};
uchar pacmanshut[] = {0x00,0x0F,0x1F,0x01,0x1F,0x0F,0x00,0x00,'\n'};
//Display Config.
#define MAX_DISPLAY_CHAR 19
//LCD Registers addresses (PORT B)
#define LCD_CMD_WR      0x00
#define LCD_DATA_WR     0x01
#define LCD_BUSY_RD     0x02
#define LCD_DATA_RD     0x03
//LCD Commands
#define LCD_CLS             0x01  //clean the screen, cursor to 0 position,
#define LCD_HOME            0x02  //cusor to 0 position
#define LCD_SETMODE         0x04
#define LCD_SETVISIBLE  0x08
#define LCD_SHIFT           0x10
#define LCD_SETFUNCTION     0x38// 0x20 8 bit one line*******0x38 8 bit two
lines
#define LCD_SETCGADDR       0x40
#define LCD_SETDDADDR       0x80
#define E_PIN_MASK      0x04
void disp(uint lcdnum);
```

```
void lcd_init();
void adc_init();
void lcd_wait();
void clearscreen();
void wrcmd(uchar cmdcode);
void wrdata(uchar data);
void pause(uint num);
void eat();
void Delay_mS(uint D);
void clearscreen ();
void adc_start() ;
void InitialiseADC (unsigned char ADC_Channel);
void adc_enable(unsigned char channel) ;
void adc_read();
void readout(uchar data);
void disptext(uchar text);
void disp1(uint lcdnum);
void check_error();
void max_min();
void Delay_m(uint D);
uint i;
uint advalf0;
uint adval0;
uint adval1;
uint vbias;
uint max;
uint min;
uint bias_a;
uint bias_b;
float error;
signed int error_int;
uint aim_point;
uint flag;
 uchar text[] = {'0','.','0','0','0'};
uchar ok[]={'o','k',' ','!'};
void main()
 {
   uint i,lednum,lednum1;
   float dacout,num1,num2;

  // uchar a0,a1,a2,a3,a4;
   lcd_init();
   adc_init();
   TRISC=0x00;
   PORTC=0x00;
Delay_mS(1000);
```

```
//max_min();
//vbias=(bias_b+bias_a)/2;
//vbias=160;
readout(vbias);
adc_start();
disp(vbias);
//Delay_mS(7123);
adc_init();
adc_start();
clearscreen ();
check_error();
          while(1){
                    if(error_int>7)
                   { vbias=vbias+1;
                    readout(vbias);
                    Delay_mS(2000);
                    check_error();}
                    else if(error_int<-10)
                                                  {
                    vbias=vbias-1;
                    readout(vbias);
                   Delay_mS(2000);
                   check_error(); }
                   else(abs(error_int)<7);
                   {
                    check_error();
                   }
}
 }
/************** error check ******************/
void check_error(){
  float dacout,num1,num2;
       if(flag<1)
          {       adc_start();
                  Delay_mS(1000);
                  aim_point=adval0;
                  disp(aim_point);
                  num1=adval0;
                  disp(num1);
                  error=(aim_point-num1);
                  error_int=error;
                    wrcmd(0xC0);
                  //disp1(abs(error_int));
                  Delay_mS(2000);
                  wrcmd(LCD_CLS);
                  flag++;
```

```
          }
                    adc_start();
                  Delay_mS(1000);
                  num2=aim_point;
                  disp(num2);
                  num1=adval0;
                  disp(num1);
                  error=(num2-num1);
                  error_int=error;
                    wrcmd(0xC0);
                  disp1(abs(error_int));
                  Delay_mS(2000);
                  wrcmd(LCD_CLS);
}
/************** adc_enable ******************/
void adc_enable(unsigned char channel) {
  ADCON0 = (channel << 3) + 0x81;  // ADC on, Fosc/32
}
/************** adc_read ********************/
void adc_read() {
  ADGO = 1;                      // start A/D-conversion
  while(ADGO)                     // wait
    continue;
}
/************** adc_start ******************/
void adc_start() {
   uint adres0;
   uint adres1;
    float advalf1;
    float advalf2;
    adc_enable(0);                // chanel 0
    adc_read();                   // beginn
    adres0 = ADRESH;         // AD-Wert save
    adres0 = adres0 << 8;
    adres0 = adres0 | ADRESL;
advalf1=(adres0/1023.0)*3.5;//==2.3843
   adval0=advalf1*1000;
//adval0=advalf1/255;
return;
}
/*************************adc_int*******************************/
void adc_init()
{
        TRISA=0x09;//set the port 1 2 3 as input

        TRISB=0x00;
```

```
        PORTA=0;

        ADCON1=0x85;   //set up the up and low vavle
        Delay_mS(10);
}
/*************************pause************************************************/
 void pause(uint num)
 // Utility routine to pause for
 // a period of time.
  { while(num--)
     {/*do nothing */
     }
  }
/************DRIVER*****************/
void lcd_init()
// Initialise the LCD Display.
 { TRISB = PORTB = 0x00;
   TRISD=0x00;
   wrcmd(LCD_SETFUNCTION);                  // 8-bit mode - 2 line - 5x7 font.
   wrcmd(LCD_SETVISIBLE+0x04);               // Display no cursor - no blink.
   wrcmd(LCD_SETMODE+0x02);
   //wrcgchr(pacmanshut, 8);         // Automatic Increment - No Display shift.
   //wrcgchr(pacmanopen, 0);
   wrcmd(LCD_SETDDADDR);            // Address DDRAM with 0 offset 80h.
 }
void clearscreen ()
 { wrcmd(LCD_CLS);
   wrcmd(LCD_SETDDADDR+0x00);
 }
void wrcmd(uchar cmdcode)
        {
        PORTB=cmdcode;
        RS=0;

        RW=0;

    Delay_mS(1);
        E=1;

        Delay_mS(1);
        E=0;

        return;
        }
void wrdata(uchar data)
        {
```

```
        PORTB=data;
        RS=1;

        RW=0;

        Delay_mS(1);
        E=1;

        Delay_mS(1);
        E=0;

        return;
        }
void Delay_mS(uint D)
        {
        unsigned int i,j;
        for(i=0;i<D;i++)
        for(j=0;j<1000;j++);
        }
void Delay_m(uint D)
        {
        unsigned int i,j,k;
for(k=0;k<D;k++)
for(i=0;i<6000;i++)
        for(j=0;j<4548;j++);
        }
/**********************disp**********************/
void disp(uint lcdnum)
{
  unsigned char *textptr = text;
  unsigned int i;
     text[0] = lcdnum/1000+48;
     text[2] = lcdnum%1000/100+48;
     text[3] = lcdnum%100/10+48;
     text[4] = lcdnum%10+48;
   for(i=0;i<5;i++)    // Write the String.
//while(*textptr)
 {
        wrdata(*textptr++);
        pause(10);
      }
}
//************DAC FUNCTION*************************************//
void readout(uchar data){
PORTC=data;
        CS=1;CS=0;
```

```
   WR=1;WR=0;

Delay_mS(1);
          WR=1;CS=1;

          return;}
/**********disptext*****************/
void disptext(uchar text)
{
uchar *textptr=text;
while(*textptr)
{wrdata(*textptr++);
pause(10);}
wrcmd(LCD_CLS);
}
/*********************disp1*******************************/
void  disp1(uint lcdnum){
  unsigned char *textptr = texta;
  unsigned int i;
if (error>0)
{texta[1]='+';}
else
{texta[1]='-';}
      texta[2] = lcdnum/1000+48;
      texta[3] = lcdnum%1000/100+48;
      texta[4] = lcdnum%100/10+48;
      texta[5] = lcdnum%10+48;
    for(i=0;i<6;i++)    // Write the String.
//while(*textptr)
 {
         wrdata(*textptr++);
         pause(10);
       }
}
void max_min()
{
float a,b;
uint tempa;
uint tempb;
uint i;
        readout(1);
        adc_start();
        tempb=adval0;
        max=tempb;
        min=tempb;
     bias_a=1;
```

```
    bias_b=1;
Delay_mS(2000);
clearscreen ();
   for(i=1;i<256;i++)    // Write the String.
     {  disp(i);readout(i);
        Delay_mS(1000);
        adc_start();
        pause(10);
        tempb=adval0;

  if(tempb<min)
                  {        min=tempb;
         bias_b=i;}

         if(tempb>max)
                  {        max=tempb;
         bias_a=i; }
Delay_mS(1000);    clearscreen ();
}
disp(max);
disp(min);
wrcmd(0xC0);
disp(bias_a); disp(bias_b);
}
```

E: Design specifications

This designed optical transmitter's specification is seen below:

Parameters	Values	Units	Notes
Optical Characteristics			
Wavelength	1550	nm	
Optical Output power(DFB laser)	20	mW	
Optical Connector type		FC	
Optical output Fiber	Corning/Fujikura SM PUV/UV250(Panda)		
Maximum Operating Temperature Variation Rate	1	1°C/min	
Insertion loss(MZM)	6	dB	
Photodiode Responsivity(MZM)	10^{-3}		
RF Characteristics			
Operational Bandwidth	0-30.4	GHz	
RF input impedance	50	Ω	
1 dB Compression Point	-9.45	dBm	
RF Connector	V-connector		
Maximum input power	25	dBm	
Insertion loss(MZM)	-2	dB	
$V\pi$	4.935	V	
Link performance			

Link Gain	-18	dB	With ZVA +213
Noise Figure	13		
Spurious Free Dynamic Range	102.34	dB	
S11 return loss	<-8.9	dB	
S22 return loss	<-10	dB	
Power supply			
Input voltage	±12, ±5	V	
Max Current	2	A	
Storage Temperature Range	-40 ~ +85	°C	
Operating Temperature Range	0 ~ +70	°C	